UNIVERSITY OF CATANIA

INTERNATIONAL PhD IN CHEMICAL SCIENCES

XXXIII CYCLE

PhD THESIS

Mimimorena Seggio

Design and Development of Photoactivatable Systems for Ophthalmic Therapies

Company Partners

CYCLOLAB MEDIVIS

Tutor
Prof. Salvatore Sortino

PhD Coordinator
Prof. Salvatore Sortino

SUMMARY

List of abbreviation

ABF: 4-amino-7-nitrobenzofurazane
ACN: acetonitrile
AMD: age-related macular degeneration
βCD: β-cyclodextrin
γCD: γ-cyclodextrin
BTX: betaxolol
CFU: colony forming units
cGMP: cyclic guanosine monophosphate.
CL: contact lens
CNV: chorioidal neovascularization
CoS: isopropanol
DAN: 2,3-diamminonaphtalene
DCC: N,N'-dicyclohexylcarbodiimide
DCM: dichloromethane
DEPT: The Distortionless Enhancement by Polarization Transfer
DIPEA: N,N-Diisopropylethylamine
FDA: Food and Drug Administration
DMAP: 4-(dimethyl)aminopyridine
DMF: N,N-dimethylformamide
DMSO: dimethylsulfoxide
EtOAc: ethylacetate
FRET: Förster resonance energy transfer
GSNO: S-nitrosoglutatione
GTN: glyceril trinitrate
HCE-2: Human Corneal Epithelial cells
HSQC: heteronuclear single quantum coherence spectroscopy
IOP: intraocular pressure
IR: infrared
ISC: intersystem crossing
ISDN: isosorbide dinitrate
ISMO: isosorbide 5-mononitrate
MALDI: Matrix Assisted Laser Desorption
MDR: multidrug resistance

ME: microemulsion
MRP: multidrug resistance protein
MTT: 3-(4,5-dimethylthiazol-2-yl)-2,5-diphenyltetrazolium bromide tetrazolium
NBF: nitrobenzofurazane
NHS: N-hydroxysuccinimide
NIR: near Infrared
NMR: nuclear magnetic resonance
MS: mass spectroscopy
NO: nitric oxide
NOPDT: nitric oxide photodynamic therapy
NOPD: nitric oxide photodonor
NOS: nitric oxide synthase
O: lauroglycol FFC
OD: optical density
PBS: phosphate buffered saline
PDT: photodynamic therapy
PETN: pentaerythrityl tetranitrate
P-gp: P-glicoprotein
PS: photosensitizer
PTT: photothermal therapy
Rf: retentions factor
PI: Polydispersity index
ROS: reactive oxygen species
S: Labrasol
SA: succinic anhydride
sGC: soluble guanylyl cyclase
SIRC: Statens Seruminstitut Rabbit Cornea
STF: artificial tears solution
TEA: triethylamine
TEM: transmission electron microscopy
THF: tetrahydrofuran
TLC: Thin layer chromatography
UV/ Vis: ultraviolet/visible
W: water

Chapter 1

Abstract

The general goal of the research is the design, characterization and potential industrial scale-up of photoactivatable systems including nanoparticles, gels and thin films for innovative ophthalmic therapies. In particular, this project aims to develop innovative constructs incorporating suitable photo-precursors generating nitric oxide (NO) and/or singlet oxygen ($^1O_2$) under visible light stimuli. If produced with accurate spatio-temporal control, these species, can act as "unconventional" therapeutics against infections, glaucoma and macular degeneration. In addition, they also offer two great advantages compared to conventional therapeutic agents: i) absence of multidrug resistance and ii) short lifetimes which avoid typical undesired systemic effects.

The purpose is to improve the therapeutic efficacy using the photodynamic action of the above transient species through different mechanisms of action either with or without the use of conventional drugs in order to maximize the therapeutic effect and minimize the side effects of drugs. Photons represent an ideal tool in this context as they are easily manipulated in terms of intensity, duration, and wavelength and do not influence the physiological parameters of pH, temperature and ionic strength.

Appropriate NO-photodonors (NOPD), activatable by visible light, already developed in the research group, constitute a solid starting point for their suitable

modifications to improve the photobehavior and encapsulation capability, in order to develop systems with multimodal therapeutic strategy. The use of prodrugs based on the NOPD can be applied in ophthalmic field, for the antibacterial properties and for the capability of lowering the intraocular pressure (IOP) in glaucoma. This latter is a strategy of increasing interest on the market of ophthalmic drugs for the accurate spatio-temporal control of the NO release and the accessibility of the eye to the light.

The photoactivatable systems using designed using already approved FDA polymeric materials and precursors, such us, Pluronics® or cyclodextrin based polymers. The systems will be designed in such a way as to preserve the properties of the components in the nanocarrier, considering the biological barriers that it must overcome to reach the specific target. All systems are characterized in terms of their chemical-physical (shape, size, surface charge), photo-chemical and photo-physical properties (quantum yields of NO and $^1O_2$ release) and biological effects.

The development and the combination of new polymers and photo-receptors both offer space for innovation and for the development of new potential photo-nanomedicine.

Chapter 2

Introduction

2.1 Anatomy and physiology of the eye

The eye is a dedicated sensory organ composed of a complex optical system that collects light from the surrounding environment to form an image. The image is converted into a set of electrical signals and transmitted to the brain through complex neural pathways that connect the eye, via the optic nerve, to the visual cortex and other areas of the brain. This organ comprises several different structures with specific physiological functions. The eyeball comprises three coats: outer (fibrous coat), middle (vascular coat) and inner (nervous coat also called retina). The human eye can be divided into front and back portion called anterior and posterior segments. The anterior segment includes cornea, iris, ciliary body. Immediately behind there are crystalline lens (which is suspended from the ciliary body by zonules) and two aqueous humour-filled spaces: anterior and posterior chambers. The posterior segment comprises sclera, choroid, retina and vitreous humor (Figure 1).

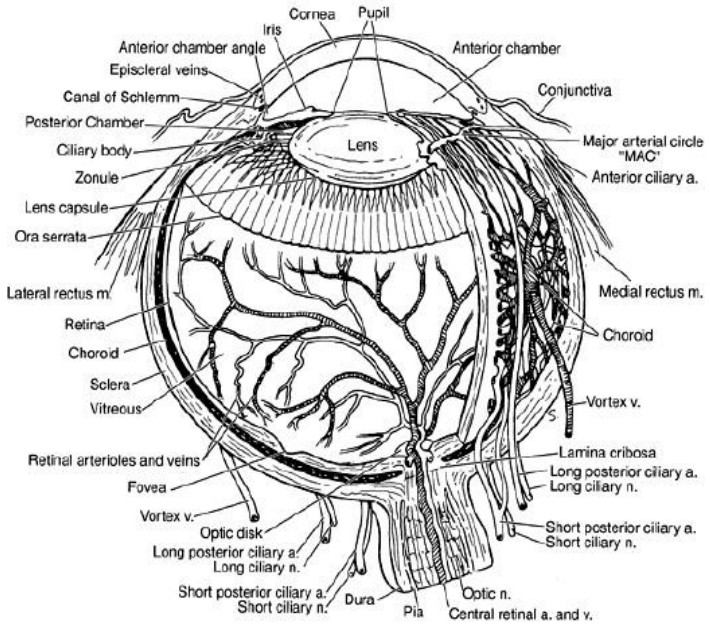

Figure 1: Anatomy of the eye globe.

The cornea is a transparent and avascular tissue and for this reason it gets its nutrition from tears on the outside, aqueous fluid on the inside, and from blood vessels located at the periphery. On the borders of the cornea and adjacent to the sclera is located a transition zone called limbus. The human cornea includes five layers i.e., corneal epithelium, Bowman's membrane, stroma, Descemet's membrane, and endothelium. The aqueous humour is a colourless and transparent liquid present in the anterior segment of the eye, and it is the major source of nutrition to the crystalline lens and cornea. It is secreted by the ciliary body and it is trained in the anterior chamber through the trabecular meshwork. The rate of production and reabsorption of the aqueous humour is accomplished in such a way as to maintain the intraocular pressure (IOP) between the normal range. Excessive production of aqueous humour or obstacles to its outflow can lead to ocular hypertension, a condition that predisposes the onset of glaucoma.

The iris is the colored portion of the eye comprising pigmented epithelial cells and circular muscles (constrictor iridial sphincter muscles). The opening in the middle of the iris is called pupil. The lens is a crystalline and flexible unit consisting of layers of tissue enclosed in a capsule. It is suspended from the ciliary muscles by very thin fibers called the zonules. The conjunctiva is a clear mucous membrane that lines the inside of the eyelids and spreads from the anterior surface of the sclera up to the limbus. It facilitates lubrication in the eye by generating mucus and helps adherence of the tear film. The sclera is a white sheath surrounding the eyeball. The retina is a multi-layered sensory, light sensitive tissue. It contains millions of photoreceptors or photosensitive elements that capture light rays and convert them into electrical impulses. The vitreous humor is a jelly-like substance or a hydrogel matrix, distributed between retina and lens. The retina is the innermost of the three membranes that form the walls of the ocular globe and extends from the point of entry of the optic nerve up to the pupil edge of the iris.

2.2 Ocular pharmacokinetics and physiological limitations

The eye is protected from external materials through to its compartmental organization, the waterproof epithelium, tear secretion and ocular drainage ways.[1] The ocular structures possess peculiar barriers and the administration of medications via local or systemic routes must overcome these barriers to achieve the effective concentration. Barriers in ocular drug delivery are classified as physiological and anatomical. Physiological barriers include tear turn over, naso-lachrymal drainage and blinking. Anatomical barriers include static and dynamic barriers. Static barrier consists of corneal epithelium, stroma, and blood–aqueous barrier. While dynamic barriers involve in conjunctival blood and lymph flow as well as tear drainage.[2] In addition, efflux pumps such as P-glycoprotein (P-gp), multidrug

resistance protein (MRP), and breast cancer resistance protein (BCRP) expressed on the capillary endothelium, represent important barrier to drug absorption.[3]

The physiological limitations imposed by the protective mechanisms of the eye lead to low absorption of drugs and a consequent low therapeutic response exhibited by conventional ophthalmic solutions.[4,5,6] Several formulation approaches are employed to overcome the absorption barriers and improve the ocular bioavailability. Numerous formulations can prolong the residence time of the pharmacological agent on the surface of the eye: gels, ointments, solid preparations, contact lenses and collagen protections.

Majority of the elimination of topically administered drugs from anterior segment are lost through the nasolacrimal duct followed by systemic absorption.[7]

The main property required for ophthalmic preparation and devices is sterility. Unlike the majority of sterile products that are intended for single use, many ophthalmic medications are designed for multiple dosages and the protection from microbial growth is assisted using microbiological preservative. In this perspective, the use of pharmaceutical forms incorporating nitric oxide donors could be useful to maintaining sterility of formulation. Nitric Oxide (NO) has been demonstrated to exert in vitro microbicidal or microbiostatic activity against a rapidly expanding list of helminths, protozoa, yeasts, mycobacteria, bacteria, and viruses.[8]

2.3 Physiological and therapeutic role of NO and NO photodynamic therapy (NOPDT)

NO is an ubiquitous gaseous messenger which plays important roles in many physiological and pathological processes, for example: neurotransmission, hormone secretion, vasodilatation, wound repair, cancer biology and shows an antibacterial and antiviral activity. The biological effects of NO have been shown to

be highly site-, concentration-, and dosage-dependent, creating a complex role for this molecule in opposing beneficial and injurious events.[9] Endogenous NO is produced enzymatically by three distinct nitric oxide synthases (NOS) *via* L-arginine conversion (Figure 2). The NO generated by each enzyme differs considerably in its pattern of expression and regulation, likely reflecting site specific functions.[10]

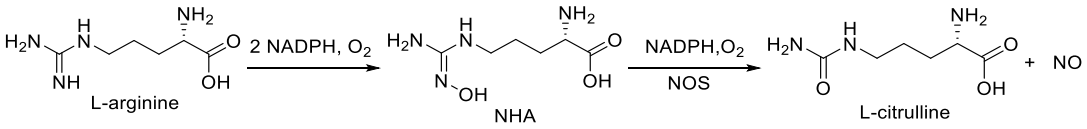

Figure 2: Scheme of endogenous biosynthesis of NO.

The established paradigm of NO biochemistry from production by NO synthases to activation of soluble guanylyl-cyclase (sGC) to eventual oxidation to nitrite (NO_2^-) and nitrate (NO_3^-) may only represent part of NO's effects *in vivo*.

In the eye, NO is synthesized from L-arginine by nitric oxide synthase (NOS) and activates cyclic guanosine monophosphate (cGMP). Through this mechanism, the relaxation response was mediated in the trabecular meshwork and ciliary muscle as well as in vascular smooth muscle cells in the aqueous drainage system. NO is implicated directly in the regulation of intraocular pressure (IOP) and its acute and massive release into the rabbit eye did not induce inflammation or other growth toxic effects on the ocular tissues.[11,12]

Although NO's bio-molecular role is still not completely understood, researchers have used current knowledge to propose and formulate NO-based therapies, some of which have demonstrated success in clinical settings.[13,14,15]

In general, current therapies may be categorized into two groups:

- drugs that alter the body's enzymatic production of NO;
- materials that actively release NO.

Thanks to its small dimension and lipophilicity, NO is capable to diffuse some micrometers (40–200 μm) in the cellular environment, with important role in intra- and extra-cellular signalling. Due to its half-life of approximately 5 seconds in tissues, this radical species offers the advantage to confine its reactivity in the restricted region of space where it has been generated.

Due to of the instability of NO, NO-precursors are used for controlled release of reactive nitrogen species. This kind of reactions can be spontaneous or controlled. The most important stimuli exploited for releasing NO are pH, temperature, enzyme and light.

NO gas is notoriously difficult to handle. Nevertheless, the gas itself can be used therapeutically, particularly in pulmonary hypertension[16] both in adult and in neonates[17], where it is delivered to the lungs via inhalation. Except these two cases, often was used molecular carriers of NO (NO-donor) to stabilize the radical until its release is required, as a result of a specific stimulus. Numerous compounds capable of releasing NO under the control of different stimuli have been developed. The organic nitrates are the most used NO donor drugs. These latters are nitric acid esters of mono- and polyhydric alcohols and they represent the oldest class of NO donors that have been clinically applied. Representative organic nitrates include glyceryl trinitrate (GTN), pentaerythrityl tetranitrate (PETN), isosorbide dinitrate (ISDN), isosorbide 5-mononitrate (ISMO), and nicorandil. The major biological effects of nitrates are attributable to the formation of NO, that requires either enzymatic or non-enzymatic bioactivation where a three-electron reduction is involved.[18,19]

Another class of NO-donor are amine NONOates, also known as amine diazeniumdiolates; dialkylamine NONOates have been used extensively in chemistry and biology as sources of NO, as these compounds decompose in a predictable pH-dependent manner to produce two molecules of NO.[20,21]

Moreover, there are NO donors [22] activated through light stimulation. For example, the compounds belonging to the class of the metal nitrosyl compounds (M-NO, M = Ru, Cr, Mo, etc.) which can be activated through light stimulation between 320 and 400 nm.[23] Sodium nitroprusside (SNP) ($Na_2[Fe(CN)_5NO]$) is the most widely studied compound belonging to this category. For over 70 years, SNP has been used clinically to reduce blood pressure in hypertensive emergencies.[24,25]

Recently, the potential of iron-sulfur cluster nitrosyls and other metal nitrosyl compounds (M-NO, M = Ru, Cr, Mo, etc.) as NO donors have received much attention. On the basis of the well-known affinity of ruthenium centers for NO, ruthenium nitrosyls have drawn considerable attention as photosensitive precursors of NO.[26,27,28,29] However, toxicity issues related to the transition metals and their elaborate structures make them more difficult to be manipulated than organic compounds may represent potential drawbacks.[30]

Organic NO-photodonor, first synthetized in 1909,[31] was nitrosothiols (RSNOs), and an example belonging to this class of compound is S-Nitrosoglutathione (GSNO).[32,33,34] Furthermore, nitrobenzene derivatives have also been developed as photo-controllable NO-donor. These compounds generate NO from the aryl-nitro group. Irradiation of nitrobenzene conduce to a photo-rearrangement followed by release of NO and formation of a phenol derivative as a stable product that does not absorb in the visible region.[35] The photoreactivity of this kind of molecule has been rationalized on the basis of an intramolecular nitro to nitrite rearrangement followed by cleavage of the nitrite intermediate.[*36*] The twisted geometry of the nitro group with respect to the aromatic plane plays a key role in triggering such a photoprocess.[37] This kind of structure has many qualities. It absorbs in visible range and can be easily functionalized. The modification of this compound can lead to obtain a NO release triggered by more “bio-friendly” light.[38]

Due to NO playing a multifaceted role in the bioregulation of vital function, is critical the control of release in terms of space, time and dosage. [39,40] In particular, dosage may result in opposing beneficial and innocuous events. Thanks to the specific characteristic of light (power, colour and localization), it is possible to have an accurate space-time control system of NO release in a desired biological environment.[41,42,43] For this reason, light-triggered release appears as much more appealing than those based on spontaneous thermolysis for potential use in medicine.

Moreover, light represents a "biofriendly" and easily manipulated reactant, and it offers the great benefit of not affecting physiological parameters such as temperature, pH, and ionic strength, a fundamental requisite for biomedical applications. For this reason, NO photo-donors have been investigated as promising new therapeutic devices.

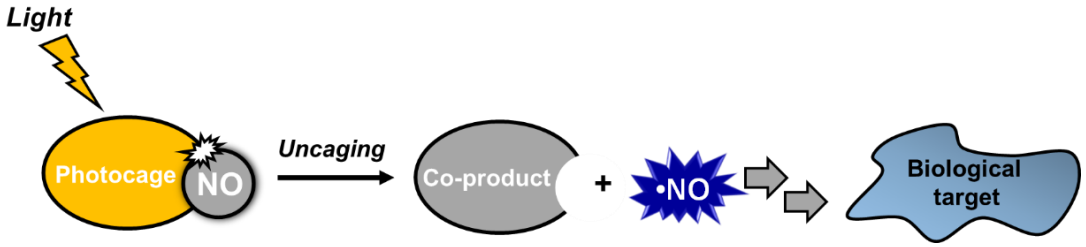

Figure 3: NO-release scheme under light control.

These compounds, to be employed in NO-based photodynamic therapy (PDT), namely NOPDT must:

- be stable in the dark and non-toxic;
- be activated by biocompatible light;
- be having an efficient quantum yield of NO production;
- form non-toxic co-products;

NO has shown an excellent broad-spectrum antibacterial activity towards both Gram-positive and Gram-negative bacteria, mainly because of its reactive byproducts such us peroxinitrite and diidrogentroxyxinitrite which affect the integrating of bacteria membrane and cell function via oxidaitive and nitrosative stress. The dose of NO required to kill bacteria is demonstrated to be non-toxic. NO-based antimicrobial strategy therefore represents good candidates to answer the alarming low turnover of new clinically approved antibiotic drugs.

The benefits of nitric oxide, in addition to the fields of application mentioned above can be exploited in the cardiovascular, pulmonary and anticancer therapy. Moreover, NO can be applied as synergistic agent in PDT. Despite NO is not generated through a photocatalytic process, it offers the advantage of not requiring molecular oxygen and thus NOPDT can complement traditional PDT under hypoxic conditions, such as hypoxia PDT induced as a result of oxygen consumption and hypoxia associated with infections and tumoral condition.

2.4 PDT and therapeutic applications in the ophthalmic field

The therapeutic use of light begins in 1900 when Raab reported that the combination of acridine orange and light could destroy living organisms (paramecium).[44] Currently, it is used in many clinics fields that include oncology, dermatology, cosmetic surgery, ophthalmology, and dentistry. The numerous fields of application of PDT derive from the nature of the treatment which involves the formation of a highly reactive cytotoxic species without selectivity for the substrate. The light source in PDT could be or not monochromatic light. The light wavelength depends primarily on the photosensitizer (PS) and then on the tissue to be treated. About 20 years ago PDT in eye disease was approved for age-related macular degeneration (AMD) and for choroidal neovascularization (CNV) in pathological

myopia. The first photosensitizer approved by FDA in ophthalmology was verteporfin in 2002. The vascular damage and blood flow stasis, followed by vascular occlusion, appears to be the predominant mechanism of damage induced by PDT *in vivo.*[45,46]

PDT is a therapeutic strategy based on production of reactive oxygen species (ROS), mainly singlet oxygen $^1O_2$ ($^1\Delta_g$), as bioactive species. PDT is a photocatalytic process that requires the concomitant presence of three components: molecular oxygen, a PS and light. The PS is an harmless molecule which under irradiation at a specific wavelength achieves a transition from a singlet ground state S_0 toward an excited state S_1. Then intersystem crossing (ISC) permits the population of the long lasting excited triplet state T_1. The extended life-time of T_1 allows it to react in two possible ways named type I and type II mechanisms. Type I mechanism implies interaction of the excited *PS by hydrogen-extraction or electron transfer and leads to the formation of free radicals. These free radicals can react with molecular oxygen and generate ROS such as superoxide radical anion $O_2^{\bullet -}$. Singlet oxygen $^1O_2$ is produced through type II mechanism, by an energy transfer process from the excited *PS toward molecular oxygen $^3O_2$ (Figure 4). These two pathways can occur simultaneously. The ratio between the two mechanisms depends on the nature of the PS and the availability of the subtract.

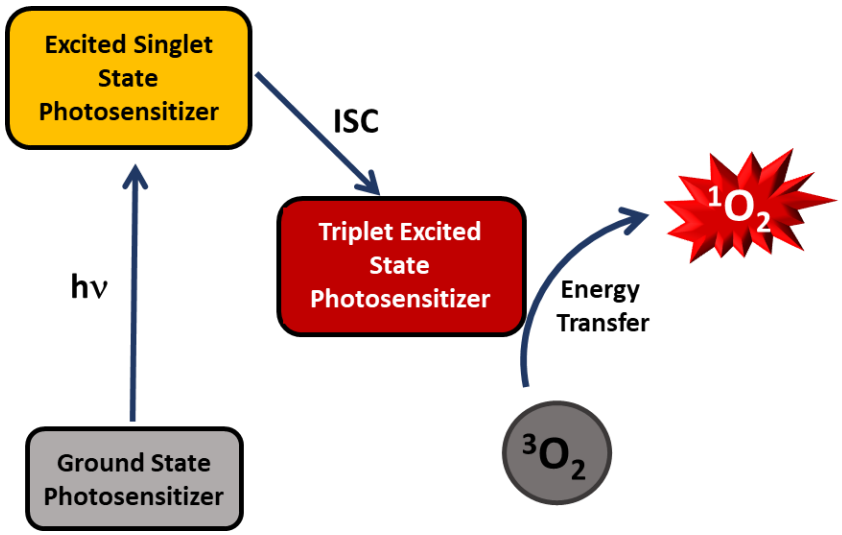

Figure 4: Photocatalytic process scheme of $^1O_2$ production involved in PDT.

The possible biological targets of singlets oxygen and free radicals include nucleic acid, enzymes and cellular membranes, leading to cell damage and cell death.[47] In recent years, the use of NO in conjunction with other therapies has been suggested to be high desirable opening new possibilities in the field of multimodal therapeutic strategies; in particular in combination with PDT and photothermal therapy (PTT).[48] These new treatment modalities aim at exploiting synergistic effect in order to obtain an amplification of therapeutic action minimizing the side effects.

Chapter 3

Results and discussions

3.1 Materials and methods

Chemicals: All solvents and chemicals used were of spectrophotometric grade and were purchased from Sigma Aldrich and used without further purification, included Pluronic® P123 (PEO_{20}–PPO_{70}–PEO_{20}, MW ca. 5.750 g mol^{-1}), Pluronic® F127 (PEO_{100}–PPO_{70}–PEO_{100}, MW ca 12.600 g mol^{-1}). Monthly SMART-NAU CL from Safilens (45% methafilcon) were used. Phthalocyanine (component **1**) was obtained from Sigma-Aldrich. Component **2** was synthesized according to our already reported procedure.[49]Labrasols and Lauroglycols FCC were kindly gifted by Gattefosse` (France). The water used was Milli-Q. All cyclodextrins were provided by CycloLab Ltd. Irradiation was performed in a thermostated quartz cell (1 cm path length, 3 mL capacity) using continuum lasers with λ_{exc} = 405 nm or 532 nm, light emitting diode (LED) (λ_{exc} = 415–420 nm), or 150 W xenon lamp.

Instrumentation: ^{1}H NMR spectra were recorded on Varian 200, Varian UNITY Inova 500 MHz or Varian DDR NMR spectrometer 600 MHz.

UV/vis absorption spectra were recorded in a quartz cell with a 1.0 cm path length and 3 mL capacity or a specific holder for thin films on a Jasco V 650 spectrophotometer.

Fluorescence emission spectra were performed with Fluorolog-2 (Model, F111) spectrofluorimeter in right angle mode for solution or in front face mode for film samples. Fluorescence lifetimes were recorded with the same spectrofluorometer equipped with a TCSPC Triple Illuminator. Solutions were excited by a Nanoled pulsed diode excitation source at 455 nm or 370 nm. The system measured fluorescence lifetimes with a resolution >200 ps.

Laser flash photolysis: All of the samples were excited with the second harmonic of a Nd–YAG Continuum Surelite II-10 laser (532 nm, 6 ns FWHM), using quartz cells with a path length of 1.0 cm. The excited solutions were analyzed with a Luzchem Research mLFP-111 apparatus with an orthogonal pump/probe configuration. The probe source was a ceramic xenon lamp coupled to quartz fibre-optic cables. The laser pulse and the mLFP-111 system were synchronized by a Tektronix TDS 3032 digitizer, operating in pre-trigger mode. The signals from a compact Hamamatsu photomultiplier were initially captured by the digitizer and then transferred to a personal computer, controlled by Luzchem Research software operating in the National Instruments LabView 5.1 environment. The solutions were deoxygenated via bubbling with a vigorous and constant flux of pure nitrogen (previously saturated with solvent). In these experiments, the solutions were renewed after each laser shot (in a flow cell with a 1 cm optical path), to prevent photodegradation. The sample temperature was 295 ± 2 °K. The energy of the laser pulse was measured at each shot with a SPHD25 Scientech pyroelectric meter.

Singlet oxygen detection: The NIR luminescence of $^1O_2$ at 1.27 mm results from the forbidden transition $^3\Sigma^-_g \leftarrow {}^1\Delta_g$. This steady-state emission was registered with the same spectrofluorometer as above equipped with a NIR-sensitive liquid nitrogen cooled photomultiplier, exciting the air-equilibrated samples with a 670 nm continuum laser (100 mW). The timeresolved emission of $^1O_2$ was probed orthogonally to the exciting beam of the same 532 nm pulsed laser as above, with a preamplified (low impedance) Ge-photodiode (Hamamatsu EI-P, 300 ns resolution) maintained at 196 °C and coupled to a longpass silicon filter (41.1 mm) and an interference filter (1.27 mm). The pure signal of $^1O_2$ was obtained as the difference between the signals in air and Ar-saturated solutions. The temporal profile of the luminescence was fitted to a single-exponential decay function with the exclusion of the initial portion of the plot, which was affected by scattered excitation light, fluorescence, and the formation profile of singlet oxygen itself.

Amperometric NO detection: NO release was measured with a World Precision Instrument, ISO-NO meter, equipped with a data acquisition system, and based on direct amperometric detection of NO with short response time (< 5 s) and sensitivity range 1 nM – 20 µM. The analog signal was digitalized with a four-channel recording system and transferred to a PC. The sensor was accurately calibrated by mixing standard solutions of $NaNO_2$ with 0.1 M H_2SO_4 and 0.1 M KI according to the reaction:

$$4H^+ + 2I^- + 2NO_2^- \rightarrow 2H_2O + 2NO + I_2$$

Irradiation was performed in a thermostated quartz cell (1 cm path length, 3 mL capacity) under gentle stirring and under continuum laser light at different λ_{exc}.

Chemical Detection of NO: NO release was also measured indirectly by means of the well-known, highly sensitive (detection limit on the order of the picomoles) fluorimetric bioassay of Misko et al. [50] based on the ring closure of the nonfluorescent DAN with nitrite to form the highly fluorescent product. The samples were immersed in 2 mL of artificial tears solution (STF) and exposed to daylight or kept in the dark. Afterwards, 2 mL solution was added of 200 µL of DAN (2,3-diamminonaphtalene) solution (DAN 0.30 M in 0.62 M HCl) and stirred for 20 min at room temperature. Then 300 µL of NaOH 3 M was added in the previous solution and stirred for 20 min at room temperature. The resultant solution was put into a quartz cell and the fluorescence emission and excitation spectra were recorded at λ_{exc} = 360 nm and λ_{em} = 405 nm, respectively. A standard calibration curve was carried out by using freshly prepared solutions of sodium nitrite in a phosphate buffer 10 mM at pH 7.4.

Fluorescence Quantum Yields: Fluorescence quantum yields (Φ_f) were determined using optically matched solutions at the excitation wavelength of compounds, and Fluorescein NaOH 0.1 M ($\Phi_{f\,(s)}$ = 0.98) as a standard through the following equation:

$$\Phi_f = \Phi_{f\,(s)}\,(I\,n^2/_{(s)}n^2_{(s)})$$

where $\Phi_{f\,(s)}$ is the fluorescence quantum yield of the standard; I and $I_{(s)}$ are the areas of the fluorescence spectra of compounds and standard, respectively; n and $n_{(s)}$ are the refraction index of the solvents used for compounds and standard. Absorbance at the excitation wavelength was less than 0.1 in all cases.

NO photorelease quantum yield: The photodegradation quantum yield, Φ_{NO}, was determined at λ_{exc} used, within 20% photo-transformation of the compounds by using the following equation:

$$\Phi_{NO} = [\text{Photocage-NO}] \times V/t \times (1–10^{-A}) \times I$$

where [Photocage-NO] is the concentration of the phototransformed compound, V is the volume of the sample, t is the irradiation time, A is the average absorbance of the sample at the excitation wavelength and I is the intensity of the excitation light source. The concentration of the phototransformed compounds were determined spectrophotometrically, and I was calculated by potassium ferrioxalate actinometry.

3.2 Photobactericidal contact lens

3.2.1 Design and preparation

As mentioned previously, the absence of microbial contamination is an indispensable requisite for ophthalmic devices and formulation. Due to microbial contamination, ocular infection is one of the main risks associated with the use of ophthalmic pharmaceuticals forms and with the wearing of contact lens (CL), which demands novel straightforward strategies to find reliable solutions. One of the most promising approaches is based on the use of NO since it is a powerful broad spectrum antibiotic agent with the capability to avoid the Multy-drug resistance problem encountered with several drugs often target-specific.[51]

On these grounds in this work a photo-responsive molecular CL was developed embedding in the devices a molecular hybrid developed in our laboratory. [52,53] This latter is composed of two functional moieties: the NO-photoreleaser (NOPD) and a latent fluorophore (coumarin). Coumarin-NOPD hybrid was loaded in a commercial CL generating a medical optical device with antibacterial properties and a fluorescent reporter function. Indeed, this compound acts like an exact optical counter that monitor the release of the bioactive species. The presence of a blue fluorescent reporting functionality which activates concomitantly to the NO photorelease, allows the easy monitoring of the NO delivery in real-time and confirms that the doped CL works under light exposure. The coumarin component has an intense fluorescence emission spectrum overlapping the absorption spectrum of the nitroaniline NO photo-donor. This condition: the close proximity of the two chromophores and the flexibility of the alkyl spacer are key prerequisites to make the fluorescence of the coumarin significantly quenched in the coumarin-NOPD by a Förster resonance energy transfer (FRET) mechanism. Excitation with

visible light is expected to trigger NO photo-release from the nitroaniline moiety leading to a phenol derivative.[54,55] In contrast to the nitroaniline chromophore the photoproduct is not able to accept the energy from the excited coumarin since its absorption spectrum, falling in the UV region, does not overlap any more the emission spectrum of the coumarin. This condition makes the FRET process thermodynamically not feasible. Consequently, the coumarin fluorescence is expected to be restored upon NO photorelease (Figure 5).

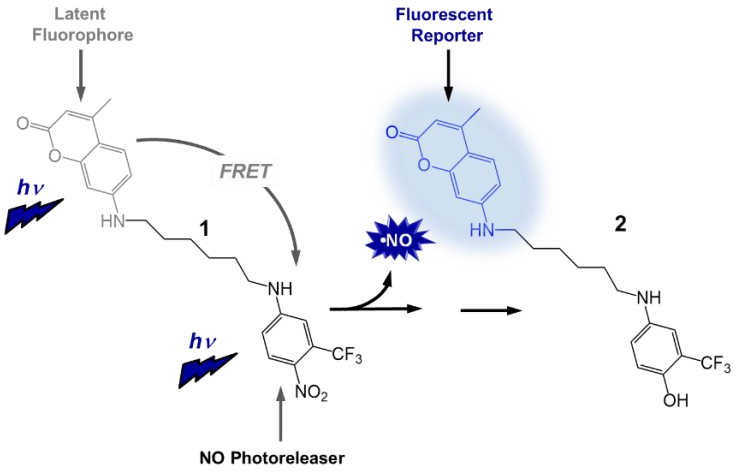

Figure 5: The working principle of the functional molecular hybrid coumarin-NOPD.

The loading was done using the "lens soaking" technique. The method involves soaking the preformed CL in the ethanolic solution of coumarin-NOPD (0.59 mM). The process was monitored spectrophotometrically at different times until reaching a plateau (inset of Figure 6). After loading, the CL appears slightly coloured in a pale yellow as shown in the actual image C in Figure 6. The amount of drug loaded in the CL was calculated from the absorbances at λ = 404 nm (ε_{404} = 8000 M^{-1} cm^{-1}, pathlength 0.1 cm). The reproducibility of the loading technique was demonstrate performing four time the procedure, obtaining an average concentration of 146 µM

of coumarin-NOPD loaded. Furthermore, the loading was monitored following increase of excitation spectra of coumarin-NOPD (Figure 6D).

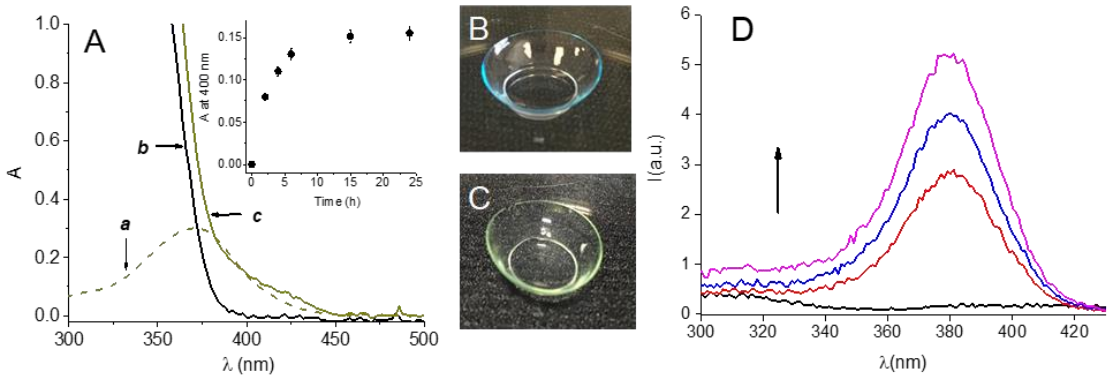

Figure 6: (A) Absorption spectra of an ethanol solution of coumarin-NOPD (a) and the CL before (b) and after (c) loading with **1**. (B) and (C) show the actual images of the CL before and after loading with coumarin-NOPD, respectively. (D) CL excitation spectra at λ_{em}= 460 nm at different times from the beginning of drug loading.

3.2.2 Photochemical characterization

To proceed with characterization tests, the lens was washed with MilliQ water for 15 minutes in order to eliminate any traces of drug on the surface, eliminate ethanol and rehydrate the polymer. Afterwards, the loaded lens was submerged in artificial tears solution (STF) ($NaHCO_3$ 26 mM, KCl 18 mM, NaCl 116 mM, CaCl 0.4 mM, pH 7.4) in which the photo-release tests were conducted by exposition to sunlight (between 11 am and 16 pm on a sunny day). Emission spectral changes were observed at λ_{exc} = 380 nm at different time upon exposition to sunlight (Figure 7). According to the FRET process occurring in Figure 5, the non-irradiated CL show a negligible fluorescence which, in contrast, increases dramatically upon exposure of the CL to daylight. This finding confirms that the formation of the highly fluorescent photoproduct concomitantly to the NO release occurs also within the CL polymeric network. As illustrated in the inset of Figure 7A, we found an excellent linear correlation between the concentration of NO photogenerated and the

increase of the fluorescence intensity of the optical reporter. Note that, the amount of NO released after 30 min exposure represents about 0.2 % of the total NO reservoir available in the CL. As a consequence, even by considering a constant sunlight flux for the whole day, the loaded NOPD results in more than enough to ensure NO photorelease during one full day of light exposure. Interestingly, the process can be also followed at the naked eye. Figure 7B,C show the actual images of CL (350 nm light excitation) before and after 30 min of daylight exposure where it is possible to note the unambiguous increase of the blue fluorescence of the optical reporter in the case of the irradiated sample. Such a fluorescence increase of the CL after irradiation confirms well that the photoproduct remains entrapped therein. This was further supported by the absence of any detectable fluorescence observed in artificial tears solution after immersion of the irradiated CL for 24 h.

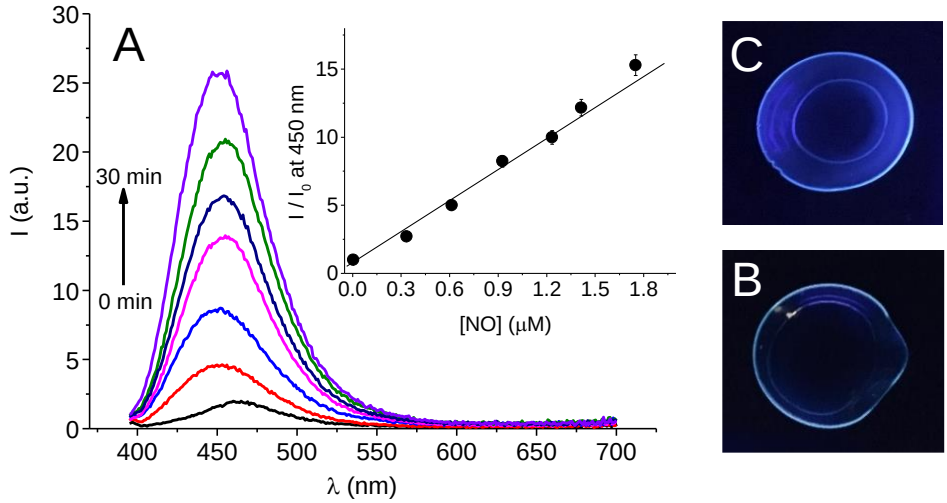

Figure 7: (A) Fluorescence emission (λ_{exc} = 380 nm) spectral changes observed for CL loaded with coumarin-NOPD exposed to daylight at regular intervals of five min. The inset shows the correlation of the fluorescence increase and the concentration of NO released from the CL (I and I_0 represent the fluorescence intensities after and before the irradiation, respectively). (B) and (C) show the actual fluorescence images of the CL (diameter = 14 mm) observed upon 350 nm of light excitation before and after 30 min exposition of the CL to daylight, respectively.

NO detection from CL by amperometric method was carried out immobilizing the lens to one of the wall of quarz cell and submerging in 3 mL of artificial tears solution. The sensor was immersed in the solution outside the light path in order to avoid NO signal artefacts due to photoelectric interference. The measurement was conducted under stirring and under irradiation with continuum laser at λ_{exc} = 405 nm at 100 mW. As shown in Figure 8 the signal remains initially stable and exhibits an increase by turning on the laser light. This means that the release of NO takes place only after a light stimulus. To exclude trivial signals, the same experiment was carried out under the same conditions with empty CL. This experiment demontrate a drastically smaller response compared to the loaded CL (Figure 8).

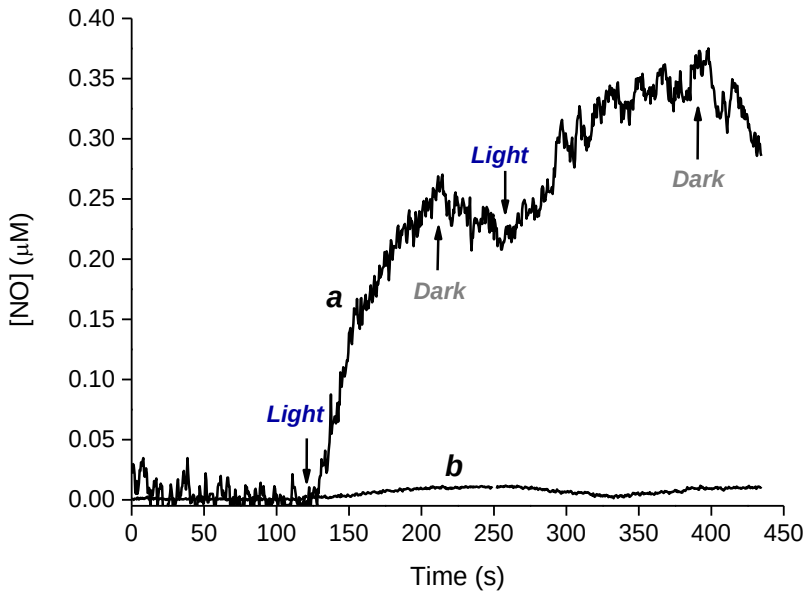

Figure 8: NO release profile observed upon On/Off alternative irradiation cycles with a continuum laser at 405 nm (100 mW) on of CL loaded (a) and unloaded (b) with coumarin-NOPD and immersed in 3 mL of artificial tears solution.

Furthermore, NO release was evaluated by the fluorometric detection method of DAN as previously described,[64] after exposure to sunlight of the CL loaded with

coumarin-NOPD. The irradiation of loaded CL was carried out in sunlight between 1:00 and 3:30 pm. To carry out the reaction of formation of naftotriazolate anion, 200 µL of the DAN stock solution (50 mg/L in 0.6 M HCl) was added to 2 ml of irradiated solution, and it was left under stirring for 20 minutes. 300 µL of NaOH 6 M and was added to the mixture and it was stirred for another 10 minutes. All emission spectra were registered with λ_{exc} = 360 nm and all excitation spectra with λ_{em} = 405 nm. The quantification was carried out using a calibration curve, which correlates the fluorescence intensity at 404 nm and concentration of NO. The NO release follows linearly proportional to the time of exposure to sunlight but it remains stable in the dark. (Figure 9B)

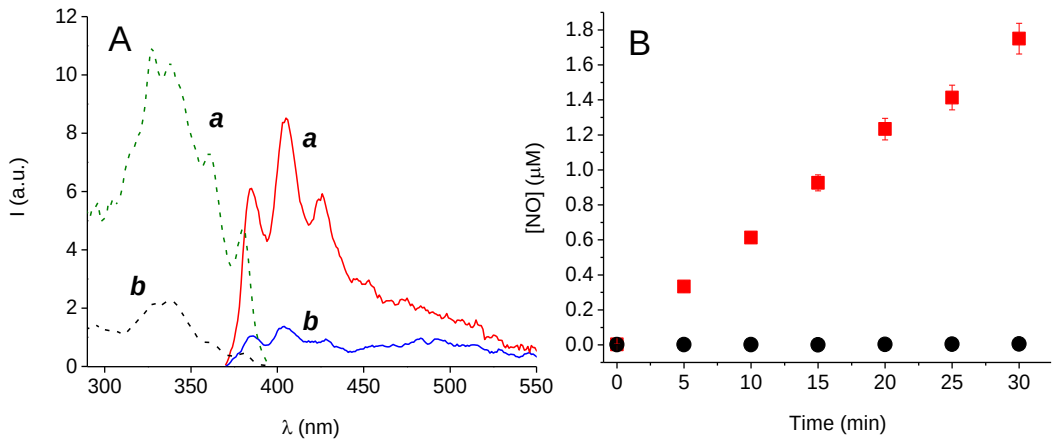

Figure 9: (A) Representative fluorescence emission (solid, λ_{exc} = 360 nm) and excitation (dotted, λ_{em} = 405 nm) spectra obtained after fluorometric assay of CL loaded with coumarin-NOPD, immersed in 3 mL of artificial tears solution, and exposed to daylight (a) or kept in the dark (b). (B) NO concentration, determined by the fluorimetric assay, observed after exposure of the CL loaded with coumarin-NOPD to daylight for different times (■) or kept in the dark (●).

Any premature loss of coumarin-NOPD from CL was evaluated and leakage of photodegradation products was tested by recording CL absorption spectra after one week of storage in CL solution. The absorption spectrum was unchanged (data

not shown). This could be an indication of the exclusive NO release, which does not involve a release of coumarin-NOPD and secondary photodegradation products by the CL polymer. This is due to the poor solubility of coumarin-NOPD in aqueous solvents.

The NO photoreleasing CL are well-tolerated in both dark and light conditions by corneal cells while being able to induce good growth inhibition of Staphylococcus aureus under visible light irradiation.

3.2.3 Biological evaluation

Antibacterial activity of CL loaded with coumarin-NOPD and, for comparison, unloaded CL were tested against Gram-positive *S. aureus*, a human pathogen responsible for a significant morbidity due to the high resistance pattern towards traditional antibiotics. The bacterial cultures (*S. aureus* ATCC® 6538) were incubated with the CL and kept in the dark or irradiated for 40 min with a 150 W Xenon lamp equipped with a cut-off filter at 400 nm. Pure culture was inoculated in 10 mL Muller–Hinton Broth and incubated at 37 ◦C for 24 h. The overnight broth culture was centrifuged at 3500 rpm for 15 min and suspended in PBS. The bacterial suspension was standardized to 2×10^5 CFU/mL by optical density measurements at 570 nm. One hundred µL of the bacterial suspension (20,000 CFU/mL) were placed into a 96-well microplate containing at the bottom a portion of the CL (circular disk, diameter = 6 mm) and irradiated for 40 min by using a 150 W Xe lamp equipped with a cut-off filter $\lambda > 400$ nm or kept in the dark. Afterwards, the bacterial suspension was diluted in PBS and seeded in duplicate as a spot on the Mueller–Hinton agar (Oxoid) plate. The CFUs were counted after incubation at 37 °C for 24–48 h. The results illustrated in Figure 10 show a negligible bactericidal activity of the CL in the dark. On the other hand, a good bacterial growth inhibition was observed for the loaded CL under illumination reaching almost 90% inhibition, in contrast to

the moderate antibacterial effects noted upon illumination in the unloaded sample. Interestingly, the control experiments carried out with all CL showed no relevant cytotoxicity on human corneal epithelial (HCE-2) cells both in the dark and under identical irradiation conditions adopted for the antibacterial test. Parallel experiments were also performed by incubating the CL with corneal cells to evaluate the phototoxicity of the system. The photocytotoxicity experiments were carried out by irradiating human corneal epithelial (HCE-2) cells incubated with CL for 40 min (with the same lamp and in analogous conditions used for the antibacterial test). Cell proliferation was assessed by 3-(4,5-dimethylthiazol-2-yl)-2,5-diphenyltetrazolium bromide tetrazolium (MTT) assays, based on the conversion of a substrate containing a tetrazolium ring to spectrophotometrically-detectable formazan by mitochondrial dehydrogenases. Briefly, cells were seeded at an initial density of 8×10^3 cells/microwell in 96-well microplate, 200 µL of complete DMEM without phenol red was added and incubated at 37 °C for 24 h in a humidified atmosphere containing 5% CO_2. CL were placed in the well and irradiated. Thereafter, the CL were withdrawn and 20 µL of 0.5% 3-(4,5-dimethylthiazol-2-yl)2,5-diphenyl-tetrazolium bromide in PBS were added to each well. Following 4 h of incubation at 37 °C, the supernatant was removed and replaced with 100 µL of DMSO. The optical density (OD) was measured with a microplate spectrophotometer reader at 550 nm. Cell viability (%) was calculated from the following equation:

$$\text{Cell Viability (\%)} = [OD_{Before} - (OD_{After}/OD_{Before})] \times 100$$

OD_{Before} and OD_{After} are the absorbance values of the sample before and after irradiation, respectively.

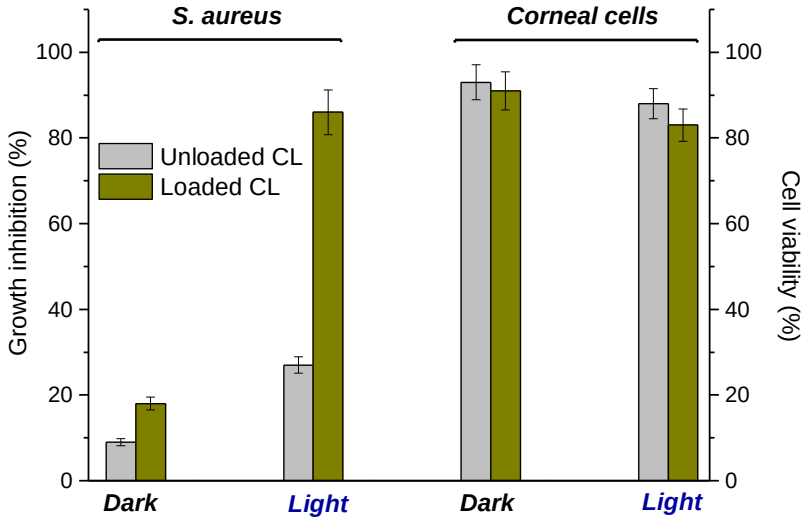

Figure 10: *S. aureus* growth inhibition and human corneal epithelial (HCE-2) cells viability of unloaded and loaded CL in the dark and upon illumination with visible light (λ_{exc} > 400 nm).

3.2.4 Conclusions

In conclusion, we achieved a NO photodelivering CL through a simple procedure which takes advantage of the effective interactions between the CL polymeric network and a tailored, water insoluble compound. Despite its non-covalent incorporation, the molecular hybrid shows a high association extent to CL, which prevents any premature leaching. The photochemical properties of the NOPD are very well preserved upon its incorporation in the host CL. In fact, the loaded CL are stable in the dark towards NO release that, in contrast, is promptly observed upon daylight exposure. The sustained NO release can be followed in real-time by the intense blue fluorescence of the by-product formed concomitantly to the NO release. The photoproduct acts as a convenient optical reporter of the NO concentration and provides a very easy way to check both the correct working of the doped CL and the exhaustion of the NO reservoir. Once photogenerated, the

NO radical promptly diffuses out of the polymeric matrix to reach the biological target. The CL show good light-dependent bactericidal activity against the Gram-positive *S. aureus* without any relevant toxic effects on human corneal cells. These results open intriguing possibilities for further engineering of CL with NOPD in the perspective of innovative ocular devices activatable by sunlight.

3.3 A thermoresponsive gel photoreleasing nitric oxide for potential ocular application

3.3.1 Design and preparation

Topical instillation of drugs through eyedrops is the most important and well-accepted route of administration for the treatment of various eye disorders. The residence time of most conventional ocular solutions is 5–25 min and only about 10% of the topically applied drug is absorbed. A smart strategy to increase or prolong the contact time of ophthalmic formulations with the ocular tissues is to use in situ gel-forming ophthalmic drug delivery system prepared from polymers that exhibit reversible phase sol-gel temperature dependent. The thermo-responsive polymers most widely used in ophthalmic formulations are Pluronics®, xyloglucan and poly(N-isopoprylacrilamide) (PNIPAAm). Pluronics® are a family of commercially available triblock copolymers that have the following trade names: Pluronics®, Poloxamers® or Tetronics®. They are non-ionic polymers (polyoxyethylene-poly-oxypropylene-polyoxyethylene; PEOn–PPOn–PEOn) and are temperature sensitive. Pluronics® F-127 (copolymer polyoxyethylene$_{106}$–polyoxypropylene$_{70}$–polyoxyethylene$_{106}$) contains approximately 70% ethylene oxide, which contributes to its hydrophilicity. It is nontoxic, with low viscosity below 4-5°C and forms a semisolid gel at body temperature. This transformation is reversible, returning it to a liquid state at low temperatures. The capability to form thermo-responsive gels is maintained even if placed in mixtures with other poloxamers, obtaining gels with excellent rheological characteristics. For this purpose, it was decided to modify the Pluronics® P-123 with a NOPD (Figure 11)[56].

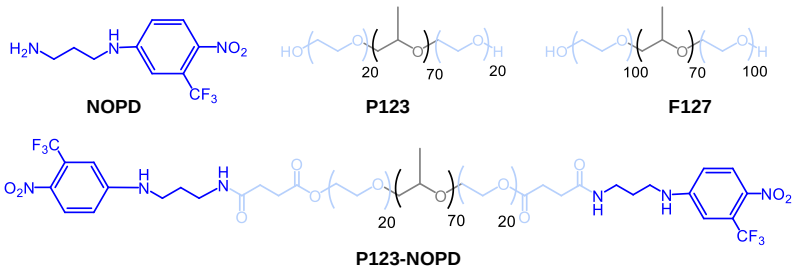

Figure 11: Molecular structures of the components used in this work.

The free NOPD was synthesized according to our previously reported procedure.[57] P123-NOPD was synthesized in a two step-synthesis. At first, we converted P123 in its bis-carboxylic derivative (P123-COOH) and then we condensed this polymer with NOPD to obtain P123-NOPD.

P123-COOH. Carboxylation of P123 followed the procedure used by Zalipisky *et al*.[58] with some modifications. Briefly P123 (10.0 g, 3.44 mmol OH), 4-(dimethyl)aminopyridine (DMAP, 420 mg, 3.44 mmol), triethylamine (TEA, 480 µL, 3.44 mmol) and succinic anhydride (SA, 345 mg, 3.44 mmol) were dissolved in 20 mL of 1,4-dioxane and stirred for 48 h at room temperature. The excess of solvent was removed by rotatory evaporation and kept at -15 °C overnight. The final solution was precipitated with cold diethyl ether and dried under vacuum. A colorless gel was formed with 45 % of carboxylation (titration with NaOH). 5.0 g of P-123-COOH was obtained and by the ^{1}H NMR 500 MHz in D_2O it is possible to confirm the carboxylation by the triplet at 2.67 ppm (H^1), the multiplet at 2.54 ppm (H^2) and a doublet at 4.31 ppm (H^3). The degree of carboxylation was determined by titration with a NaOH solution previously standardized and it was found to be about 80 %.

P123-NOPD. P123-COOH (1.5 g, 0.44 mmol COOH), N,N'-dicyclohexylcarbodiimide (DCC, 91 mg, 0.44 mmol) and N-hydroxysuccinimide (NHS, 51 mg, 0.44 mmol) were

added in 25 mL of dichloromethane (DCM) and kept at room temperature under continuous stirring and N_2 atmosphere for 1 h. After removing the formed dicyclohexylurea, an equimolar amount of NOPD (116 mg, 0.44 mmol in 1,4-dioxane) was added dropwise to the resulting solution. The mixture was kept under stirring at room temperature for 48 h. The excess of DCM was removed, and the solution cooled overnight. The final solution was filtered (under vacuum with a thin layer of silica gel) followed by the precipitation with cold diethyl ether and dried under vacuum. Further purification was done by dialysis (membrane with molecular weight cut-off 3.5 kD) tracking the absorption of dialysis medium. Finally, the yellowish gel was frozen and lyophilized for 24 h, yielding 1 g (63%) of P123-NOPD. The final compound was fully characterized by ^{1}H NMR. In the spectrum the characteristic peaks of the NOPD moieties are easily identifiable at 8,06 ppm ($H^{2'}$); 7,06 ppm ($H^{3'}$); 6,9 ppm ($H^{1'}$); 2,73 ppm ($H^{4'}$); 2.58 ppm ($H^{6'}$) and 1.89 ppm ($H^{5'}$) as shown in Figure 12.

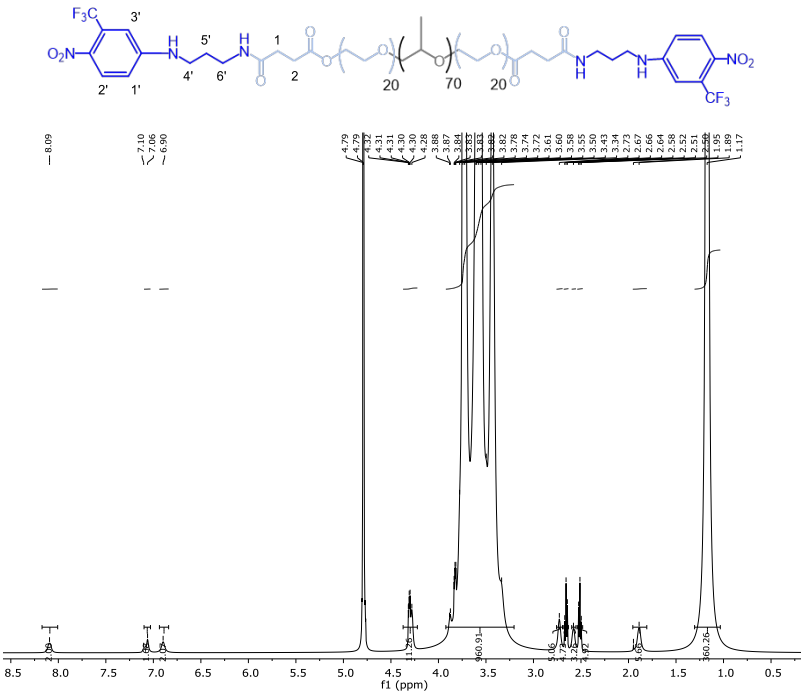

Figure 12: ^{1}H NMR (500 MHz) of P123-NOPD.

3.3.2 Rheological and physico-chemical characterization

The temperature-dependent in situ gel-forming system was prepared as follows. At an appropriate weight ratio F127/P123 Pluronics® were put into a saline solution (0.9 % NaCl), stirred at 4 °C until a clarified solution was obtained and stored at 4 °C. Preliminary experiments were carried out through the tube inversion method to find suitable F127 and P123 concentrations in order to achieve a gelation temperature in the range of 32–35 °C. The sample solution was transferred to a transparent vial conditioned at room temperature and then put into a thermostated water bath. A thermometer with an accuracy of 0.1 °C was used for the measurement. The temperature of the solution was increased at a rate of 1 °C min^{-1}. The gelation temperature was determined by the inversion tube method, recording the temperature at which the tested solution was converted to a non-flowing gel. Figure 13 shows a clear evidence of the gelation at 35 °C that simulate the temperature on the surface of the eye.

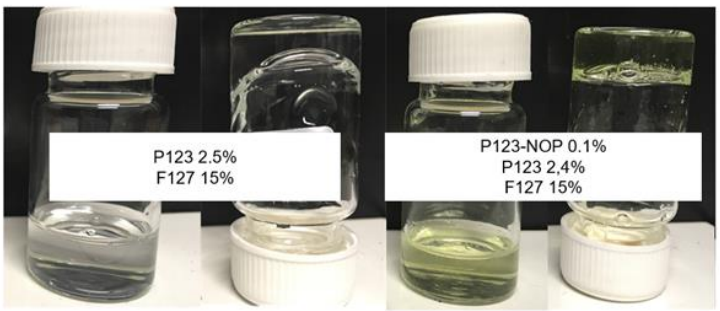

Figure 13: Gelation at 35 °C of solutions (on the left) of commercial Pluronic® F127 15% w/w P123 2.5% w/w and (on the right) of the doped with P123-NOPD.

Two different types of tests were performed to evaluate the rheological characteristic: temperature ramps and frequency sweeps. During the temperature

ramps, the temperature was increased from 20 to 42 °C, at a heating rate of 2 °C min^{-1}, and the material was subjected to a continuous oscillation with a frequency of 1 rad s^{-1} and a strain amplitude of 2%. During the frequency sweeps, the temperature was kept constant (at 24, 26, 28, 32 and 35 °C) and the material was subjected to oscillations with a strain amplitude of 2% and a frequency ranging from 0.1 to 100 rad s^{-1}. For both types of tests the linear viscoelastic properties were measured. The gelation temperature of the solutions was determined rheologically using the method of Chambon and Winter, [59] i.e. the temperature at which the two moduli are linear, and tan δ is the frequency independent over a wide frequency range. This provides the most accurate and reliable method to determine the transition from liquid-like to solid-like behavior. The results are reported in terms of the complex modulus (G*) and the loss factor (tan δ) as a function of temperature and oscillation frequency (ω), respectively. For the sake of clarity, it is worth pointing out that both parameters are easily related to the storage modulus (G''), representing the energy stored elastically from the material for each oscillation cycle, and to the loss modulus (G''), ascribed to the energy dissipated during the same cycle, according to the following equations:

$$G^* = \sqrt{(G')^2 + (G")^2} \qquad \tan\delta = G''/G'$$

where δ is the phase-shift angle between stress and strain.

The evolution of the complex moduli of the saline solution with F127/P123 or F127/P123 at 2.5 % P123-NOPD during a temperature ramp from 20 to 42°C is plotted in Figure 14A. Data demonstrate that the inclusion of P123-NOPD does have a minimal effect upon the evolution of the complex modulus. Both the systems show a 4-order of magnitude increase in the modulus when the temperature is

increased from 20 to 35° C. At room temperature the systems show relatively low complex moduli and relaxation spectra (not shown here) —with G" larger than G' and a strong dependency of the frequency—typical of viscoelastic liquids. The transition from a liquid-like behavior, where the system can flow with the application of relatively low stresses, to a gel state, where the system exhibits a solid-like behavior, takes place in the temperature range from 25 to 35° C. At 35°C the systems show relatively high moduli and relaxation spectra (not shown here) with G' and G" having very similar values over a wide frequency range typical of a stable gel. Frequency sweeps data at 35°C, plotted in Figure 14 in terms of complex modulus and tan δ as a function of the oscillation frequency, shows that the two systems have identical viscoelastic responses over the entire frequency range and that they both behave as stable gel (thus reflecting the presence of tridimensional network of interconnected micelles) with moduli of the order of 1000 Pa.

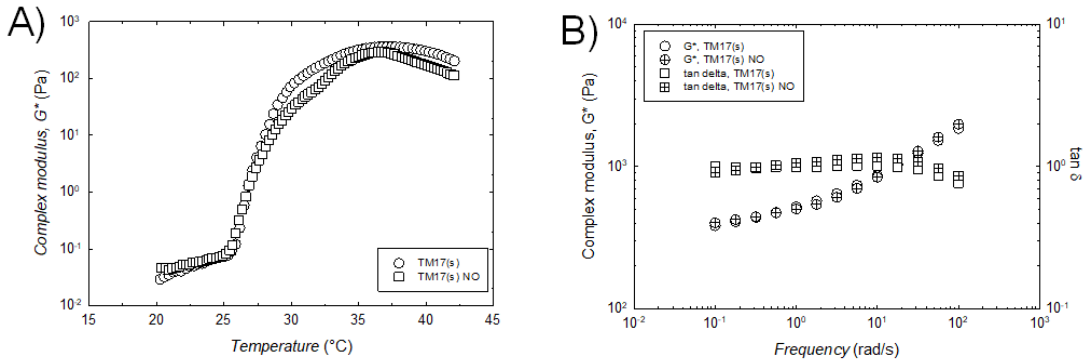

Figure 14: (A) Complex modulus as a function of the temperature for the saline solution with F127/P123 or F127/P123 at 2.5 % P123-NOPD (measurements are taken during a heating ramp, at an oscillatory frequency of 1 rad/s and a strain amplitude of 2%). (B) Complex modulus (G*) and tanδ as a function of the frequency for samples F127/P123 or F127/P123 at 2.5 % P123-NOPD (measurements are taken at 35°C and with a strain amplitude of 2%).

Afterwards, two mixture solutions with P123-NOPD 0.1% w/w, P123 at 2.4% w/w and F127 at 15% w/w and P123-NOPD 0.5% w/w, P123 at 2% w/w and F127 at 15%

w/w (named gel 0.1% and gel 0.5% respectively for sake of clarity) in saline solution was prepared and was evaluated absorbance spectra (Figure 15).

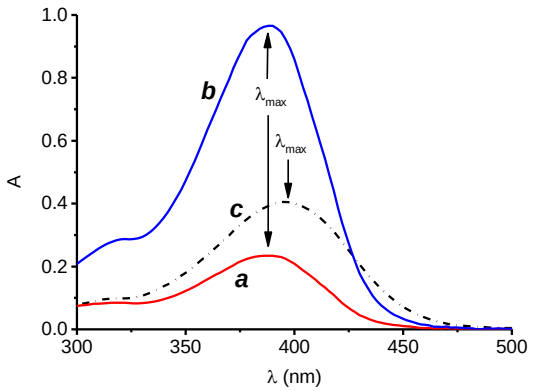

Figure 15: Absorption spectra of solutions with P123-NOPD 0.1% (black) and 0.5% (red) (pathlength 0.1 cm)

The same protocol, previously described, was used to evaluate the capacity of gelling at 35 °C for both solutions. The behavior was unchanged. Moreover, the capability of the mixture to instant gelation, drop by drop, in STF thermostated at 35 °C was tested (Figure 16).

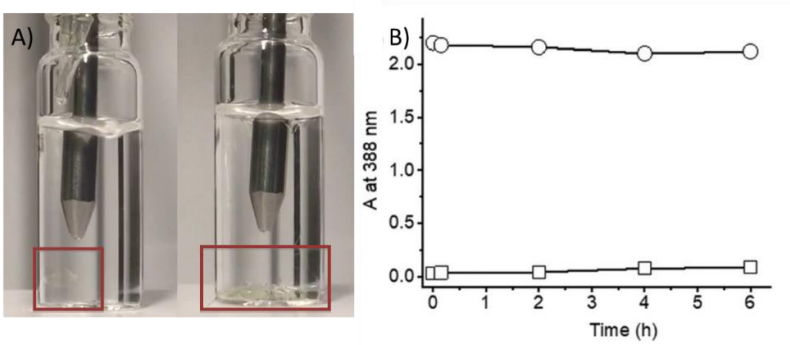

Figure 16: (A) Actual images taken immediately after (left) and 60 s after (right) the addition of the above solution of Pluronic® to STF at 35°C. The probe for temperature measurement is immersed in the solution. (B) The absorbance values, recorded at 388 nm, as a function of the incubation time for the gel placed in the STF; gel phase (○) and the supernatant solution (□). Cell pathlength = 1 cm.

3.3.3 Photochemical characterization

The photosensitivity of the polymer mixture to visible light excitation was at first investigated in solution (0.1% P123-NOPD) and it was demonstrated by illuminating the gel with blue led spotlight (415-420 nm) at 30 mW and following the modification of the absorption spectral bands. As shown in Figure 17, the bleaching of the visible absorption band observed upon light excitation is in agreement with the photochemical pathway leading to NO release. The isosbestic point at 303 nm is a proof of a clean reaction and the increase of the band under 300 nm is coherent with formation of phenol. Interestingly, comparative photolysis experiments, carried out with an optically matched solution of the free NOPD (inset in Figure 17), show that the kinetics of the photobleaching occurs more than one order of magnitude faster in the case of the polymer. This result is in excellent agreement to what recently observed for the same NOPD entrapped in micellar systems [60, 61] and other polymeric scaffolds.[62,63] This can be the results of the active role the polymeric network plays in providing easily abstractable hydrogens close to the phenoxy-radical intermediate involved in the mechanism of the NO photorelease. The inset of Figure 17 shows that the photobleaching occurs more than one order of magnitude faster in the casa of the polymer with the NO photorelease quantum yield Φ_{NO} being $8\times10^{-3}\pm 0.8\times10^{-3}$.

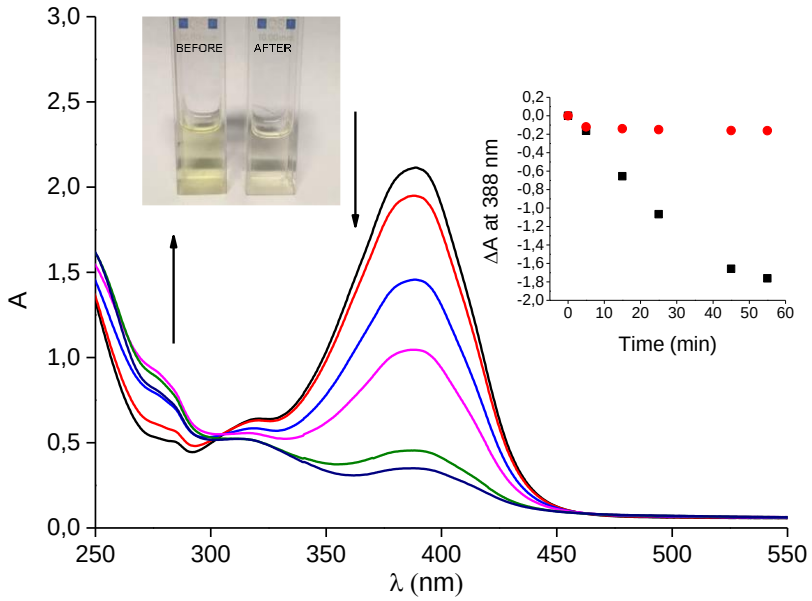

Figure 17: Photobleaching of solution (gel 0.1%) (pathlength 1 cm) observed at different times upon light irradiation with blue led spotlight 415-420 nm (30 mW). The inset shows the absorbance changes monitored at λ_{exc} = 388 nm of the Pluronic® containing solution (■) and for an optically matched solution of the free NOPD in the same solvent (●); representative picture of the Pluronic® solution before and after the photolysis are also shown.

The photorelease of NO was unambiguously demonstrated by its direct amperometric detection using an ultrasensitive NO electrode. The results illustrated in Figure 18 provide evidence that the pre-gel solution is stable in the dark but supplies NO upon illumination. The release process is strictly dependent on the external light inputs, as confirmed by the NO delivery which starts and stops as the light is switched On and Off, respectively.

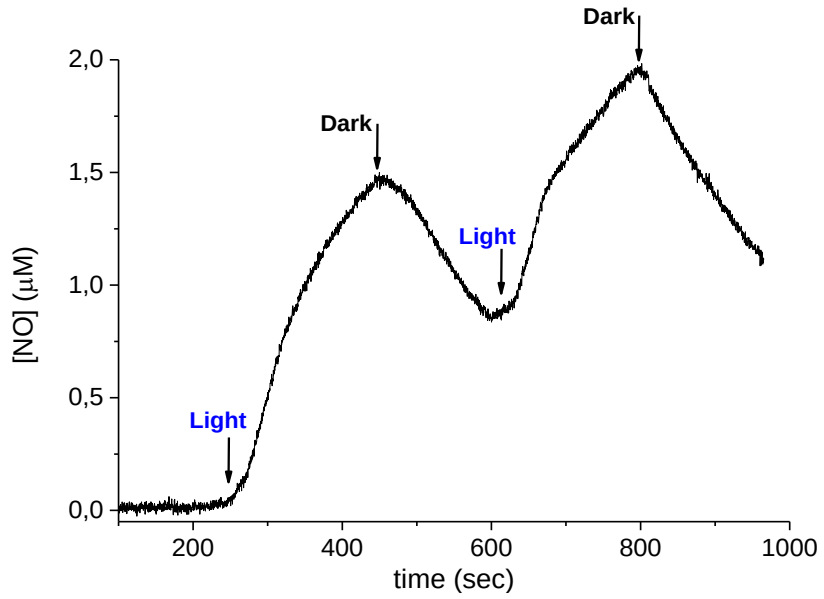

Figure 18: NO release profile observed upon On/Off alternative irradiation cycles with a continuum laser 405 nm at a power of 100 mW from the solution P123-NOPD 0.1% w/w without thermostatation.

The NO photoreleasing properties of the polymeric mixture were well-retained in the gel phase. We used both direct and indirect method to demonstrate the NO release from the gel. In a first experiment, the gel was placed at the bottom of a quartz cuvette and covered with STF at 35 °C. The light source was focused exclusively into the gel phase and the NO electrode was placed in the supernatant. In this way, the electrode is expected to detect the NO directly once it diffused from the gel to the solution phase. The results illustrated in Figure 19 provide clear-cut evidence that the gel is stable in the dark but supplies NO upon illumination with visible light.

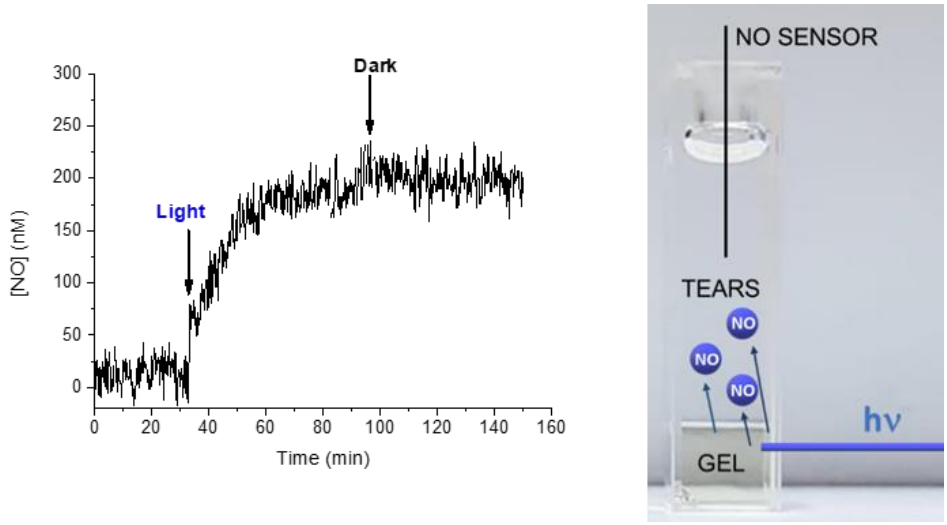

Figure 19: NO release profile observed upon On/Off alternative irradiation cycles with a laser 405 nm at a power of 100 mW on artificial tears solution from the gel P123-NOPD 0.1%, termostated at 35 °C. In the inset the schematic image of the measurement setup.

NO photorelease was further proved by the indirect assay by using the DAN assay, [64] one of the most sensitive and selective fluorescence-based methods for NO detection based on its determination as nitrite. Which is the main oxidation stable product of NO formed under aerobic conditions. Figure 20 shows an excellent linear correlation of the NO photoreleased with the time exposure as well as a dependence of the amount of NO photogenerated by the % of loading of the NO photoprecursor. The inset of Figure 20 shows representative fluorescence emission and excitation spectra of the highly fluorescent formed after the reaction of DAN with nitrite, observed only in the case of the irradiated samples. For the test a xenon wide spectrum lamp was used to simulate the full solar light spectrum. The irradiation was conducted under thermostat condition (35 ± 0.1 °C).

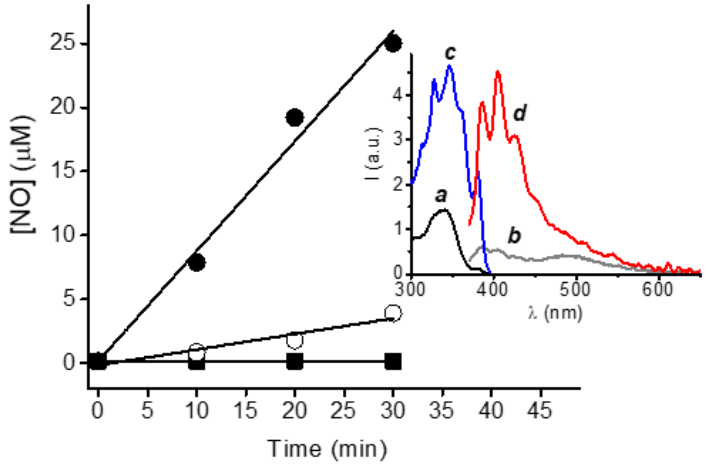

Figure 20: Release of NO from 0.5 % (blue) and 0.1% (red) gel P123-NOPD at different irradiation times with Xenon wide-spectrum lamp. The inset shows representative fluorescence excitation and emission spectra obtained after fluorimetric DAN assay of the gel from the gel P123-NOPD non-irradiated (**a** and **b**) and irradiated with a xenon lamp (**c** and **d**), under air-saturated conditions. The emission wavelength for the excitation spectra was 410 nm, whereas the excitation wavelength for the emission spectra was 360 nm.

Interestingly, NO release from the gel can be also triggered by sunlight and it can be easily followed by the naked eye. The as prepared gel was covered with a black plastic mask and left 60 min outdoor under daylight. Figure 21 shows the discoloration of the pale yellow arising only from the illuminated sites, according to the photobleaching process previously observed in solution and accounting for a remarkable spatial differentiation between the illuminated and non-illuminated areas.

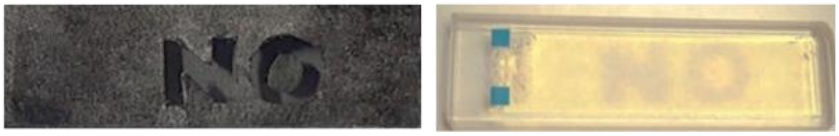

Figure 21: Bleaching of gel that goes from yellow to colorless by light irradiation with blue led spotlight 415-420 nm (30 mW) using a stencil.

3.3.4 Biological Evaluation

Preliminary biological experiments were carried out to assess the potential bactericidal activity of the gel as well as its biocompatibility. In all these experiments, we used the Pluronic® composition containing the highest content of P123-NOPD (2.5%) and for comparison, the same amount of unmodified P123. Antibacterial activity of the gel was tested on the Gram-positive *S. aureus* responsible for higher rate of morbidity due to the high antibiotic resistance pattern towards the traditional antibiotics. The bacterial cultures (ATCC® 6538) were incubated with the gel samples and kept in the dark or irradiated for 15 and 30 min with visible light. The results illustrated in Table 1 show a negligible bactericidal activity of the gel in the dark. On the other hand, a good bacterial growth inhibition was observed in the sample loaded with P123-NOPD under illumination. Almost 100% of inhibition in CFU/mL was achieved for modified P123-NOPD sample, in contrast to the lower antibacterial effects noted upon illumination of the gel containing the unmodified P123. Biocompatibility of the gel was tested by incubation with SIRC rabbit corneal cells followed by a further period of incubation in the dark or of irradiation with visible light up to 30 min. The cell viability observed in all the cases, confirms that the gel can be well tolerated.

Table 1. *S. aureus* growth inhibition and SIRC rabbit corneal cells viability observed in the dark and under irradiation of the gel containing F127/P123 (2.5 % P123-NOPD).

% P123-NOPD	Irradiation time (min)	CFU mL^{-1}	Cell viability[a] (%)
0	0	$1.3x10^5$	99
0	15	$2.3x10^4$	105
0	30	$1.9x10^3$	101
2.5	0	$1.3x10^5$	96
2.5	15	$1.7x10^4$	101
2.5	30	< 50	82

[a]Results are expressed as percentage of viable cells *vs* Ctrl cells.

3.3.5 Conclusions

In conclusion, we have achieved a thermoresponsive and photoactivatable gel addressed to NO delivery. This has been obtained through the covalent integration of a NOPD into the polymeric skeleton of P123 followed by its self-assembling with F127 and subsequent increase of temperature to 35 °C. The photochemical performance of the NOPD is enhanced upon its incorporation in the polymeric scaffold. This is the result of the reduced microenvironment polarity experienced by the NOPD and the key role of the polymer itself as reactant in the photochemical reaction leading to NO photorelease. Rheological tests highlighted that the systems investigated behave as liquids at room, thus allowing easy application to patients, while behave as relatively strong and stable gels at corneal temperatures. The gels show excellent chemical and physical stability when in contact with a simulated tear fluid and does not show any relevant premature leaching of the NOPD unit. NO delivery from the gel is exclusively triggered by visible light and occurs even under daylight conditions. Once photogenerated, the NO radical can promptly diffuse out of the gel matrix to reach biological targets. The present NO-delivering gel platform shows good bactericidal activity against the Gram-positive *S. aureus* and is well tolerate both in dark and light conditions by SIRC rabbit corneal cells. These results may open intriguing possibilities for further studies exploiting the multifaceted role of NO in ocular therapeutic treatment activated by light.

3.4 Multicargo microemulsions with bimodal photobactericidal action and dual colour fluorescence

3.4.1 Design and preparation

The potential use of microemulsions (MEs) as an ocular drug delivery carrier offers several favorable pharmaceutical and biopharmaceutical properties such as their excellent thermodynamic stability, phase transition to liquid-crystal state, very low surface tension, and small droplet size, which may result in improved ocular drug retention, extended duration of action, high ocular absorption, and permeation of loaded drugs. Further, both lipophilic and hydrophilic characteristics are present in microemulsions, so that the loaded drugs can diffuse passively as well get significantly partitioned in the variable lipophilic-hydrophilic corneal barrier. MEs are single-phase, optically isotropic nanocarriers made of oil, water and surfactants with size below 100 nm.[65] They are prepared at a low mixing rate and offer high thermodynamic stability. In recent years MEs have gained increasing attention for delivery in the bio-pharmaceutical field due to their ability to deliver both hydrophilic and lipophilic molecules. For these properties MEs may result in high drug absorption and permeation, and hence, strong possibility of drug delivery to the posterior segment of the eye.

In the context of microbial infections, the alarmingly low turnover of new clinically approved antibiotic drugs [66] and the Multi Drug Resistance (MDR) phenomena emerging for drugs actually used,[67,68,69] call for a shift of attention to other ‘‘unconventional’’ antibacterial treatment modalities. PDT constitutes one of the most promising alternatives in this regard.[70] In recent years, phototherapeutic approaches based on the photostimulated release of NO through suitable NOPDs,[71] called NO-photodynamic therapy (NOPDT), are also receiving growing attention.

Analogously to $^1O_2$, NO does not suffer MDR and confines its action to short distances (<200 µm) from the production site due to its short lifetime, reducing systemic toxicity issues common to many conventional drugs. On these grounds the combination of PSs with NOPs using suitable delivery nanoscaffolds is revealing a very appealing strategy in view of multimodal therapeutic approaches entirely controlled by light stimuli and not based on conventional drugs.[48]

In this work a ME multicargo, able to generate $^1O_2$ and NO and emitting distinct fluorescence signals under visible light stimuli was reported.[72] As shown in Figure 22 the ME co-entraps phthalocyanine (component **1**) as a red emitting PS and molecular hybrid (component **2**) as a green emitting NOPD in the oily phase. The ME has been devised in order to permit the selective excitation of components **1**, **2** or both by using red light, blue light or both excitation sources, resulting in an ensemble of cytotoxic species and fluorescence signals.

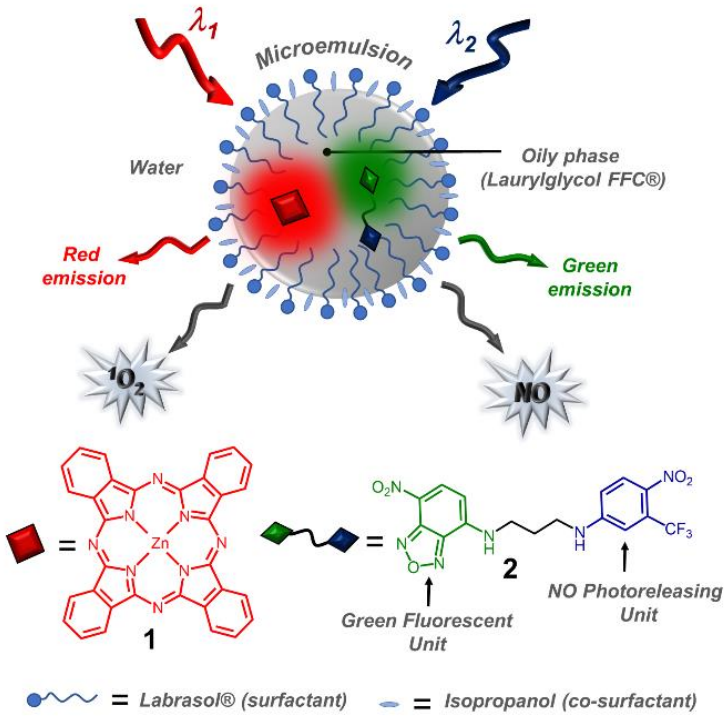

Figure 22: Schematic of the photoactivatable multicargo MEs and their working principle.

The construction of a pseudo-ternary phase diagram allows us to define the best experimental conditions in which the two photoresponsive components should be combined to form a stable microemulsion. A preliminary test was performed to determine the oil solubility of **1** and **2**. Labrasol® and Lauroglycol® FCC have shown the best results in terms of solubility of the guests and were chosen as a surfactant (S) and oily phase (O), respectively. Moreover, isopropanol was used as a co-surfactant (CoS) to achieve the ultra-low interfacial tension necessary for the formation of small microemulsion droplets. The pseudo-ternary phase diagram of S, CoS, O and water (W) was constructed at room temperature to show the relationship between the composition and phase behavior of the samples (Figure 23). The construction of the phase diagram allows selection of the correct ratio of all the components where transparent and stable microemulsions are formed. In all the cases, the areas of stable microemulsion formation extended over a more or less limited area in the S/CoS-rich part of the phase diagram. For other ratio between components, milky emulsion was obtained (Figure 23).

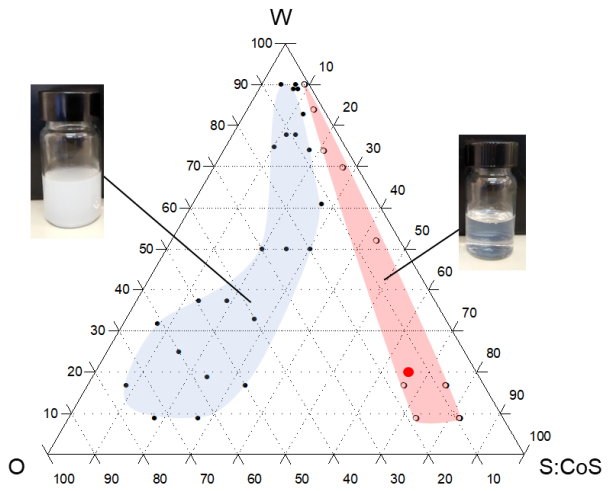

Figure 23: Pseudo-ternary plot for Labrasol®(S), isopropanol (CoS), Lauroglycol® FFC (O) and water (W) at a S:CoS 2:1 ratio by wt. Microemulsion zone (red area), emulsion zone (blue area) and representative actual images. The red dot represents the prototype microemulsion for loading **1** and **2**.

Has been selected one prototype made of Labrasol® (43.3% v/v), isopropanol (21.7% v/v) and Lauroglycol® FCC (20.0% v/v) for further investigations (red dot in Figure 23). The individual lipophilic components **1** and **2** or both were dissolved directly into the oily phase and added to the system to achieve a final concentration of **2** and **1** of 5.8 mg/mL, respectively.

3.4.2 Physico-chemical characterization

Table 2 shows that the MEs present small particle sizes and narrow size distributions, as indicated by the low (≈ 0.2) polydispersity index (PI) obtained and slightly negative Z potential (ξ).

Table 2: Composition, size and Z potential of the optimized MEs (mean SD, n = 3).

Formulation	**μg mL^{-1}(μM)**	**D_H [a] (nm)**	**PI**	**ξ (mV)**
Unloaded	-	72.8 ± 0.7	0.229	-2.8 ± 0.3
1	2 (3.4)	72.6 ± 0.8	0.234	-3.5 ± 1.2
2	6 (14)	73.6 ± 0.2	0.225	-3.8 ± 0.5
1+2	2 (3.4) + 6 (14)	73.2 ± 0.6	0.238	-3.2 ± 0.9

[a] Hydrodynamic diameter determined by Dynamic Light Scattering (DLS).

Representative TEM image of the ME co-loaded with **1** and **2** are reported in Figure 24 and clearly demonstrate the presence of spherical globules with a size in line with the values obtained by DLS.

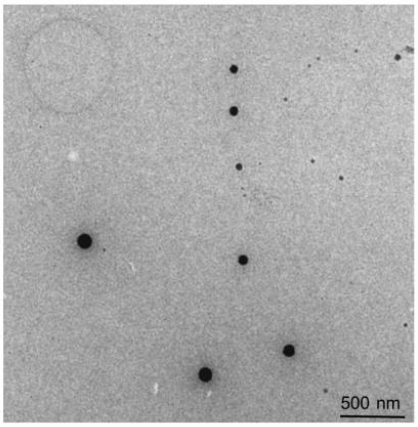

Figure 24: Representative TEM image of the ME co-loaded with **1** and **2**.

After centrifugation and freezing–thawing and heating–cooling cycles, the stability was evaluated by visual inspection and size determination. The centrifugation test allowed the evaluation of the absence of phase separation under the effect of mechanical stress. All microemulsions were found to be stable to centrifugation, as no change in any of their properties was observed (data not shown). All the systems undergoing freezing–thawing and heating–cooling cycles remained stable since neither significant changes in droplet size nor phase separation were observed (data not shown). A long-term stability study was conducted by storing the formulation for more than one year at room temperature. All the MEs remained completely transparent during storage without any significant size changes.

3.4.3 Spectroscopic and photo-delivery characterization

An important issue to address in the fabrication of phototherapeutic systems exploiting the combined effects of $^1O_2$ and NO regards the relative amounts of these cytotoxic species to produce. $^1O_2$ is generated through a photocatalytic process that, in principle, does not consume the PS, whereas photogeneration of NO implies

a neat photochemical reaction with consequent degradation of the NOPD. As a consequence, the regulation of the reservoir of NO with respect to $^1O_2$ is a critical point to consider in order to achieve effective bimodal photodynamic action. This can be accomplished by using a larger amount of the NOPD with respect to the PS and by using a PS and NOPD preferentially absorbing in different spectral regions, in this way is possible to control and modulate the development of active species by choosing the wavelength and modulating the intensity of the light. Moreover, the modular character of the noncovalent approach to nanoassemblies permits to easy regulate the relative concentrations of distinct guests assembled within the very same host, without synthetic procedures. However, this is not sufficient. In fact, for distinct photoresponsive components in close proximity operating in parallel under light inputs, their individual photochemical and photophysical properties need to be preserved. Therefore, inter-chromophoric interactions between the two photoactive guests confined in the same microenvironment need to be intentionally avoided by inspection of their lowest excited states and their redox potentials, in order to rule out undesired photoinduced energy/electron transfer processes that would preclude the final goal.

All the samples were prepared by dissolving compound **1**, **2** or both at first in the S/CoS–oil phase of the ME and remain dissolved upon water addition, because PS **1** and NOPD **2** are not soluble in water. The spectroscopic behavior of the ME loaded with **1**, **2** or both are showed in Figure 25.

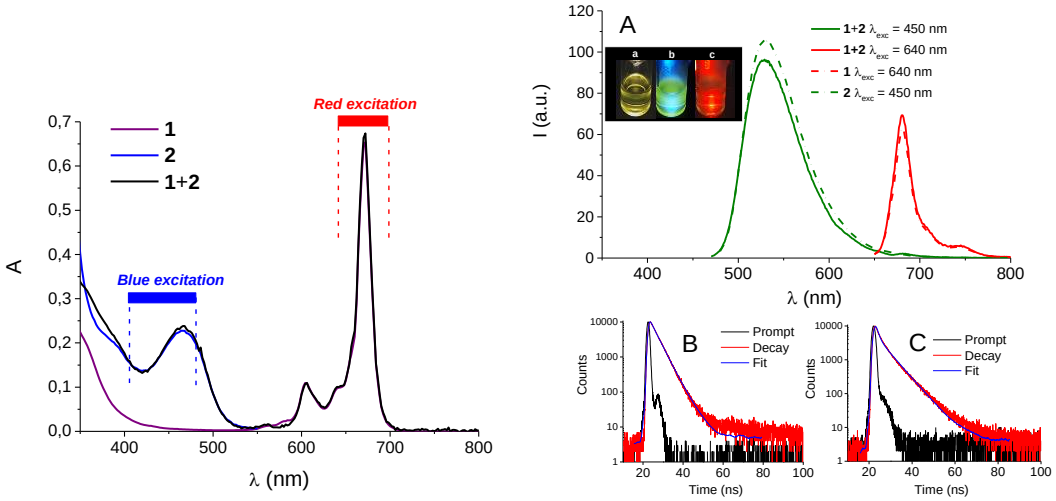

Figure 25: On the left the absorption spectrum of the ME loaded with **1**, **2** or both. [**1**] = 3.4 mM; [**2**] = 14 mM; T = 25 °C. On the right: (A) Fluorescence emission spectra of the ME co-loading **1** + **2** and, for comparison, the single components. The inset shows the actual image of the ME co-loading **1** + **2** observed under ambient light (**a**) and upon excitation at λ_{exc} = 450 nm (**b**) and λ_{exc} = 640 nm (**c**). Fluorescence decay and related fitting of the ME co-loading **1** + **2** and observed at λ_{em} = 680 nm (B) and λ_{em} = 530 nm (C). [**1**] = 3.4 mM; [**2**] = 14 mM; T = 25 °C.

The absorption spectrum of **1** in the visible window is dominated by the intense Q absorption band in the red region with a maximum at ca. 670 nm and shows only negligible absorption in the range 400–600 nm. In contrast, the absorption of compound **2** is characterized by a band at 470 nm related to the fluorescent nitro-aminobenzofurazane moiety and a shoulder at ca. 390 nm corresponding to the absorption of the NO photoreleasing trifluoromethyl nitroaniline appendage. These absorption features are basically similar to those observed for **1** and **2** in organic solvents. They are accounted for the solubilization of the guests in the oily phase mainly in the monomeric form. Interestingly, the spectrum of the ME co-entrapping both components show all the typical features of the isolated chromophores, matching very well the sum of **1** and **2**. Such an ideal spectral condition permits the two guests to be selectively or simultaneously excited by using red light, blue light,

or both excitation sources. On the right of Figure 25A it is shown the fluorescence emission spectra of the ME co-loaded with **1** and **2** and, for comparison, the ME loaded with the individual guests. Interestingly, the two different components show emission similar to that observed in organic solvents and they retain their luminescence behaviour when co-encapsulated in the ME. The selective excitation of **1** and **2** at 450 nm and 640 nm results in their typical red and green fluorescence, respectively, which is almost identical to that observed for the single chromofluorogenic guests encapsulated in the same ME. The fluorescence emission is also visible at naked eye as shown in the inset of Figure 25A. The photophysical independence of the two fluorophores was further confirmed by time-resolved emission. Figure 25 B and C show the fluorescence decays observed for the ME co-entrapping **1** and **2** monitored at 680 nm (maximum of the emission of **1**) and 530 nm (maximum of the emission of **2**). In both cases the kinetic fit was bi-exponential with dominant components of 5.9 ns and 3.3 ns, respectively. Such values remained unaltered in the case of the ME loading the isolated **1** and **2**, in excellent agreement with the steady-state fluorescence results of Figure 25A. Note that the appropriate choice of the chromofluorogenic components makes almost the entire fluorescence spectrum of **2** fall in the hole of absorption of **1** (see Figure 25). This result in a negligible value of the J-overlap integral, avoiding any FRET process and preserving the photophysical properties of the two guests dissolved in the same ME.

The photodynamic behaviour of the ME was investigated with the aid of steady-state and time-resolved techniques. Figure 26A shows the transient absorption spectrum of the degassed ME co-loading **1** and **2** observed at different delay times with respect to the initial laser pulse. The spectrum observed at 1 μs shows a maximum at ca. 470 nm and bleaching in correspondence with the ground-state

absorption of **1**, in agreement with the typical features of the excited triplet state of **1**.[73] The time evolution of the absorption reveals that no new transient species are formed concurrently with the triplet decay, ruling out any possible reaction of this species with the guest **2**.

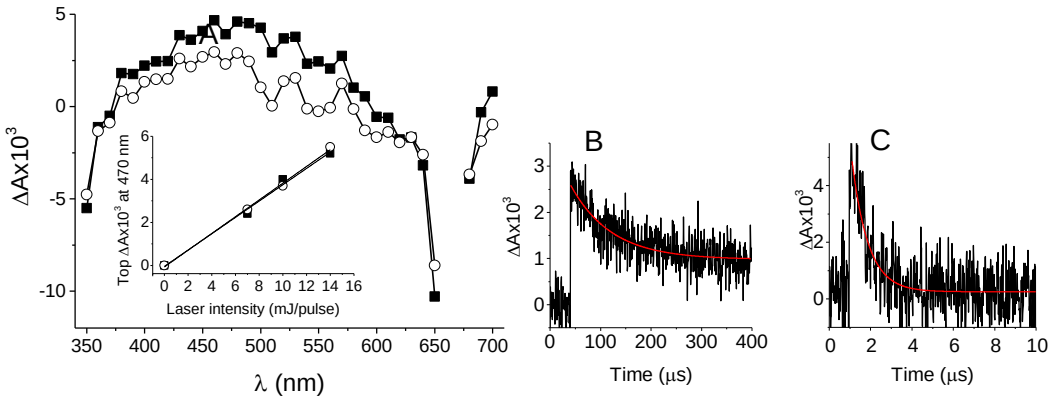

Figure 26: (A) Transient absorption spectra observed 1 μs (■) and 35 μs (○) after 532 nm laser excitation (E_{532} = 12 mJ per pulse) of the N_2-saturated ME co-loading **1** + **2**. The inset shows the top ΔA at 470 nm observed at different laser intensity for the same ME (■) and, for comparison, for an optically matched ME loaded only with (○). Decay trace monitored at 470 nm and the related first-order fitting for the N_2-saturated (B) and air-equilibrated (C) ME co-loading **1** + **2**. [**1**] = 3.4 mM; [**2**] = 14 mM; T = 25 °C.

The excited triplet state decays mono-exponentially with a lifetime τ_T = 82 μs (Figure 26B) and was effectively quenched under aerobic conditions, where τ_T was 0.75 μs (Figure 26C). This spectroscopic and kinetic scenario was very similar to that observed for the ME loaded only with the PS **1**. In particular, the inset of Figure 26A reports the top ΔA of the triplet state measured as a function of the laser intensity in the case of the ME co-loading **1** and **2** and, for comparison, loading **1** alone. The behavior observed is typical of a one-photon process and the slope of each set of data points is proportional to the product $\Phi_T \times \varepsilon_{T-T}$, where Φ_T and ε_{T-T} are the quantum yield of the triplet state and its molar absorption coefficient, respectively. Considering that all the solutions are almost matched in terms of the excitation

wavelength and by assuming the same value of ε_{T-T} for both samples, it can be safely concluded that in both cases very similar values of Φ_T are obtained. Energy transfer from the triplet of **1** to molecular oxygen results in the photogeneration of $^1O_2$.

An additional proof of this phenomenon is the presence of the typical luminescence signal of $^1O_2$ at 1270 nm with a lifetime on the microsecond time-scale. The ME were prepared in deuterated water since under these conditions the $^1O_2$ lifetime is longer and the intensity of the NIR signal is larger than in water. The spectrum shown in Figure 27 provides clear-cut evidence for the photogeneration of $^1O_2$ by the ME upon red light excitation. Furthermore, the lifetime measured for $^1O_2$ under these conditions was ca. 25 μs (see the inset Figure 27), in excellent agreement with that observed for other PSs encapsulated in MEs prepared using D_2O.

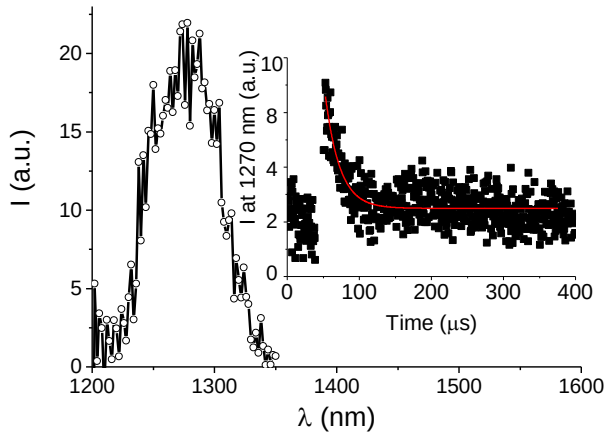

Figure 27: $^1O_2$ luminescence detected upon 670 nm light excitation of the ME co-loading **1** + **2**. The inset shows the $^1O_2$ decay and the related first order fitting observed at 1270 nm. [**1**] = 3.4 mM; [**2**] = 14 mM; T = 25 °C.

The NO photorelease of the ME was investigated by the direct amperometric detection using an ultrasensitive NO electrode. The results, illustrated in Figure

28A, demonstrate that the MEs co-loading **1** and **2** supply NO exclusively upon illumination with blue light whereas they are stable in the dark. As illustrated in Figure 28B, before and after the NO photorelease experiment the most significant spectral changes were observed in the region of absorption of the NO photoreleasing moiety at ca. 390 nm, in agreement with the photochemical pathway leading to the NO release previously proposed in the case of the single NO photodonor unit. Comparative photolysis experiments carried out with an optically matched solution of the ME loaded with **2** alone show that the photobleaching monitored at 390 nm proceeds with the same rate as observed for the multicargo ME (inset Figure 28B). Once again, this result well supports the absence of mutual interactions between **2** and **1** inside the oily components of the ME upon light excitation.

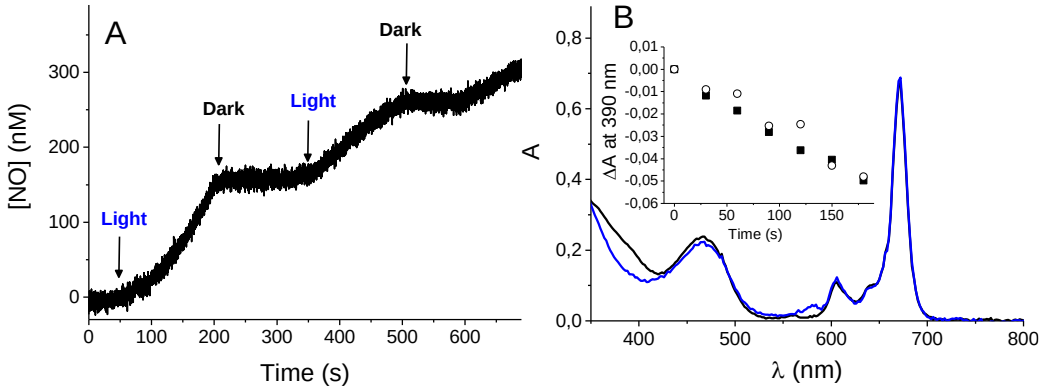

Figure 28: (A) NO release profile observed upon ON/OFF alternate irradiation cycles at 405 nm of the ME co-loading **1** + **2**. (B) Absorption spectra observed before (black line) and after (blue line) the NO photorelease experiment shown in (A). The inset shows the kinetic profiles monitored at λ = 390 nm and observed upon 405 nm light irradiation of the ME co-loading **1** + **2** (■) and, for comparison, **2** alone (○). [**1**] = 3.4 mM; [**2**] = 14 mM; T = 25 °C.

3.4.4 Biological evaluation

The bimodal photodynamic activity of the ME was investigated against *S. aureus* ATCC 6538. In view of the photocatalytic generation of $^1O_2$ by the PS, the red-light source was adjusted so that it was ca. 4-fold less intense than the blue light, which triggers NO generation non-catalytically through photodecomposition of the NOPD. The pure culture was inoculated in 10 mL Muller-Hinton Broth and incubated at 37 °C for 24 h. The overnight broth culture was centrifuged at 3500 rpm for 15 minutes and suspended in PBS. The bacterial suspension was standardized to 1×10^9 CFU/mL by optical density measurements at 570 nm. For the antibacterial assay, 90 mL of appropriately diluted ME (1:1, 1:3, and 1:5 in water) was loaded into a 96-well microplate. Afterwards, 10 mL of the standardized bacterial suspension was inoculated. The microplate was irradiated for 45 min by using a blue LED (λ_{exc} = 415– 420 nm) and a red LED (λ_{exc} = 620–630 nm), having an irradiance on the samples of ca. 19 mW / cm^2 and ca. 4.4 mW / cm^2, respectively. At the end of the irradiation, an aliquot (20 mL) of each sample was diluted in PBS and seeded in duplicate as a spot on a Mueller Hinton Agar plate. The CFU were counted after incubation at 37 °C for 24–48 h. Figure 29 reports the results obtained at 3 different amounts of the ME co-loaded with **1** + **2** and either kept in the dark or irradiated with blue, red and simultaneous blue and red light to activate the photorelease of NO, $^1O_2$ or both species, respectively (unloaded ME gave a log reduction of the initial bacterial burden <1.7). Under blue light, a clear reduction of the cell number (1.85–3.6 log reduction) was achieved with increasing ME amounts. On the other hand, negligible reduction of bacteria was observed upon irradiation with red light, suggesting that under these experimental conditions the amount of $^1O_2$ produced is not enough to kill bacteria. Interestingly, the combination of blue and red light allowed the highest reduction at all ME amounts tested, resulting in marked cell killing. These results indicate that the antibacterial activity of NO is well-

complemented by $^1O_2$ and that their orchestrated photorelease can represent a valuable strategy to achieve considerable bacterial killing.

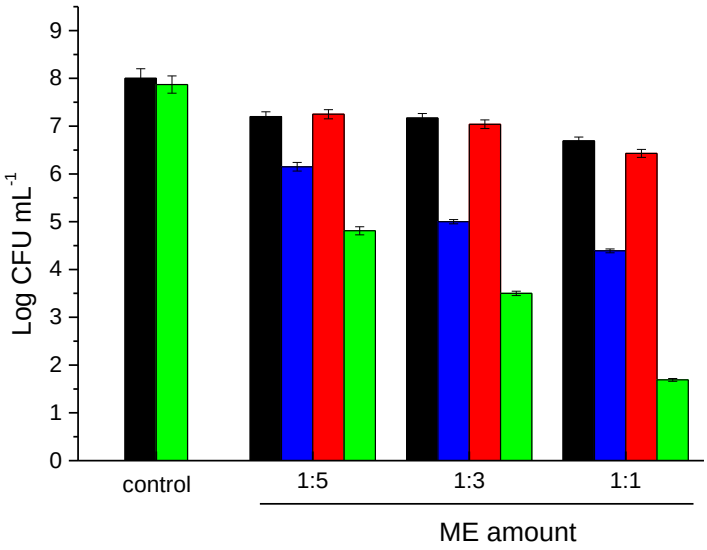

Figure 29: *S. aureus* (1×10^8 CFU mL^{-1}) incubated with the ME loaded with **1** + **2** ([**1**] = 3.4 μM; [**2**] = 14 μM) at different dilutions and either kept in the dark or irradiated with blue light (ca. 50 J cm^{-2}), red light (ca. 11 J cm^{-2}) and both light sources. Untreated bacteria were used as a control.

3.4.5 Conclusions

In conclusion, multicargo photoresponsive MEs co-solubilizing a PS and a NOPD in their oily phase was prepared. These MEs are very stable in the dark, maintaining their physico-chemical properties for more than one year. The photochemical independence of the two guest components in the ME permits them to operate either individually or in tandem by using visible light of an appropriate wavelength. In particular, red light excitation triggers the generation of $^1O_2$ and red emission from the PS, whereas blue light excitation triggers the release of NO and green emission from the NOPD. In view of the key role $^1O_2$ and NO play as ‘‘unconventional’’ therapeutic agents, the present ME represent an intriguing

model system for potential multimodal phototherapeutic applications. In fact, we have demonstrated that amplified bacterial cell killing can be achieved upon simultaneous excitation of the ME with blue and red light. To our knowledge, this represents the first example of therapeutic MEs activatable by visible light showing the convergence of dual modal photodynamic action and dual colour fluorescence emission.

3.5 A high-performing metal-free photoactivatable NOPD with a green fluorescent reporter loaded in thermoresponsive gel

3.5.1 Design and preparation

As discussed in the introduction, the biological effects of NO have been shown to be highly site- and dosage-dependent. For this reason, quantification, and localization of NO released has a central role in the therapeutic approaches involving NO. One way to address this task is to use systems which are based on the principle of the "release with fluorescence reporting". In other words, in this kind of systems, the fluorescence is quenched and restored only after the NO release acting as an optical counter. In this work a novel NOPD developed in the group (Figure 30),[74] was loaded in the thermoresponsive Pluronics® based formulation, whose development was described above.[56] **NBF-NO** is a nitroso-derivative of the 4-amino-7-nitrobenzofurazane (ABF), modified with a short alkyl chain to facilitate its entrapping into hydrophobic carrier system. It belongs to the family of intramolecular charge transfer molecules, with the amino group which act as an electron donor and the nitro group which act as an electron acceptor.[75,76] The choice to use a derivative of ABF was driven by different reasons: the main absorption band with "push-pull" character of these compounds falls in the blue region of the Vis range and is characterized by a considerably high absorption coefficient (larger than 10^4 $M^{-1}cm^{-1}$). Moreover, they exhibit excellent fluorescence in the green region with quantum yield values, Φ_f which strongly depend on the solvent polarity.

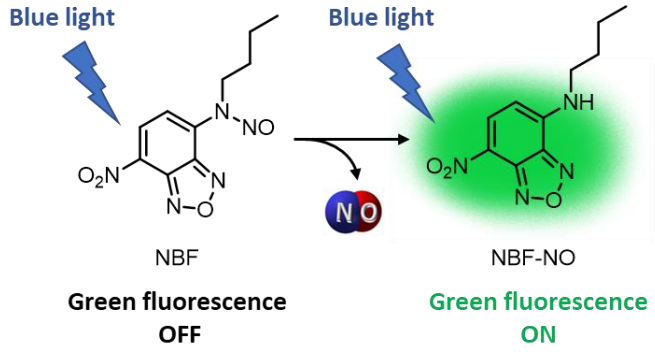

Figure 30: Structures of the **NBF-NO** and of its stable photoproduct **NBF** which is generated after NO release.

The synthesis of **NBF-NO** has been performed following the procedure reported in Scheme 3. All syntheses were carried out under a low intensity level of visible light.

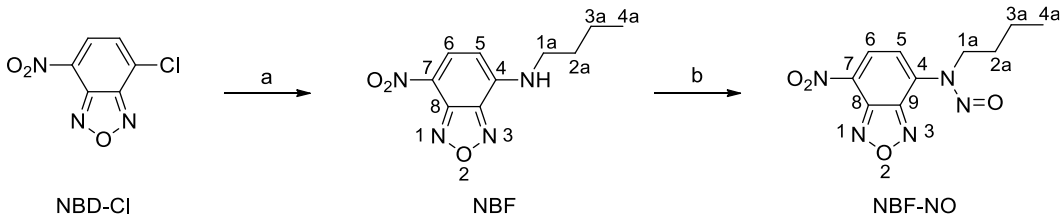

Figure 31: a) Butylamine, CH_3CN dry, N_2, room temperature, 2 hours, 97%; b) $NaNO_2$, CH_3COOH:THF 1:1, room temperature, 12 hours, 50%.

N-butyl-7-nitro[1,2,3]benzoxadiazol-4-amine (NBF). To a solution of NBD-Cl (100 mg, 0.5 mmol) in dry CH_3CN (40 mL) stirred at room temperature under N_2, butylamine (250 µL) was added dropwise. The reaction mixture was stirred at room temperature for 2 hours and then the solvent was removed under reduced pressure. DCM (20 mL) was added to the residue which was washed with water (3 x 15 mL) and brine (3 x 15 mL), dried over Na_2SO_4 and concentrated to dryness. Purification of the residue by flash chromatography, using cyclohexane/ ethyl

acetate 4/1 as eluent, gave NBF as an orange solid (115 mg, 97%). Melting point 91-93 °C. HRMS (ESI): $[M+H]^+$= 237.09778. ^{1}H NMR (200 MHz, $CDCl_3$): δ 8.51 (d, *J* = 8.7 Hz, 1H, ^{6}CH), 6.19 (d, *J* = 8.7 Hz, 1H, ^{5}CH), 3.61 – 3.40 (m, 2H, $^{1a}CH_2$), 1.94 – 1.69 (m, 2H, $^{2a}CH_2$), 1.67 – 1.38 (m, 2H, $^{3a}CH_2$), 1.03 (t, *J* = 7.2 Hz, 3H, $^{4a}CH_3$).

N-butyl-N-(7-nitro[1,2,3]benzoxadiazol-4-yl)nitrous amide (NBF-NO). To a solution of **NBF** (60 mg, 0,25 mmol) in THF:CH_3COOH (1:1 v/v; 10 mL) cooled at 0 °C with an ice bath, sodium nitrite (140 mg, 2 mmol) was added; the reaction mixture was stirred at 0 °C for 1 hour and at room temperature for 12 hours. The solvent was removed under reduced pressure and the residue was purified through flash chromatography, using ethyl acetate/cyclohexane 1/4 as eluent, to give NBF-NO as a yellow solid (34 mg, 50%). Melting point 59- 60 °C. HRMS (ESI): $[M+H]^+$ = 266.08779. ^{1}H NMR (200 MHz, $CDCl_3$): δ 8.64 (d, *J* = 8.3, 0.7 Hz, 1H, ^{6}CH), 7.81 (d, *J* = 8.3, 0.7 Hz, 1H, ^{5}CH), 4.47 – 4.37 (m, 2H, $^{1a}CH_2$), 1.66 – 1.47 (m, 2H, $^{2a}CH_2$), 1.45 – 1.26 (m, 2H, $^{3a}CH_2$), 0.94 (td, *J* = 7.3, 0.7 Hz, 3H, $^{4a}CH_3$). ^{13}C NMR (50 MHz, $CDCl_3$): δ 145.09, 144.47, 137.93, 132.30, 114.51, 44.72, 29.50, 20.71, 14.11.

3.5.2 Spectroscopic and photochemical characterization

Figure 32A reports the absorption spectra in MeOH:H_2O (1:1 v/v) of **NBF-NO** (black) and of the corresponding non nitrosate compound (green), which corresponds exactly with the first and last spectra of photodegradation process, respectively. The absorption spectrum of non nitrosate compound presents a main absorption band at *ca.* 470 nm which is blue-shifted by *ca.* 90 nm in the absorption spectrum of **NBF-NO** due to the introduction of the NO group at the amino functionality. However, the large extinction coefficient and the broad band shape make possible to excite **NBF-NO** in the visible region. The introduction of the NO group on the

amino functionality leads also to a drastic quenching of the intense green fluorescence (see figure 32B): the fluorescence quantum yield value passes from 0.13 for **NBF** to 0.01 for **NBF-NO**, more than 1 order of magnitude of difference.

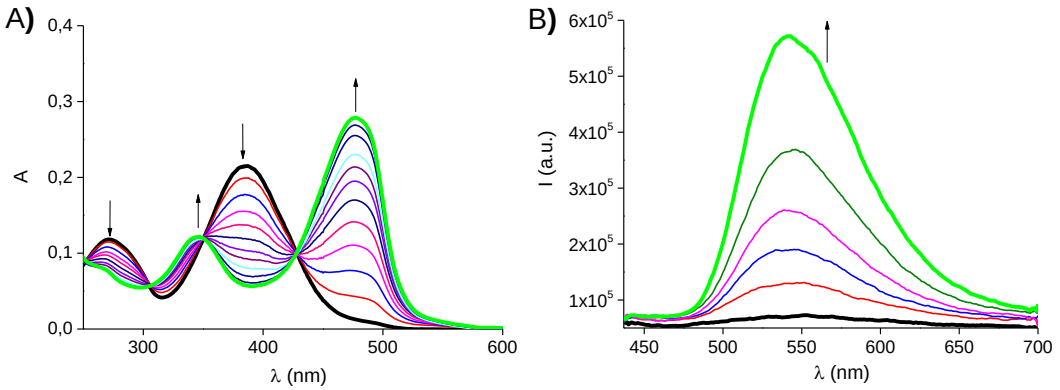

Figure 32. (A) Absorption spectral changes observed upon exposure of a solution of **NBF-NO** (15 μM) at λ_{exc} = 420 nm (ca. 20 mW cm^{-2}) for time intervals from 0 to 75 s. The arrows indicate the course of the spectral profile with the illumination time. (B) Evolution of the fluorescence emission spectra corresponding to the sample of figure A and recorded at λ_{exc} = 427 nm (isosbestic point).

As shown in Figure 32A the photolysis was almost complete in less than 2 min of irradiation accounting for very effective photochemical reaction. The quantum yield for the NO photorelease, Φ_{NO} is 0.15, a value which is ca 1 order of magnitude larger than that reported for other organic NOPD activatable with visible light. This value founds a rational explanation in the mechanism which is at the basis of the NO release; excitation of **NBF-NO** leads to the homolytic cleavage of the N-NO bound and to the formation of an anilinyl radical which is stabilized by the nitro group. The anilinyl radical evolves to the stable photoproduct **NBF** via H-transfer from solvent, a mechanism already seen in the case of the other N-nitrosamine after loss of NO.

In view of a biological application, an important issue to be faced regards the encapsulation of **NBF-NO** within biocompatible polymeric carriers and the

evaluation of the preservation of its photochemical performances also once encapsulated. For this purpose, it was thought to incorporate the compound into the thermoresponsive gel described above (commercial Pluronic® F127 15% w/w P123 2.5% w/w).

The black spectrum of Figure 35A shows the absorption spectrum of a solution of **NBF-NO** encapsulated within Pluronics® gel. This spectrum represents the proof of the occurred encapsulation since **NBF-NO** is poorly soluble in pure water but effectively solubilizes in the presence of Pluronic® gel as confirmed by the appearance of its typical absorption spectrum with maximum at 385 nm.

Irradiation with blue light of this thermoresponsive preparation leads to the same spectral changes observed in the absence of Pluronics®, according to the formation of **NBF** as stable photoproduct. However, the photoreaction was completed in less than 15 seconds (against the 75 seconds needed for the reaction in MeOH:H_2O 1:1). The quantum yield Φ_{NO} in this case is 0.80, a remarkably high value even if compared with other organic NOPDs encapsulated in carrier systems. This enhanced photoreactivity can be explained considering the active role that the polymeric network plays in providing easily abstractable hydrogens close to the anilinyl radical.

Figure 33B shows the dramatic revival of the green emission, demonstrating that the fluorescence activation upon light irradiation typical of the **NBF** fluorophore is well preserved also when compound is loaded in the thermoresponsive solution.

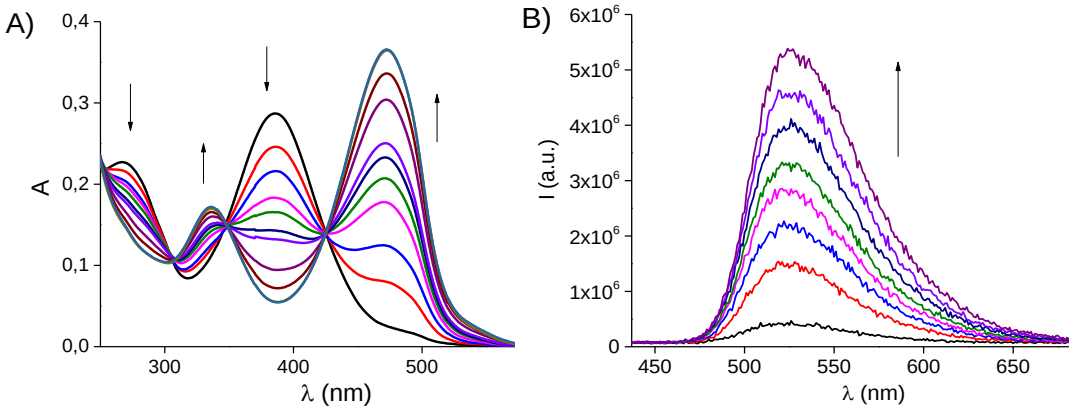

Figure 33: (A) Absorption spectral changes observed upon exposure of a solution of **NBF-NO** (15 µM) encapsulated in Pluronics® thermoresponsive gel at λ_{exc}=420 nm (ca. 20 mW cm^{-2}), for time intervals from 0 to 15 s. (B) Evolution of the fluorescence emission spectra corresponding to the sample of Figure A and recorded at λ_{exc} = 427 nm (isosbestic point).

The loading of the guest within the polymeric mixture had no effect on the gelation temperature (Figure 34A). Then a black mask was used (Figure 34C) to cover the gel and the sample was left 5 min outdoor under daylight. Interestingly, we observed that NO release from the gel is also effectively triggered by sunlight and can be easily followed by naked eye (Figure 34B). This latter figure shows the restoring of the typical green fluorescence of the reporter exclusively in the illuminated sites clearly visible at naked eye, accounting for a remarkable spatial differentiation between the illuminated and non-illuminated areas. This finding shows clearly that NO can be delivered to a specific location by either the covering of the surrounding areas or by appropriate focusing of the employed light source.

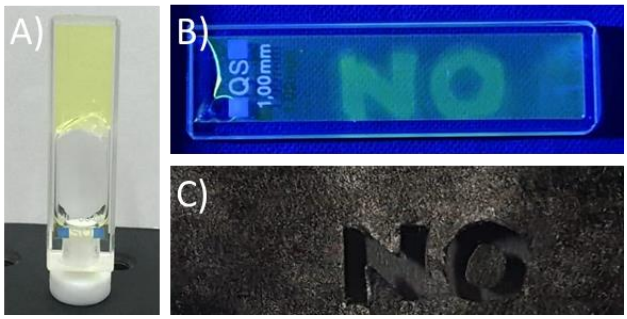

Figure 34: (A) Actual images of the aqueous solution containing F127 (15%) and P123 (2.5%) loaded with **NBF-NO**. after the gelation. (B) Actual fluorescence image (λ_{exc}=420 nm) of the gel after selective exposition to sunlight for 5 min and removing the mask. (C) Black mask placed on top of the **NBF-NO** loaded gel.

NO release was once again demonstrated by the direct detection of this radical through amperometric technique; the amperogram clearly shows that the release of NO is exclusively regulated by light since it stops in the dark and restart once the illumination is turned on again. A similar thermoresponsive solution of **NBF** was used as control; any detectable signal was observed in this case proving that the signal observed can be safely attributable to the NO released from **NBF-NO** and cannot be ascribed to other effects like the intense fluorescence restored.

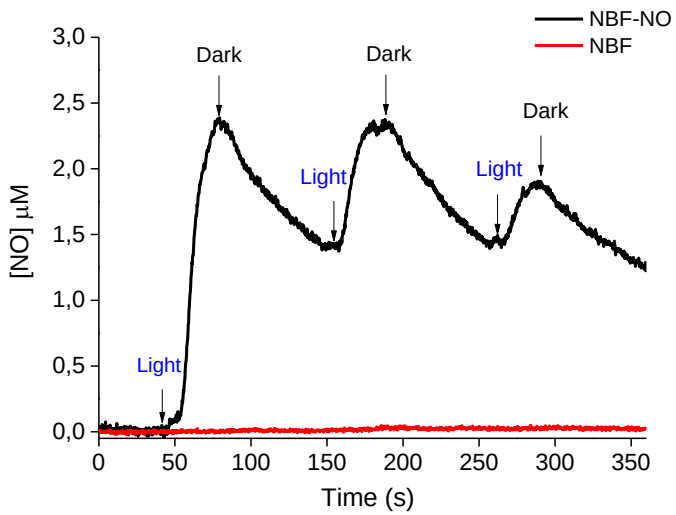

Figure 35: NO release profiles observed for thermoresponsive gel loaded with **NBF-NO** (15 µM) and of **NBF** (15 µM).

3.5.3 Biological Evaluation

It is well known that NO reduces IOP in glaucoma and ocular hypertensive patients for its capability to modulate the conventional aqueous humor outflow system, directly improving outflow through the trabecular meshwork, Schlemm's canal and distal scleral vessels. For this reason, the formulation was tested in its capability in IOP reduction. Albino rabbits of the "New Zeland" species were used for this test. All animals were treated according to the guidelines of the Animal Care and Use Committee of the Association for Research in Vision and Ophthalmology (ARVO). The IOP was measured before (baseline) and after (30, 60, 90, 120 and 180 minutes) the administration of the ophthalmic formulation (30 µl/eye) based on **NBF-NO** (20 mM). Intraocular pressure was measured using the Tono-Pen XL® (Bio-Rad) tonometer. The animals were exposed under blue led light (λ_{exc}=420 nm) for all the duration of the experiment. As shown in Figure 36, a good reduction in IOP is visible in the first 30 minutes after administration. The reduction of effectiveness at prolonged times is linked to the loss of active principle from the site of administration.

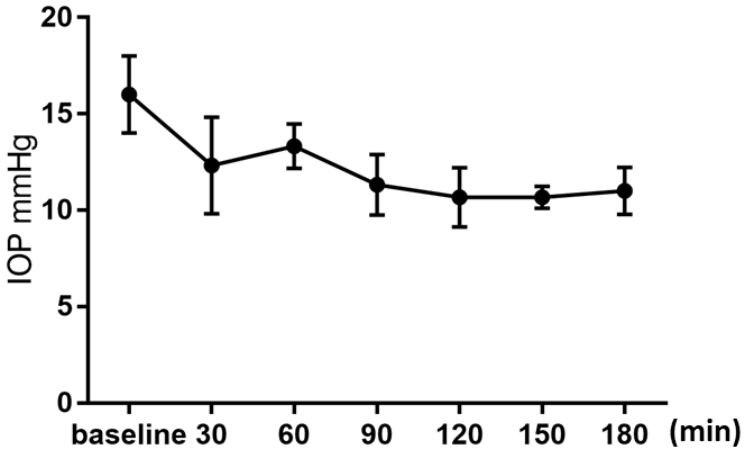

Figure 36: IOP values after topical ocular administration of **NBF-NO**; n = 4.

3.5.4 Conclusions

In conclusion, the developed **NBF-NO** can be effectively encapsulated in biocompatible thermoresponsive solution Pluronic® based, where it preserves the nature of the photo-process but increases further its photochemical efficiency. The gel results stable in the dark and maintains its capability to release NO with a good spatiotemporal control even under activation by daylight. The release process can be followed at naked eye thanks to the intense green fluorescence of the reporter. These features make the gel suitable for ophthalmic applications and shows a good reduction in IOP, linked to the NO release.

3.6 Visible light-activatable cyclodextrin based systems for the efficient delivery of nitric oxide and their inclusion complexes with betaxolol

Cyclodextrins (CDs) are cyclic oligosaccharides consisting of 6, 7 or 8 glucopyranose units (α-, β- or γ-CD, respectively), well-known for their capability to complex, stabilize and solubilize guest compounds.[77,78,79,80,81] The modification of the CDs ring through functionalization of the primary and/or secondary hydroxyl groups with suitable appendages, allows to obtain multifunctional nanocarriers with intriguing properties while maintaining the macrocycle capacity for guests encapsulation.[82,83] Furthermore, it is possible to produce cyclodextrin-based polymeric systems while preserving their peculiar capabilities both in terms of inclusion capacity and phototherapeutic properties.[62] The aim of this work was to develop cyclodextrin-based system modified with photo-responsive units. Two different photoresponsive units were chosen to modify the βCDs scaffolds: a nitrobenzene derivative and a *N*-nitroso amino-nitro-benzofurazan derivative. These compounds are of great interest in bio-pharmaceutics field due to its photo-behaviour, as recently proven by a variety of photoresponsive CD-based molecular constructs with potential phototherapeutic applications.[84,85]

As model compound to investigate the host-guest complexation properties was chosen betaxolol (**BTX**), a well-known β-blocker drug used against glaucoma for the reduction of intraocular pressure.[86,87] In view of the already proven effects of NO on eye, [88,89,90] such a host-guest system might have a potential interest as eye drop formulations for combined ocular therapy stimulated by environmental light.

3.6.1 β-Cyclodextrin-conjugates for the efficient delivery of nitric oxide with fluorescent reporter

3.6.1.1 Design and Synthesis

The first compounds are two β-cyclodextrin (βCD) monomer, **βCD-NBFNO1** and **βCD-NBFNO2**, covalently integrating an *N*-nitroso amino-nitro-benzofurazan in the primary and secondary hydroxyl rims of the βCD scaffold, respectively through flexible spacers of different length. [91]

This work was inspired by our recently developed NOPD, **NBF-NO** [74] (see Figure 37) and based on the same N-nitroso amino-nitro-benzofurazan moiety. This compound is poorly fluorescent but concomitantly to NO, releases the highly fluorescent non-nitrosated derivative is formed as the sole stable photoproduct, representing an optical reporter useful for the NO detection even at the naked eye. Despite the excellent photochemical performances, **NBF-NO** has poor solubility in an aqueous medium, which limits its potential bio-applications in the absence of any carrier system. On the contrary, both βCD conjugates shows an excellent water-solubility and the capability to release NO under the input of either blue or green light. Moreover, these compounds exhibit an excellent contrast between the fluorescence green emission of the chromogenic moiety before and after the NO release. This characteristic permits the easy and real-time quantification of the amount of NO generated, in a spectral region which does not interfere with cell autofluorescence. Although the presence of the appendages, these βCD derivatives are also able to complex betaxolol (**BTX**), a β-blocker drug [86,87] widely used for the reduction of the intraocular pressure.[88,89,90]

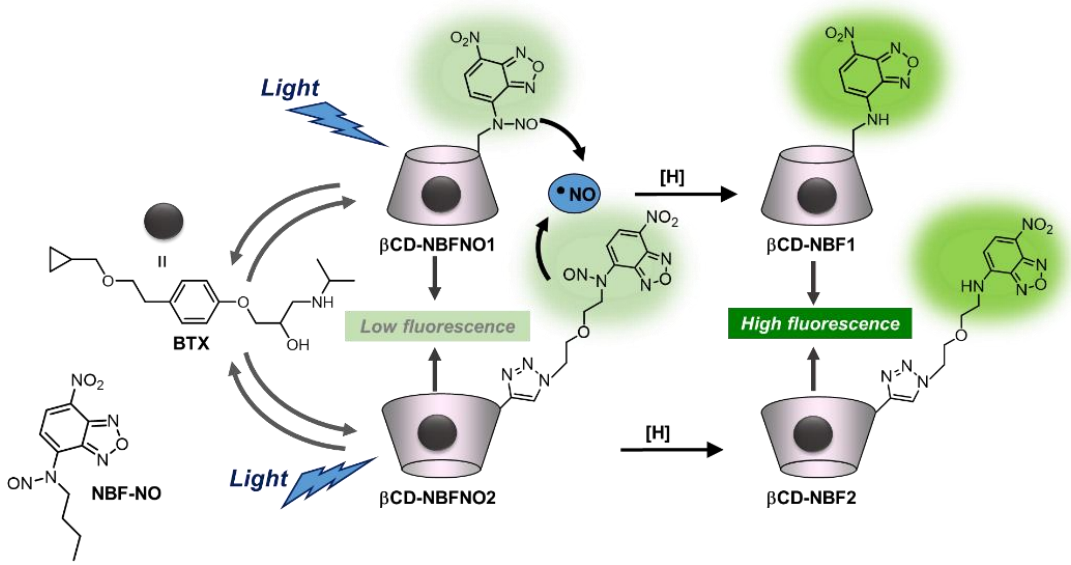

Figure 37: Structures of **βCD-NBFNO1**, **βCD-NBFNO2**, their respective fluorescent photoproducts **βCD-NBF1**, **βCD-NBF2** formed after NO photorelease, **BTX** used as guest molecule and the NOPD **NBF-NO**, which inspired this work.

βCD-NBFNO1. In Figure 38, the synthesis scheme for **βCD-NBFNO1** is shown. 6-Monodeoxy-6-monoamino free base **(2)** was obtained by precipitation of the corresponding hydrochloride salt with concentrated ammonia. 6-Monodeoxy-6-monoamino-βCD hydrochloride (11.70 g, 10 mmol) was solubilized in water (50 mL) and the solution was added to ammonia 25% solution (80 mL) under vigorous stirring. The white precipitate was filtered on a sintered glass filter (porosity 3), the solid was washed with methanol (2 x 15 mL) and placed into a vacuum drying box overnight in the presence of P_2O_5 and KOH (10 g, 88% yield). m.p.: 203-205 °C (dec.). R_f: 0.26-0.29 in 1,4-dioxane:25% aqueous NH_3:1-propanol = 10:7:3. ^{1}H-NMR (D_2O): δ(ppm) 5.10-5.05 (m, 7H, H1, H1'), 4.10-4.05 (m, 1H, H3'), 3.99-3.75 (bs, 25H, H3, H5, H6), 3.67-3.47 (bs, 15H, H2, H4, H6'), 3.26-3.20 (m, 1H, H6'). ^{13}C-NMR (125 MHz, D_2O): δ(ppm) 101.94 (C1), 101.38 (C1'), 83.02 (C4'), 81.36 (C4), 81.30 (C4), 81.27

(C4), 81.24 (C4), 73.23 (C3), 73.00, 72.59, 72.17, 71.94, 68.00 (C3'), 60.45 (C6), 40.36 (C6').

The nitrobenzofurazanyl group was installed onto the CD scaffold without using any additional base in order to avoid the formation of NBF-related by-products. It is worth noticing that 4-chloro-7-nitrobenzofurazan would react with any additional base in the mixture thus creating new chromophoric species and complicating the purification process. 4-chloro-7-nitrobenzofurazan (NBF-Cl) (0.2 g, 1 mmol) dissolved in acetonitrile (5 mL) was added to an aqueous solution (50 mL) of **(2)** (1.13 g, 1 mmol) and the reaction mixture was heated at 50 °C for 2 h. The solvents were completely evaporated under reduced pressure (T = 60 °C), the crude was dissolved in water (20 mL) and extracted with dichloromethane (2 x 20 mL). The aqueous phase was suspended with silica gel (5 g) and the mixture was evaporated under reduced pressure until dryness. This crude mixture thus preabsorbed onto silica was purified by chromatography over silica with CH_3OH:H_2O:HCOOH (0.05%) = 9:1:0.5 as eluent in isocratic elution. The viscous solution was neutralized (NaOH 0.1 N) and precipitated with MeOH (50 mL). The obtained solid was filtered on a sintered glass filter (porosity 3), washed with methanol (2 x 15 mL) and placed into a vacuum drying box overnight in the presence of P_2O_5 and KOH (dark brown solid, 0.45 g, 35% yield). Rf: 0.35-0.77, 0.83-0.85 (NBF-Cl) in CH_3OH:H_2O:HCl (1N) = 9:1:0.5. ^{1}H-NMR (D_2O): δ(ppm) 8.53 (m, 1H, H8'), 6.62 (bs, 1H, H7'), 5.11-4.94 (m, 7H, H1), 3.35-4.26 (bs, 42H, H2, H3, H4, H5, H6).

βCD-NBFNO1 was obtained by reacting **βCD-NBF1**, solubilized in a mixture of DMSO/CH_3COOH 1:1 (2 mL). After complete solubilization, the solution was cooled at 0 °C with an ice bath and $NaNO_2$ (100 mg, 1,45 mmol) was added; the solution was stirred at 0 °C for 1 hour and at room temperature for 2 days. The reaction mixture was precipitated with acetone (40 mL). The solid was filtered-off on a glass filter (porosity 3), extensively washed with acetone (2 x 10 mL) and dried until

constant weight in a vacuum drying box (51 mg; 98% yield). A dark yellow powder was obtained.

Rf = 0.70 (9:1 = MeOH:H_2O);^{1}H-NMR (500 MHz DMSO-d_6): δ(ppm) 9.8 (d, 1H, H8'), 7.83 (d, 1H, H7'), 5.11-4.8 (m, 7H, H1), 2.9-3.95 (bs, 42H, H2, H3, H4, H5, H6).

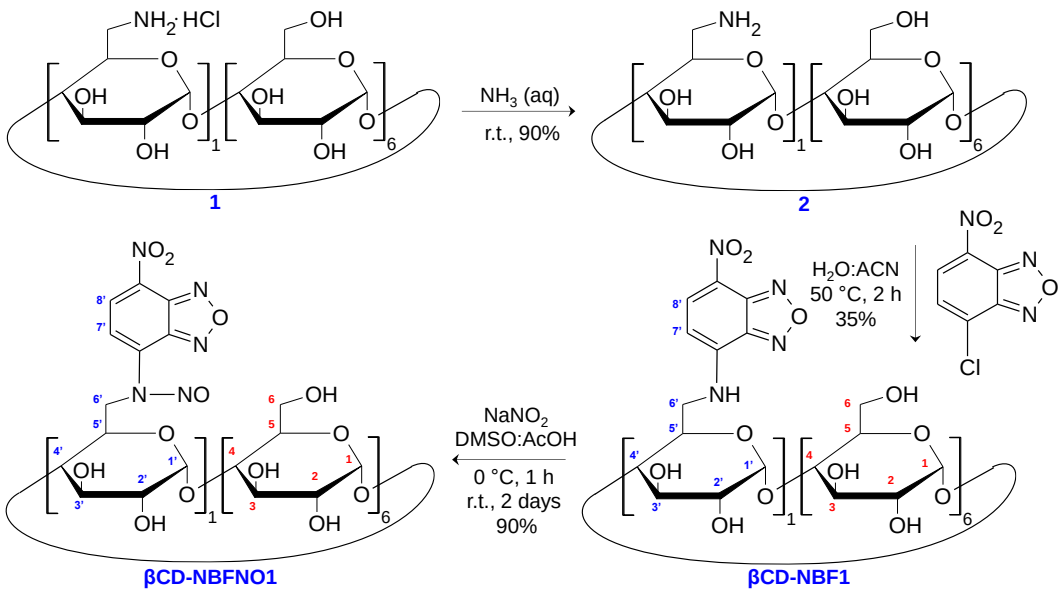

Figure 38: Synthesis scheme for **βCD-NBFNO1**.

βCD-NBFNO2. In Figure 39, the synthesis scheme for **βCD-NBFNO2** is shown. In the first step the regioselective 2-*O*-monopropargylation of βCD **(3)** was achieved in DMSO with LiH and propargyl-bromide.[92] Lithium hydride (53 mg, 6.608 mmol) was added to βCD solution 1 (5 g, 4.405 mmol) in dry DMSO (75 mL). The resulting suspension was stirred under N_2 at room temperature until it became clear (12-24 h). Propargyl bromide (solution in toluene, 80 % w/w, 491 µL, 4.405 mmol) and a catalytic amount of lithium iodide (5 mg) were then added and the mixture was stirred at 50 °C in the absence of light for 5 h. TLC (10:5:2 = CH_3CN:H_2O:25% aqueous NH_3) showed four spots with Rf values of 0.75, 0.65, 0.50, and 0.30, the last two

corresponding to monopropargylated and nonpropargylated βCD, respectively. The solution was poured into acetone (800 mL), the precipitate was filtered on a sintered glass filter (porosity 4) and washed thoroughly with acetone. The resulting solid was transferred into a round-bottom flask and dissolved in a minimum volume of water. Silica gel (10 g) was added and the solvent was removed under vacuum until powdered residue was obtained. This crude mixture was applied on top of a column of silica (25 x 6 cm), and chromatography (10:5:2 CH_3CN:H_2O:25% aqueous NH_3) yielded, after freeze-drying, 2-O-monopropargyl-βCD **(4)** (1.912 g, 1.63 mmol, 37%) as white solid. The material decomposes at 239-245 °C; [α]25D +126 (c 0.25, H_2O); Rf = 0.50 (10:5:2 = CH_3CN:H_2O:25% aqueous NH_3); IR (KBr): 3397, 2923, 2117, 1646, 1156, 1081, 1029 cm^{-1}; ^1H NMR (500 MHz, DMSO-d_6) δ(ppm) 5.98 (br d, 1H, OH), 5.88 (br s, 1H, OH), 5.79-5.69 (m, 10H, OH), 4.98 (d, 1H, 3J = 3.6 Hz, H1'), 4.84-4.82 (br s, 6H, H1), 4.54 (t, 1H, J = 5.6 Hz, OH), 4.50-4.45 (m, 8H, OH, CHC≡), 4.38 (dd, 1H, 2J = 15.8 Hz, 4J = 2.4 Hz, CHC≡), 3.78 (t, 1H, 3J = 9.8 Hz, H3'), 3.64-3.53 (m, 27H; H3, H5, H6a, H6b), 3.51 (t, 1H, 4J = 2.4 Hz, ≡CH), 3.43-3.40 (m, 2H, H2',H4'), 3.36-3.29 ppm (m, 12H, H2, H4); ^{13}C NMR (125 MHz, DMSO-d_6) δ 102.0-101.7 (C1), 100.1 (C1'), 82.2-81.4 (C4), 79.9 (C≡), 79.1 (C-2'), 77.8 (≡CH), 73.3-71.7 (C2, C3, C), 72.6 (C3'), 60.1-59.7 (C6), 58.8 ppm (CH_2C≡); MALDI-TOF: $[M+Na]^+$ calcd for $C_{45}H_{72}O_{35}Na$, 1195.4; found: 1195.58.

The conjugation of 2-*O*-monopropargyl-βCD **(4)** and azido-diethylene glycol-nitrobenzofuraran linker **(5)** was based on a copper-assisted azide–alkyne cycloaddition. The click reaction was performed in DMF mixture at 60 °C with copper(I) bromide as catalyst. Compound **5** (0.1 g, 0.35 mmol) was solubilized in DMF (5 mL) and added to a DMF solution (20 mL) of 2-O-monopropargyl-βCD (0.36 g, 0.31 mmol). CuBr (12 mg, 0.083 mmol) was added to the solution under vigorous stirring and the reaction mixture was heated at 60 °C for 2 h. The progress of the reaction was monitored by TLC (ACN:H_2O:25% aqueous NH_3 = 10:2.5:1). The crude

reaction was filtered on a celite pad to remove copper-related material and the pad was extensively washed with DMF (3 x 10 mL). The filtrate was suspended with silica gel (5 g) and the solvent was removed under vacuum until a powdered residue was obtained. This crude mixture thus preabsorbed onto silica was purified by chromatography over silica with ACN:H_2O:25% aqueous NH_3 = 10:2.5:1 as eluent in isocratic elution. The brown solid was placed into a vacuum drying box overnight in the presence of P_2O_5 and KOH (0.37 g, 82% yield). Rf = 0.70 (ACN:H_2O:25% aqueous NH_3 = 10:2.5:1); ^{1}H NMR (500 MHz, DMSO-d_6) δ(ppm) 8.29 (d, 1H, H14'), 7.89 (s, 1H, H8'), 6.09 (br s, 1H, H13'), 4.94-4.69 (m, 7H, H1), 4.61 (overlapping with HDO signal, br s, 2H, H7'), 4.46 (m, 2H, H9'), 3.92-3.20 (m, 48H, H2, H3, H4, H5, H6, H10', H11', H12'); ^{13}C NMR (125 MHz, DMSO-d_6) assignment based on DEPT-edited HSQC spectrum δ 138.64 (C14'), 126.16 (C8'), 102.55-101.08 (C1), 81.79-80.27 (C4, C2), 74.09 (C5), 72.58 (C2), 72.57 (C10'), 72.18 (C3), 69.54 (C12'), 68.73 (C11'), 65.11 (C7'), 60.66 (C6), 51.22 (C9'). **βCD-NBFNO2** was obtained by reacting **βCD-NBF2**, solubilized in a mixture of DMSO/CH_3COOH 1:1 with $NaNO_2$. **βCD-NBF2** (56 mg, 0.04 mmol) was solubilized in a solution of DMSO/CH_3COOH 1:1 (2 mL). After complete solubilization, the solution was cooled at 0 °C with an ice bath and $NaNO_2$ (100 mg, 1,45 mmol) was added. The solution was stirred at 0 °C for 1 hour and at room temperature for 2 days. The reaction mixture was precipitated with acetone (40 mL). The solid was filtered-off on a glass filter (porosity 3), extensively washed with acetone (2 x 10 mL) and dried until constant weight in a vacuum drying box (51 mg; 98% yield) and a dark yellow powder was obtained. Rf = 0.75 (9:1 = MeOH:H_2O); ^{1}H NMR (500 MHz, DMSO-d_6) δ (ppm) 8.8 (d, 1H, H14'), 8.03 (br s, 1H, H13'), 7.71 (s, 1H, H8'), 4.97-4.45 (m, 7H, H1), 4.51 (br s, 2H, H7'), 4.4 (m, 2H, H9'), 4.2-2.80 (m, 48H, H2, H3, H4, H5, H6, H10', H11', H12');

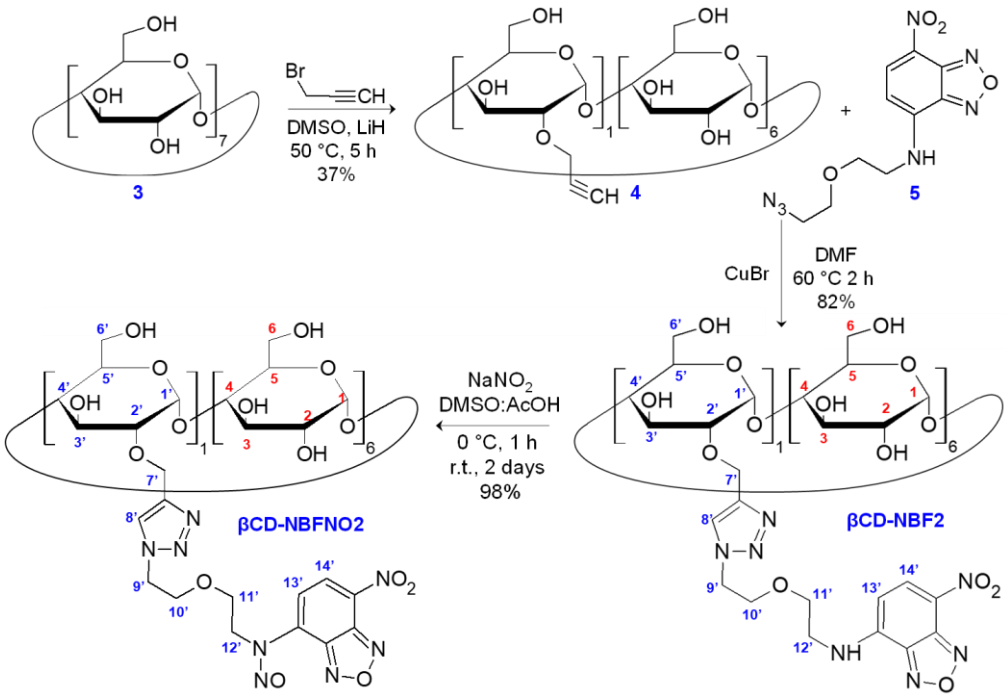

Figure 39: Synthesis scheme for **βCD-NBFNO2**.

The synthetic strategy for compound **5** is shown in Figure 40. The preparation of the linker was divided in two parts. First 2-(2-azidoethoxy)ethan-1-amine **(L4)** was synthesized by modifications of existing synthetic procedures.[93,94] Compound **5** was prepared globally in 4 synthetic steps starting from the commercially available diethylene glycol **(L1)**. Diethylene glycol **(L1)** (50.0 g, 0.47 mol) was dissolved in CH_2Cl_2 (480 mL) and TsCl (180.0 g, 0.942 mol) was added. The solution was cooled to 0 °C and crushed KOH (211.0 g, 3.77 mol) was slowly added. The suspension was additionally stirred at 0 °C for 3 h. The reaction mixture was monitored by TLC using hexane:EtOAc = 1:1 as eluent and detection was achieved with potassium permanganate solution. The mixture was warmed to room temperature and $CHCl_3$ (400 mL) was added. The mixture was extracted with water (3 x 400 mL) and the organic phase was collected.

Compound **L2** was converted to the corresponding diazido diethylene glycol **(L3)** in DMF with excess of sodium azide. Isolation of the compound **L3** was based on liquid-liquid extraction. Diethylene glycol ditosylate **(L2)** (169.6 g, 0.41 mol) was dissolved in DMF (800 mL) and NaN_3 (106.7 g, 1.64 mol) was added. The suspension was stirred at 80 °C for 8 h. The reaction mixture was monitored by TLC using hexane:EtOAc = 1:1 mixture as eluent and detection was achieved with potassium permanganate solution. The suspension was cooled to room temperature and water (750 mL) was added. The solution was extracted with Et_2O (1600 mL). The organic phase was then concentrated to a volume of approximately 800 mL on a rotary evaporator at room temperature. To the solution was added HCl 1 M (800 mL), and the biphasic mixture was stirred vigorously. Partially reduction of diazido diethylene glycol based on Staudinger reaction and *ad hoc* developed work-up afforded the 2-(2-azidoethoxy)ethan-1-amine **(L4)** in good yield and purity. PPh_3 (123.0 g, 0.47 mol) was then added slowly and the mixture was stirred overnight. The reaction mixture was monitored by TLC using hexane:EtOAc = 1:1 mixture for the starting diazide **(L3)** and CH_2Cl_2:MeOH:25% aqueous NH_3 = 3:3:1 mixture for the product **(L4)**; detection was achieved with potassium permanganate. The precipitated triphenylphosphine oxide was filtered off and washed with water. The organic phase was separated and the aqueous solution was subsequently extracted with Et_2O (3 x 500 mL). The aqueous solution was cooled to 0 °C and KOH (300 g) was slowly added. The basic aqueous solution was then extracted with CH_2Cl_2 (6 x 600 mL). The product was dried at room temperature using an oil rotary pump. The product was obtained as an yellowish oil, in 64% yield (39 g). IR (KBr): 3357, 2860, 2101 ν(azide), 1595, 1440, 1344, 1269, 1120 cm-1. ^{1}H NMR (300 MHz, $CDCl_3$):δ = 3.65 (t, J = 5.2 Hz, 2H, H-3), 3.52 (t, J = 5.1 Hz, 2H, H-2), 3.39 (t, J = 5.1 Hz, 2H, H-4), 2.88 (t, J = 5.1 Hz, 2H, H-1) ppm. ^{13}C NMR (100 MHz, $CDCl_3$):δ = 73.15 (C-2), 70.00 (C-3), 50.80 (C-4), 41.73 (C-1) ppm. ESI MS: for $C_4H_{10}N_4O$calcd: m/z 130.1, found

131.2 $[M+H]^+$. HRMS: for $C_4H_{10}N_4O$calcd: m/z 130.0855, found 131.0933 $[M+H]^+$, Δ 4.6 ppm. ^1H NMR spectrum was consistent with the literature (Klein et al.). Chromophore 4-chloro-7-nitrobenzofurazan (NBF-Cl) was finally reacted with compound **L4** in absolute ethanol. NBF-Cl (0.8 g, 4 mmol) was solubilized in EtOH (20 mL) and slowly added to a EtOH solution (10 mL) of 2-(2-azidoethoxy)ethan-1-amine **(L4)** (1.3 g, 10 mmol) under vigorous stirring. The mixture was stirred at r.t. for 2 h. The reaction was monitored by TLC (DCM:hexane = 8:2) and detection was achieved under UV-Lamp at 254 nm. The reaction mixture was evaporated under reduced pressure at 40 °C and the obtained oil was diluted with DCM (50 mL) and extracted with water (3 x 50 mL). The organic phase was extracted with HCl 1 M (3 x 100 mL), dried over $MgSO_4$ and concentrated under reduced pressure. The obatined oil was purified by chromatography with DCM as eleunt in isocratic elution. the product was concentrated under reduced pressure and a dark oil was obtained (1.2 g, 42% yield). Rf = 0.20 (8:2 = DCM:Hexane); ^1H NMR (500 MHz, $CDCl_3$) δ(ppm) 8.47 (d, 1H, H2), 6.72 (br s, 1H, NH), 6.23 (d, 1H, H3), 3.88 (t, 2H, H8), 3.76-3.74 (m, 4H, H7-H9), 3.45 (t, 2H, H10).

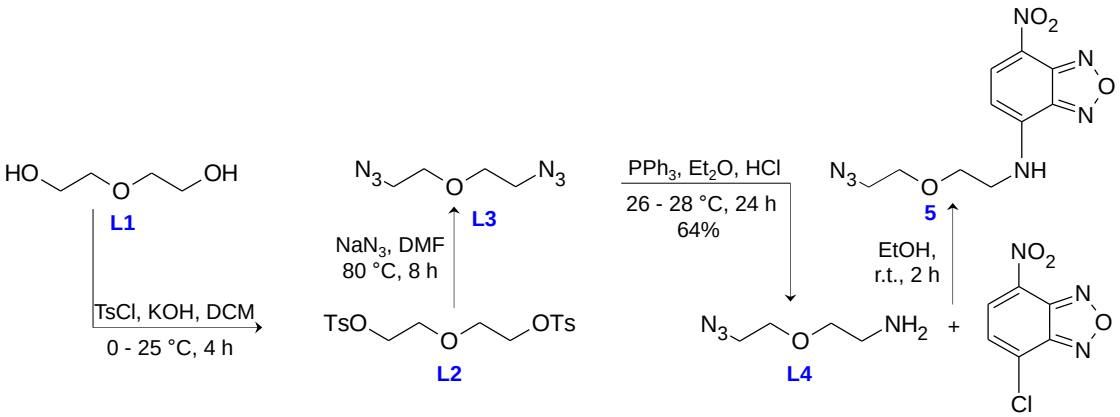

Figure 40: Synthesis scheme for compound **5**.

Both the final products, **βCD-NBFNO1** and **βCD-NBFNO2** show excellent solubility in water up to ca 10^{-2} M. In Figure 41 are shown the UV-Vis spectroscopic features of aqueous solutions of the two derivatives and, for the sake of comparison, those of the non-nitrosated βCD conjugates **βCD-NBF1** and **βCD-NBF2** in the same solvent.

3.6.1.2 Spectroscopic and photochemical characterization

The absorption spectra of **βCD-NBFNO1** and **βCD-NBFNO2** (Figure 41A) exhibit an intense absorption at ca. 380 nm and a shoulder at 475 nm. The main absorption is blue-shifted by more than 90 nm as compared to that of the non-nitrosated analogues (Figure 41B) as a consequence of the loss of the "push-pull" character due to the introduction of the electron-withdrawing NO group at the amino functionality. Note that the shoulder in the visible region is much more intense if compared with that observed for **NBF-NO**, bearing the very same chromogenic unit but non-linked to the βCD scaffold. In principle, this can be due to either intra or intermolecular non-covalent interaction between the N-nitroso appendages and the βCD moiety. However, the presence of this intense shoulder, even in very dilute solutions, ruled out the latter hypothesis. Analogously to what already observed for **NBF-NO**, the presence of the nitroso group has a significant effect on the emission properties. **βCD-NBFNO1** and **βCD-NBFNO2** exhibited fluorescence emission in the green region (Figure 41A) but with quite low quantum yields, being Φ_f = 0.026 and 0.018, respectively, that are values ca. 4 and 7-fold smaller than those of the analogues non-nitrosated derivatives (Φ_f = 0. 10 and 0.13) (Figure 41B).

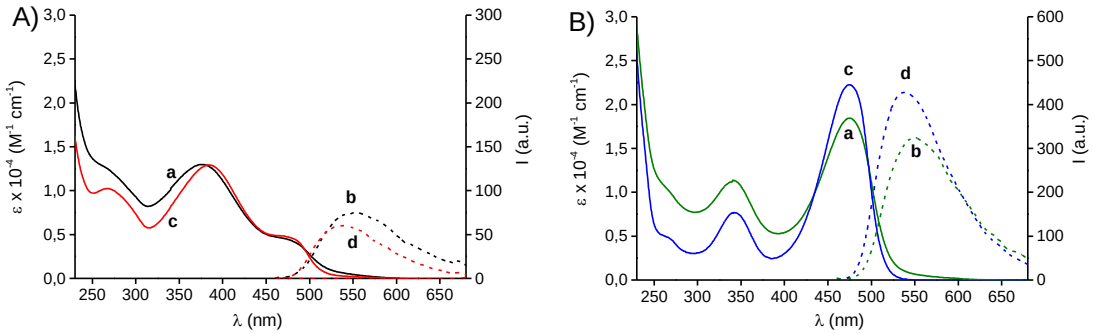

Figure 41: (A) Absorption and fluorescence emission spectra (λ_{exc} = 450 nm) of aqueous solutions of **βCD-NBFNO1** (**a** and **b**) and **βCD-NBFNO2** (**c** and **d**). (B) Absorption and fluorescence emission spectra (λ_{exc} = 450 nm) of aqueous solutions of denitrosated **βCD-NBF1** (**a** and **b**) and **βCD-NBF2** (**a** and **d**). Fluorescence emission spectra were carried out with optically matched solutions of all compounds at the excitation wavelength. T = 25 °C.

Figure 42A shows the absorption and fluorescence emission spectral changes observed when a solution of **βCD-NBFNO1** is irradiated with blue light under aerobic conditions. They show the bleaching of the main absorption band at 377 nm and the formation of a new, intense absorption at 475 nm, accompanied by the presence of 4 clear isosbestic points, which indicates the occurrence of a very clean photochemical transformation. The spectrum observed after completing the photolysis is basically identical to that of the non-nitrosated conjugate **βCD-NBF1** (compare spectra **a** in Figure 41A and B) characterized by the typical charge transfer band at 475 nm of the amino-nitro-benzofurazan moiety. The evolution of the fluorescence emission spectra observed upon irradiation shows a significant revival of the green emission with λ_{max} = 550 nm, typical of the amino-nitro-benzofurazan fluorophore (Figure 42A). [95] These findings clearly suggest the occurrence of NO photorelease from **βCD-NBFNO1** and the concomitant formation of the non-nitrosated fluorophore that can be a suitable optical reporter to follow the NO uncaging. The inset of Figure 42A shows an excellent agreement between the evolution of the absorption and fluorescence changes as a function of the

irradiation time and it indicates that the photolytic process was complete after ca. 2 min of irradiation. This accounts for a very effective photochemical reaction as proven by the high of the quantum yield for the NO photorelease, Φ_{NO} = 0.13, a value very close to that observed for the non-water-soluble **NBF-NO** (Φ_{NO} = 0.15). NO release was unambiguously demonstrated by the direct detection of this radical through amperometric technique using an ultrasensitive NO electrode. Figure 42B shows a prompt and effective NO release from the aqueous solution of **βCD-NBFNO1**, which stops in the dark and restarts once the illumination is turned on again.

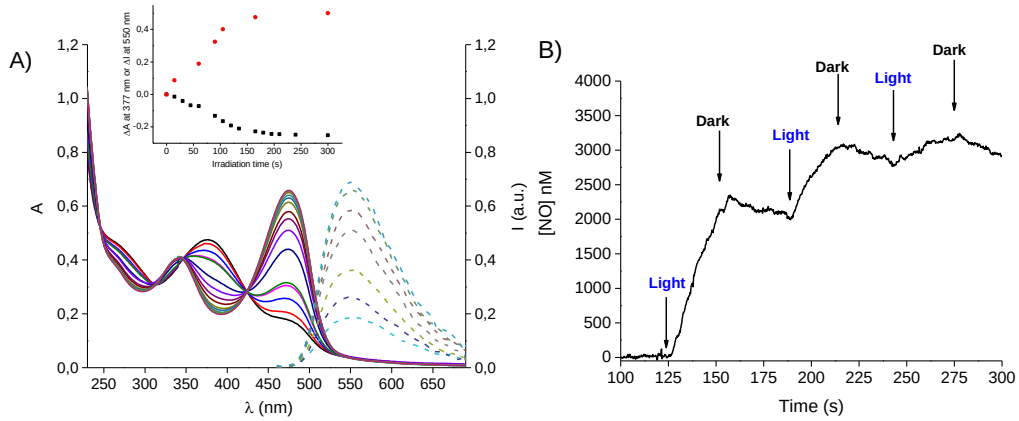

Figure 42: (A) Absorption (solid lines) and fluorescence emission, (λ_{exc} = 424 nm, isosbestic point) (dotted lines) spectral changes observed upon exposure of an aqueous solution of **βCD-NBFNO1** (35 μM) at λ_{exc} = 405 nm (ca. 20 mW cm^{-2}) for time intervals from 0 to 300 s. The arrows indicate the course of the spectral profile with the illumination time. The inset shows the different absorbance changes at λ = 377 nm (■) and fluorescence changes at λ = 550 nm (●), respectively. (B) NO release profile observed for an aqueous solution of **βCD-NBFNO1** (35 μM) upon alternate cycles of irradiation (λ_{exc} = 405 nm, ca. 20 mW cm^{-2}) and dark. T = 25 °C.

As shown in Figure 43A and related inset, **βCD-NBFNO2** exhibited a similar photobehaviour with an even higher quantum yield for the NO photorelease Φ_{NO} = 0.31, which represents the largest value among those reported for any organic

NOPD activatable in the Vis range. Interestingly, the restoring of the emission of the optical reporter is visible at naked eye (Figure 43A) and gives easily readable information about the NO produced. The NO photorelease measured by its direct monitoring was then related to the increase of the fluorescence emission for both compounds. As shown in Figure 43B, we found a very good correlation between the concentration of NO liberated by both compounds upon light stimuli and the increase of the fluorescence intensity of the related optical reporters.

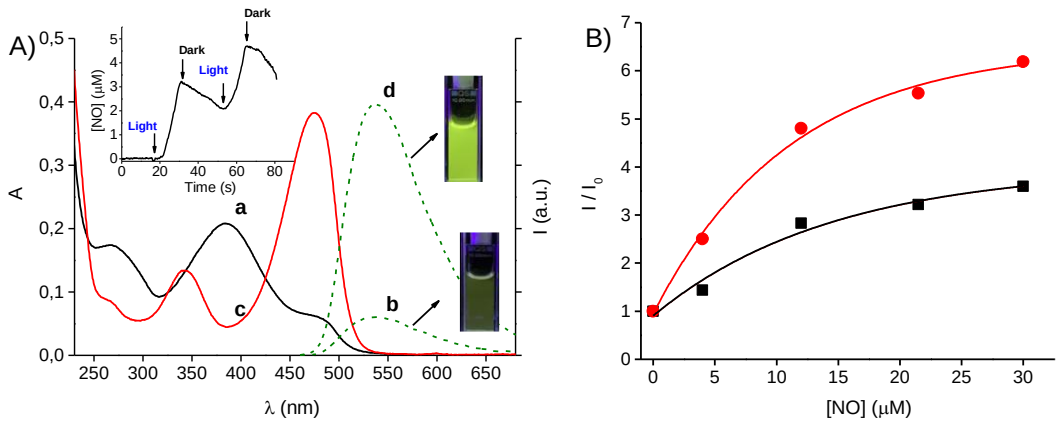

Figure 43: (A) Absorption (solid lines) and fluorescence emission, (λ_{exc} = 427 nm, isosbestic point) (dotted lines) spectra changes observed before (**a** and **b**) and after the complete photolysis (**c** and **d**) at λ_{exc} = 405 nm. (ca. 20 mW cm^{-2}) of aqueous solution of **βCD-NBFNO2** (16 μM) and actual images of the solutions before (bottom) and after (top) the photolysis acquired upon excitation at λ = 350 nm. The inset shows the NO release profile observed for an aqueous solution of **βCD-NBFNO2** (16 μM) upon alternate cycles of irradiation (λ_{exc} = 405 nm, ca. 20 mW cm^{-2}) and dark. (B) Correlation of the fluorescence increase observed upon photolysis of **βCD-NBFNO1** (■) and **βCD-NBFNO2** (●) and the concentration of NO photoreleased. I and I_0 represent the fluorescence intensities at the λ_{max} of emission after and before irradiation, respectively. T = 25 °C.

It needs to be stressed that the remarkable values of Φ_{NO} found for both conjugates permit the generation of a considerable amount of NO without the need of prolonged irradiation times, which in some cases are deleterious to cells especially when blue light is used. According to the literature, anilinyl radical derivatives

formed after the homolytic N-NO photocleavage evolve to stable photoproducts by H-transfer from the solvent medium. Since in neat water, like in our case, this process is thermodynamically not feasible, the high values observed for Φ_{NO} indicate a key role of the βCD scaffold as a reactant, providing a source of 14 easily abstractable H atoms and very close to the anilinyl radical intermediate. Furthermore, it should be noted that the absorption and emission spectral changes observed upon irradiation as well as the related kinetics were identical in the case of an N_2-saturated solution (data not shown), suggesting that both the efficiency and nature of the photochemical reaction are not dependent by the presence of oxygen. This observation rules out the participation of a long-lived excited triplet state in the photodecomposition, suggesting a NO photodetachment occurring from the short-lived excited singlet state. This hypothesis is in excellent agreement with i) the inefficient intersystem crossing to the excited triplet state reported for amino-nitro benzofurazan derivatives unless they are in very non-polar solvents (i.e., cyclohexane),[96] and ii) the very short singlet lifetimes found for **βCD-NBFNO1** and **βCD-NBFNO2**. As shown in Figure 44, both conjugates exhibited a biexponential behavior with dominant components (ca. 80%) with τ = 2.30 and 0.84 ns, respectively.

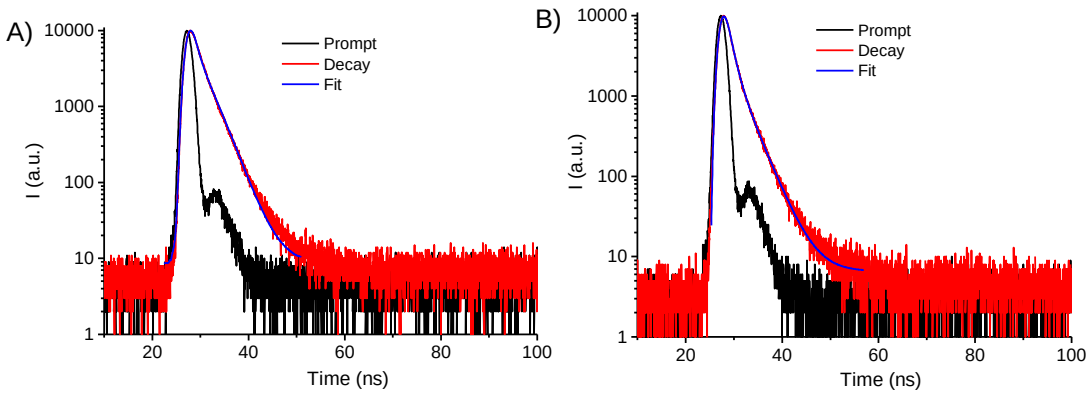

Figure 44: Fluorescence decay and the related bi-exponential fitting of the aqueous solution of **βCD-NBFNO1** (A) and **βCD-NBFNO2** (B) recorded at λ_{exc} = 455 nm and λ_{em} = 550 nm.

Moreover, the absorption spectrum of both βCD conjugates shows a pronounced shoulder extending up to the green region. These spectral features spurred us to investigate the photoreactivity of the compounds upon green light excitation. Therefore, the aqueous solution of either **βCD-NBFNO1** or **βCD-NBFNO2** was irradiated at λ_{exc} = 532 nm. We observed changes in the absorption and fluorescence emission spectral profiles basically identical to those already observed under blue light stimuli (data not shown) but with lower photochemical efficiency. In fact, the values calculated for Φ_{NO} were = 0.007 and 0.013 for **βCD-NBFNO1** and **βCD-NBFNO2**, respectively. Figure 45 shows unambiguous evidence for the NO release exclusively triggered by green light for both compounds. The photoreactivity dependence by the excitation wavelength is not surprising and may be due to the participation of upper excited singlet states populated with blue light as mediators of the photodecomposition route.

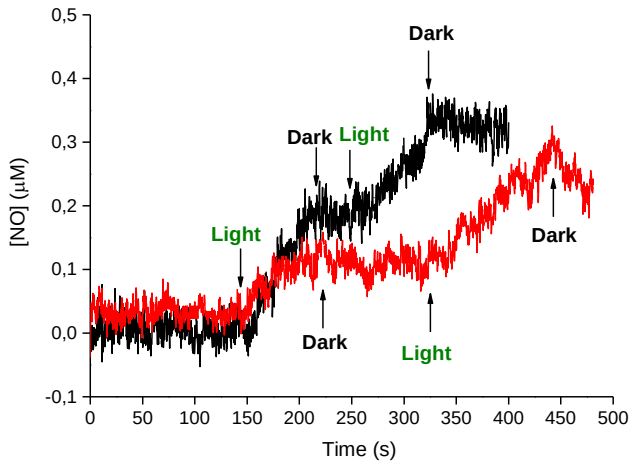

Figure 45: NO release profiles observed for an aqueous solution of **βCD-NBFNO1** (35 μM, a) and **βCD-NBFNO2** (16 μM, b) upon alternate cycles of irradiation with green light (λ_{exc} = 532 nm, ca. 100 mW cm^{-2}) and dark.

The stability of the conjugates was also evaluated in the dark at different temperatures and times. Figure 46A shows moderate decomposition for both compounds (ca. 20 %) at 25 °C, which is almost totally inhibited if samples are incubated for the same time at 4 °C. Moreover, incubation of the solution in thermostated bath at a different temperature for 15 min each showed satisfactory stability up to 40 °C (Figure 46B).

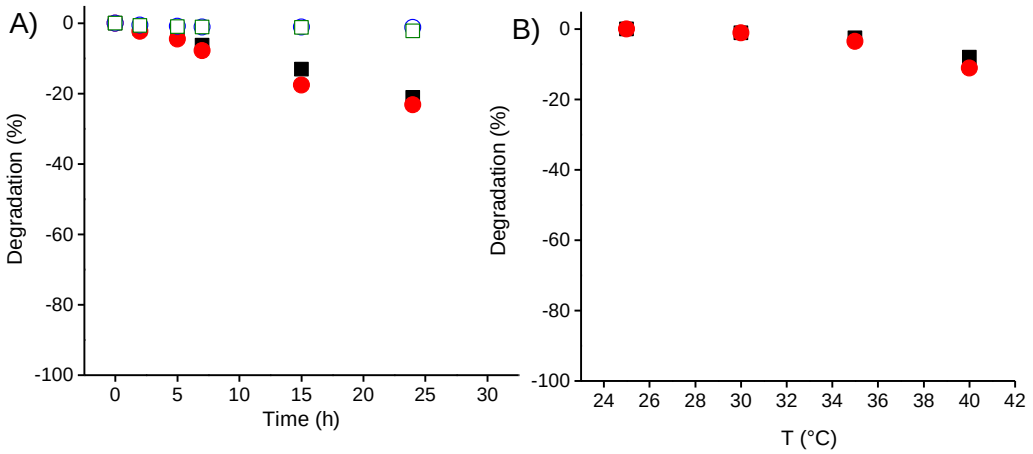

Figure 46: (A) Dark stability of the aqueous solution of **βCD-NBFNO1** (square) and **βCD-NBFNO2** (circles) incubated at 25 °C (filled symbols) or 4 °C (open symbols) at different times. (B) Dark stability of the aqueous solution of **βCD-NBFNO1** (square) and **βCD-NBFNO2** (circles) incubated for 15 min at different temperatures.

Finally, we investigated the host-guest complexation ability of the βCD conjugates. As a prototype guest, we chose **BTX** for the reasons mentioned behind. Titration of an aqueous solution of **BTX** was carried out using increasing amounts of either **βCD-NBFNO1** or **βCD-NBFNO2**. **BTX** offers good spectroscopic requisite to follow the titration by UV-Vis absorption spectroscopy since its absorption maximum falls at 275 nm, a region in which both conjugates display small absorption. Figure 47A and B show the absorption spectral changes in the **BTX** region observed upon the addition of the host molecules and after subtracting the cyclodextrin contribution

in the Uv-Vis spectra. We observed a hypochromic shift of the absorption band of **BTX** after the addition of the βCD conjugates, in accordance to typical host-guest encapsulation processes. The reciprocal of the absorbance changes at the absorption maximum was then plotted as a function of the reciprocal concentration of the host molecules, according to the Benesi-Hildebrand equation:[97]

$$\frac{1}{\Delta A} = \frac{1}{\mathrm{K}_{ass} \cdot \Delta\varepsilon \cdot [host]} + \frac{1}{\Delta\varepsilon}$$

where K_{ass} represents the association constants for the supramolecular host-guest process, $\Delta\varepsilon$ is the difference of the molar extinction coefficient between the free and complexed guest and [*host*] is the concentration of the βCD conjugates. As shown in Figure 47C and D, we obtained very good linear plots in both cases and values of K_{ass} of 500±50 M^{-1} and 1100±100 M^{-1} respectively for **βCD-NBFNO1** and **βCD-NBFNO2**, were obtained from the intercept/slope ratio. The higher value observed for **βCD-NBFNO2** is probably attributable to the longer flexible spacer between the CD scaffold and the chromogenic unit, which allows a better accommodation of the host within the hydrophobic cavity.

In order to be used in combination, one of the indispensable requisites for this host-guest system is that the encapsulation of **BTX** in the CD cavity does not affect the photochemical performances of the photoactivatable conjugates. Therefore, photolysis experiments on **βCD-NBFNO1** and **βCD-NBFNO2** were carried out in the presence of **BTX**. We observed that the presence of the guest molecule changes neither the nature nor the efficiency of the photoreactivity of both compounds, ruling out any intermolecular communication between the host and the guest through competitive photoinduced processes. This is not a trivial result for host-guest supramolecular complexes. In fact, it is known that the photoreactivity of the host and guest components can be remarkably influenced in efficiency nature or

both upon complexation as result of their close proximity and the presence of specific interactions, steric constrains and reduced polarity.[85]

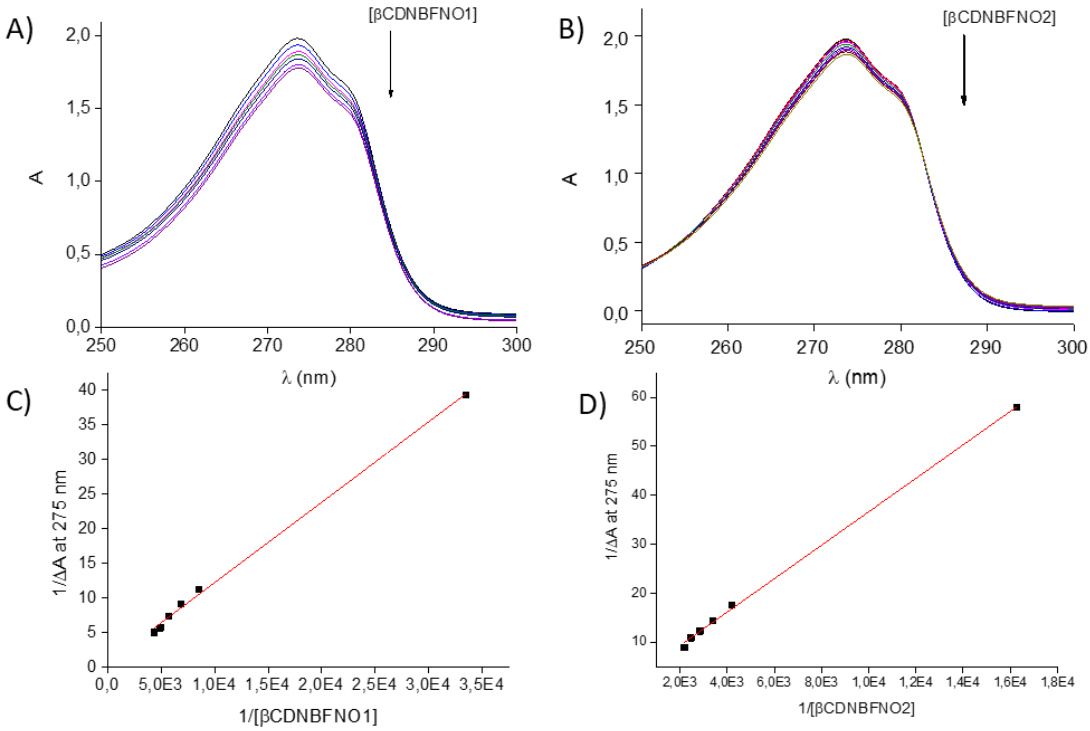

Figure 47: Absorption spectral changes observed upon addition of different amounts of **βCD-NBFNO1** (A) and **βCD-NBFNO2** (B) to aqueous solutions of **BTX** (1.4 mM). The related double-reciprocal plots and the linear fitting of the data, according to the Benesi-Hildebrand equation, are reported for **βCD-NBFNO1** (C) and **βCD-NBFNO2** (D). T = 25 °C.

3.6.2 Cyclodextrin based Polymers

3.6.2.1 Design and synthesis

A rich variety of polymers based on cyclodextrins (CDs) are receiving a growing interest thanks to their well-known complexation capability as well as their ability to stabilize and solubilize guest compounds. Moreover, the CDs polymers offer additional advantages like the possibilities of guest interaction thanks to their different binding sites and/or the option to develop integrated systems for multimodal therapeutic strategies. This work reports the synthesis and characterization of a novel β and γCD-based copolymer covalently integrating two moieties of nitric oxide photodonor (NOPD) per β-CD unit (Figure 48). The complexing capability were tested using **BTX** as a model compound for the same reasons reported above.[88, 89, 90]

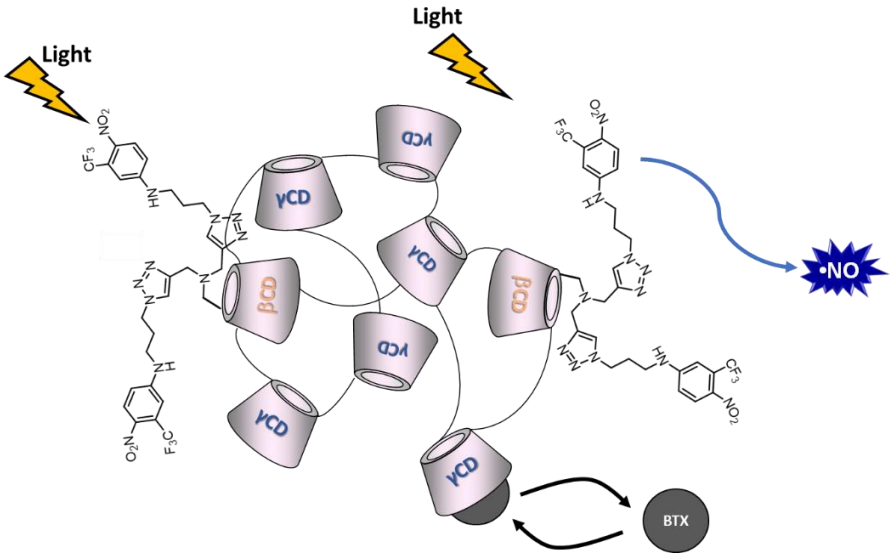

Figure 48: Schematic representation for the functioning of cyclodextrin-based copolymer.

Synthesis of azidated-NO-donor (compound 8). In order to selectively modify the cyclodextrin scaffold on the primary rim, the NO-donor-containing synthon was prepared according to the following strategy in three steps (Figure 49).

Briefly, 5-cloro-2-nitrobenzofluoride (4.5 g) was heated at 70 °C for 1 h with an excess of 3-amino-1-propanolo (17.7 g). The reaction was cooled down and was stirred at room temperature for 2 days. The solvent was removed under reduced pressure and the residue was precipitated with water. The solid was filtered-off using a glass filter (porosity 3) and it was dried in a vacuum drying box with a yield of 90% (5 g). The obtained intermediate, compound **6** (3 g), was solubilized in pyridine (50 mL), cooled down to 0 °C and 4-toluenesulfonyl chloride (2.16 mg) and DMAP (0.55 g) were added in sequence. The reaction mixture was stirred overnight. The solvent was removed under reduced pressure and the residue was washed 3 times with H_2O/CH_2Cl_2. The reaction crude was purified by chromatography (Hexan:EtOAc = 7:3) obtaining 4.5 g of yellow powder with a yield of 97 % (**7**). Compound **7** (5 g, 12 mmol) was dissolved in DMF/DMSO 1:1 (60 mL), sodium azide was added in one portion (1.55 gr, 24 mmol) and left under stirring for 2 days at 60° C. Compound **8** was extracted three times with H_2O/CH_2Cl_2, the organic phases were combined, evaporated thus yielding the target compound as yellow oil with a yield of 83 % (3g). ^{1}H NMR (500 MHz, D_2O, 298 K) δ(ppm) 7.85 (d, 1H, H3a), 6.82 (d, 1H, H2a), 6.51 (d, 1H, H1a), 3.31 (t, 2H, H1), 3.14 (t, 2H, H3), 1.76 (q, 2H, H2).

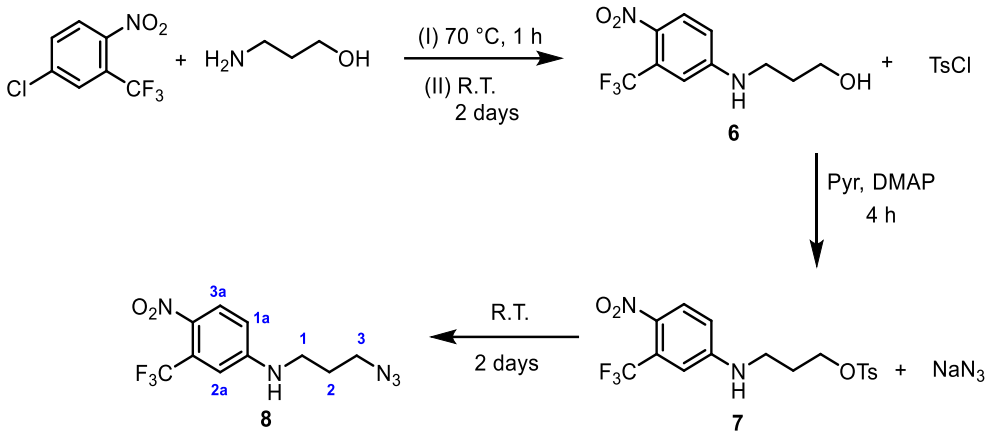

Figure 49: Synthetic strategy towards azidated-NO-donor (compound **8**).

(NOPD)$_2$-NH-BCD (9). In order to implement the azidated-NO-donor compound on the cyclodextrin scaffold, 6-monoamino-β-CD was first modified with two propargyl moieties according to the scheme shown in Figure 50. 6-monoamino-β-CD (2.3 g) was solubilized in anhydrous DMSO. After complete solubilization, DIPEA (2.58 g) and propargyl bromide (0.88 g) were added in sequence and the mixture was heated at 40 °C for 3 hours. The reaction mixture was concentrated under reduced pressure and the obtained syrup was precipitated with acetone. The solid was filtered-off, extensively washed with acetone and finally dried until constant weight in a vacuum drying box. The crude was additionally purified by chromatography; eluent THF : NH_3 water solution 25% : MeOH = 10:4:1, fractions were combined, evaporated yielding compound **9** as white powder (1.5 g; 56% yiled). MALDI MS: for $C_{48}H_{75}NO_{34}$ calcd m/z 1209.420 found 1210.510 $[M+H]^+$,^{1}H NMR (500 MHz, DMSO-d_6) δ(ppm) 5.9-5.74 (m, 7H, C3OH) 4.83-4.39 (m, 7H, H1), 4.46 (m, 2H, H9'), 3.69-3.20 (m, 48H, c), 3.36 (s, 2H, a), 3.27 (s, 2H, b); ^{13}C NMR (125 MHz, DMSO-d_6) assignment based on DEPT-edited HSQC spectrum δ 104.98 (C1), 86.91-73.66 (C2, C3, C4, C5), 102.55-101.08 (C1), 63.27 (C6), 51.78 (Ca), 45.50 (Cc), 42.96 (Cb).

The cycloaddition reaction between the compound **8** and **9** was performed as follow. Compound **8** (3 mL) and **9** (2 g) were dissolved in DMF/H_2O 2:1 and then Cu(I)Br (0.25 g) was added to the mixture as catalyst. The reaction was stirred at room temperature for 30 minutes. The solvent was partially removed under reduced pressure and the residue was precipitate with acetone. The obtained precipitate was filtered-off, washed with acetone (100 mL x 3 times) and dried (1.5 g). The crude was purified by chromatography using as eluent 1,4-dioxane:NH_3 aqueous solution 25%:1-propanol = 10:7:3, yielding a yellow powder (2.3 g). MALDI, ^{1}H NMR, DEPT-edited HSQC spectra of compound **10** are shown in Figure 51,52 and 53, respectively.

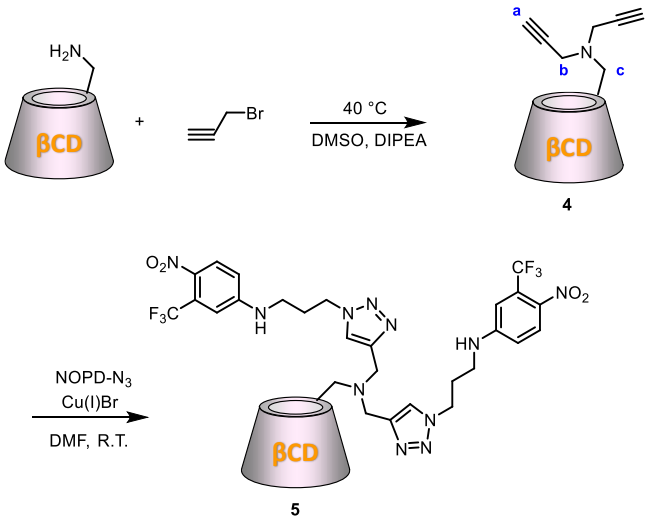

Figure 50: Synthetic strategy towards NO-donor appended βCD.

In Figure 51 the MALDI spectrum of compound **10** is shown. The molecular weight reported is different than the expected one due to the decomposition of nitro group into amino group caused by the laser desorption ionization.

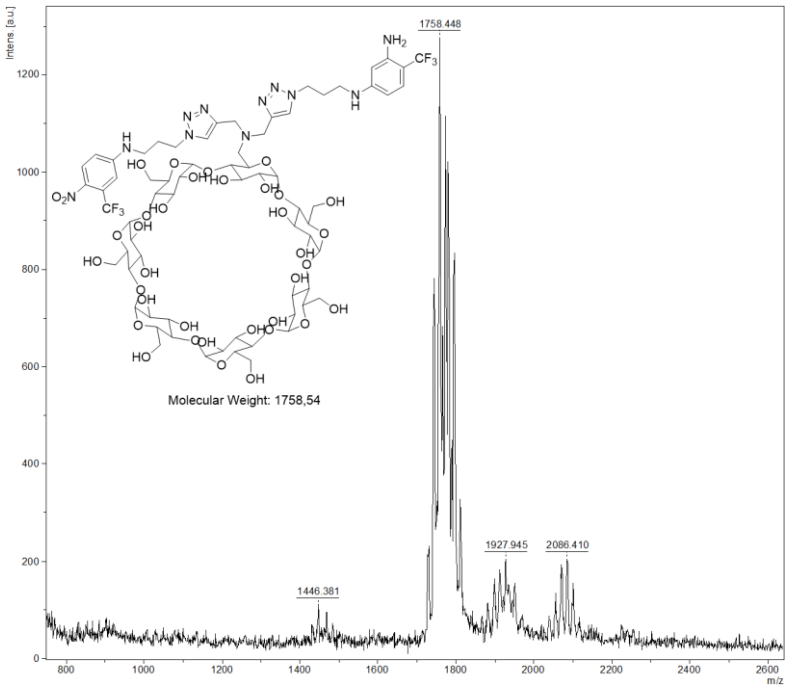

Figure 51: MALDI spectrum of compound **10.**

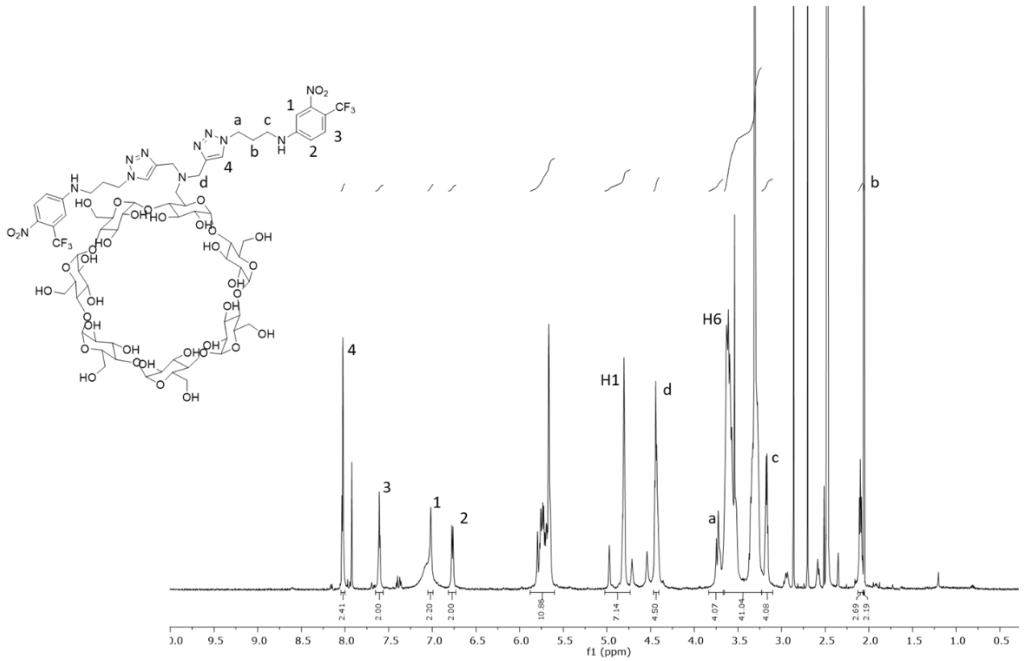

Figure 52: ^{1}H spectrum of compound **10** with partial assignment (DMSO-d_6, 600 MHz, 298 K).

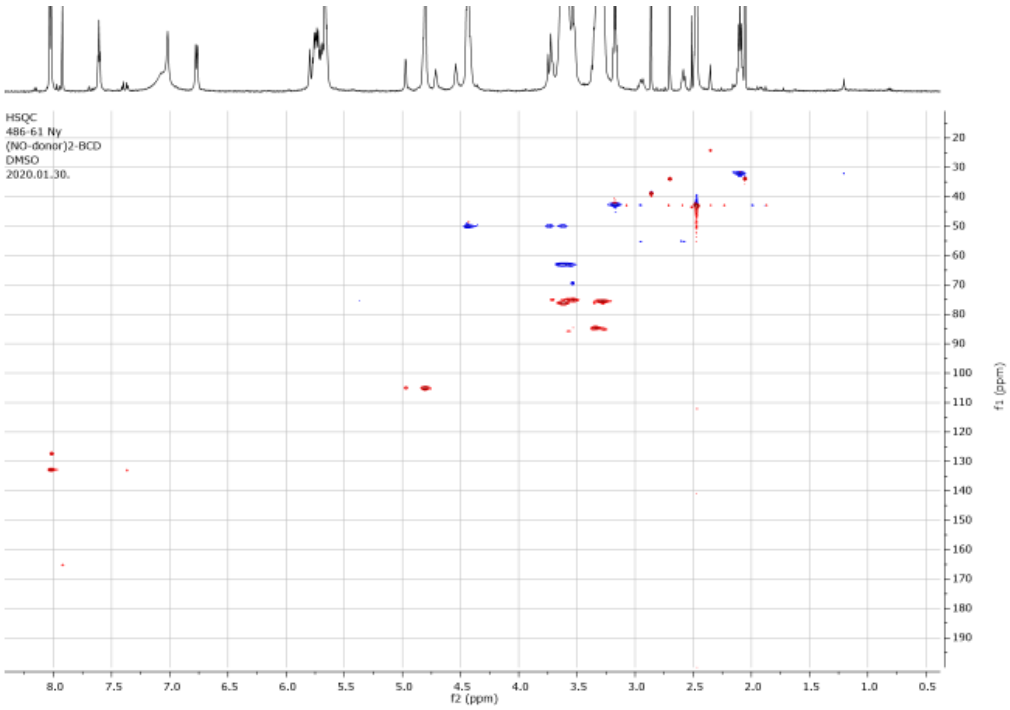

Figure 53: DEPT-edited HSQC spectrum of compound **10** (DMSO-d_6, 600 MHz, 298 K).

The final step of the synthesis of the polymer was conducted to have a copolymer of γCD and compound **10** as shown in Figure 54.

Polymerization. Compound **10** (1.5 g) and γCD (12 g) was solubilized in 25 mL of a water solution of NaOH 2M. and epichlorohydrin was added dropwise (60 minutes) by keeping the temperature constant at 60 °C. The reaction mixture was stirred at 60 °C for additional 2 hours, cooled down to 30 °C and left rest overnight at room temperature without stirring. The crude reaction was neutralized with HCl solution 1 N (10 mL) and then extensively dialyzed, filtered to remove insoluble residue (glass filter porosity 3), dialyzed and freeze drying. The copolymer integrating two moieties of NO photodonor per each unit of βCD (**copolymer-NOPD**) was obtained. The degree of functionalization with **10** obtained is 1.6 %.

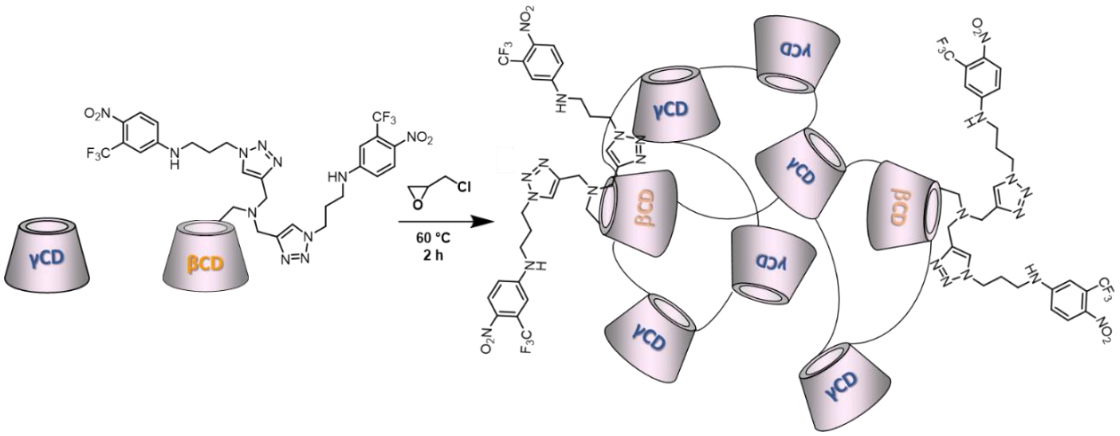

Figure 54: Synthetic strategy towards **Copolymer-NOPD**.

The use of cyclodextrins branched polymers is increasingly emerging in view of their unique topological structures and appealing physico-chemical properties such as three-dimensional globular structure, reduced hydrodynamic radius, improved multifunctionality, enhanced encapsulation capabilities and water solubility.[98]

3.6.2.2 Dimensional and photochemical characterization

Characterization of the dimension of particle of copolymer in water solution was performed through Dynamic light scattering (DLS), revealing hydrodynamic particle diameters of about 13 nm in aqueous solution (Table 3).

Table 3: Table of values obtained from DLS.

Mean (µm)	PI
0.013*	0.05*

*Average value

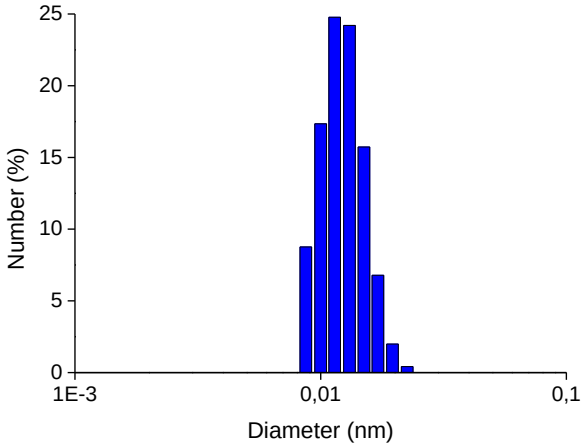

Figure 55: Representative image of particle size determination by dynamic light scattering (DLS).

The Photosensitivity of the compound was evaluated upon irradiation with blue light and the absorption spectral changes is in agreement with the typical decrease of the band characteristic of nitroaniline moieties and a slight increase in the UV region for the formation of phenol derivative as the only stable photoproduct (as shown in Figure 56A).[54,55] Moreover, the production of NO was monitored directly by an amperometric technique using an ultrasensitive NO, alternating cycles of light/dark. Figure 56B shows that NO generation in the micromolar range is achieved upon blue light excitation; it stops as the light is turned off and restarts when the light is turned on again. The quantum yield for the NO photogeneration was $\Phi_{NO} = 0.007 \pm 0.001$.

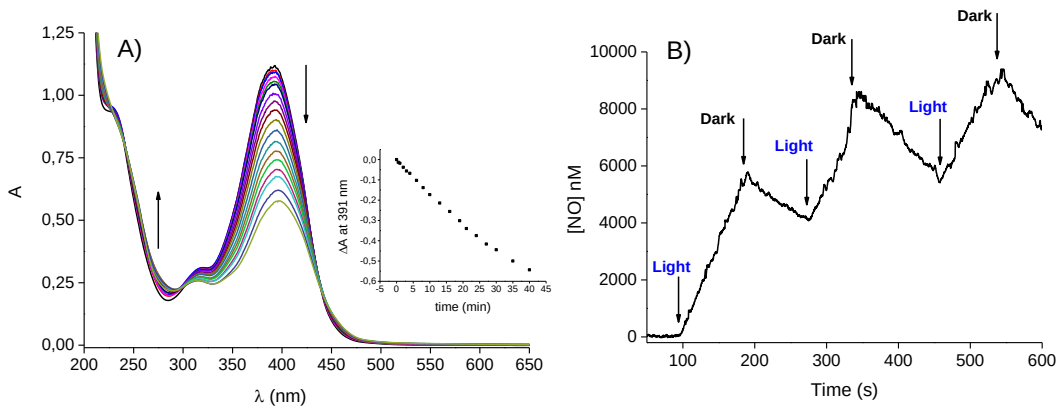

Figure 56: (A) Photobleaching of cyclodextrin polymer in aqueous solution (4 mg/mL) observed at different times upon light irradiation with continuum laser λ_{exc} 405 nm (100 mW), in the insert ΔA at 391 nm as a function of irradiation time was reported. (B) NO release profile observed upon On/Off alternative irradiation cycles with a laser 405 nm at a power of 100 mW.

Finally, the non-covalent drug entrapment capability of this new polymeric material was also evaluated using **BTX** as guest. Titration of an aqueous solution of **BTX** was then carried out using increasing amounts of **copolymer-NOPD**. Figure 57A shows the absorption spectral changes in the **BTX** region, observed upon the addition of the host molecules and after subtracting the cyclodextrin contribution in the Uv-Vis spectra. We observed a hypochromic shift of the absorption band of **BTX** after the addition of the βCD conjugates, according to typical host-guest encapsulation processes. The reciprocal of the absorbance changes at the absorption maximum was plotted as a function of the reciprocal concentration of the host molecules, according to the Benesi-Hildebrand equation[97] and K_{ass} was calculated as previously explained. As shown in Figure 57B, we obtained very good linear plots in both cases and values of K_{ass} of 400 ± 40 M^{-1} were obtained from the intercept/slope ratio.

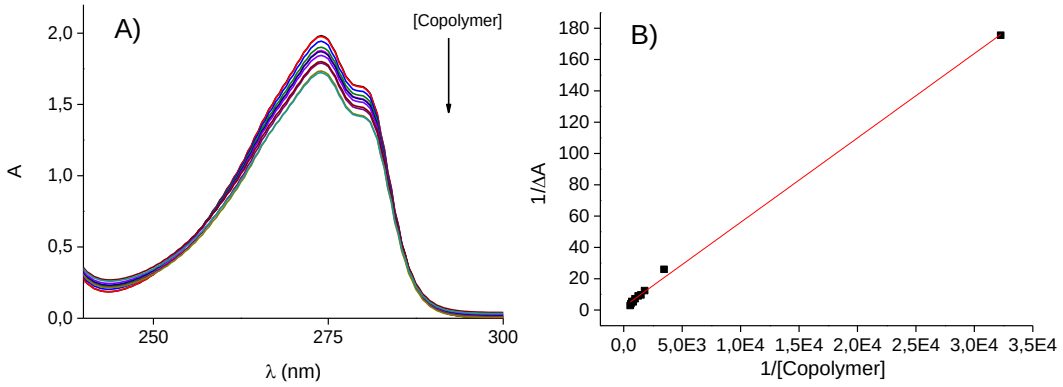

Figure 57: (A) Absorption spectral changes observed upon addition of different amounts of **copolymer-NOPD** to aqueous solutions of **BTX** (1.4 mM). (B) The related double-reciprocal plots and the linear fitting of the data, according to the Benesi-Hildebrand equation. T = 25 °C.

In order to be used in combination with other therapeutic agents, one of the indispensable requisites for this host-guest system is that the encapsulation of **BTX** in the CD cavity does not affect the photochemical performances of the photoactivatable conjugates. Therefore, photolysis experiments were repeated in the presence of **BTX**. We observed that the presence of the guest molecule maintains almost unchanged the nature and the efficiency of the photoreactivity of compounds (Φ_{NO} = 0.006 ± 0.001) as shown in Figure 58.

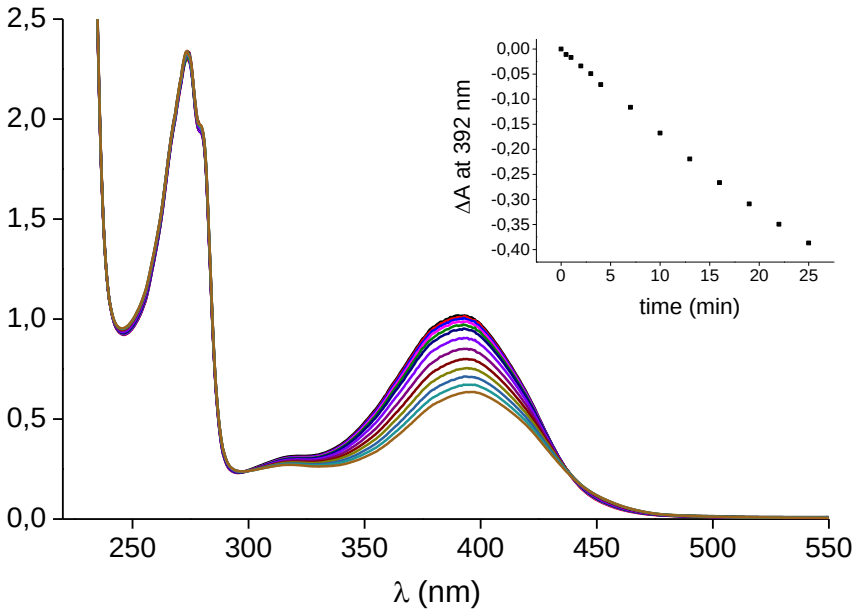

Figure 58: Photobleaching of cyclodextrin polymer in aqueous solution (4 mg/mL) in presence of **BTX** (1.4 mM) observed at different times upon light irradiation with continuum laser λ_{exc} 405 nm (100 mW).

3.6.3 Conclusions

In conclusion, two novels photoactivatable βCD conjugates and a cyclodextrins based copolymer were designed, synthesized, and characterized. These compounds present remarkable advantages with respect the isolated photoactive unit not linked to the βCD scaffold, show an excellent water solubility, good stability in the dark within 24 h at room temperature and the capability to release the biologically relevant NO under blue light.

In particular, βCD conjugates shows the highest quantum yields ever observed for non-metal based NO photoreleaser triggered by visible light and these give the possibility to release nitric oxide even under the stimulus of the more biocompatible green light, although with lower efficiency. Moreover, the release

process can be followed at naked eye thank to the difference between the poorly fluorescent starting compounds and the highly fluorescent stable photoproducts (reporter). The reporter can be excited by using the same excitation wavelength used for NO uncaging, facilitating the real-time monitoring of NO.

On the other hand, although the polymer shows a lower yield of NO release, compared to the βCD conjugates, gives the possibility to integrate the system with molecules employed in imaging or to strengthen the system with other therapeutic or phototherapeutic functions (e.i. verteporfin).[62]

Interestingly, the functionalization of the CD scaffold with photoactivatable moieties does not preclude the encapsulation guest as demonstrated by the association of both conjugates with the β-blocker **BTX**. In this regard, in view of the well-known vasodilator properties of NO, the present work may open intriguing prospects for biological studies on formulations for ocular application against glaucoma, addressed to explore the combinatory effect of **BTX** and NO. These studies are currently underway in our laboratories.

Chapter 4

General conclusion

During the PhD work, different photoactivatable moieties were successfully integrated into scaffolds suitable for ophthalmic administration, maintaining the original capability to release the active species (NO and $^1O_2$). In this contest visible light has been demonstrated to be a perfect trigger for production of active species for the control of release in term of space, time, and dosage and for the easy accessibility of the eye to the light. For the well-known properties of reactive species, the developed systems can find application against bacterial infections in therapy of glaucoma and AMD. Preliminary in vivo studies were conducted with promising results and further studies will be done to evaluate the effectiveness of the systems to reduce the IOP.

Acknowledgements

I thank my tutor Prof. S. Sortino and all his research group for giving me this opportunity. I thank Dr. M. Malanga and the CycloLab Ltd, Dr. D. Aleo and the Medivis S.r.l, and Prof. F. Quaglia and her group for their contribution in part of this work.

Bibliography

1. Achouri D, Alhanout K, Piccerelle P, Andrieu V; Recent advances in ocular drug delivery. *Drug Dev Ind Pharm.* (2013) 39, 1599–1617.

2. Ghate D, Edelhauser H. F; Ocular drug delivery, Expert Opin*. Drug Deliv.* (2006) 3*,* 275-287*.*

3. Gaudana R, Jwala J, Boddu SH, Mitra AK; Recent perspectives in ocular drug delivery; *Pharm Res*. (2009) 26, 1197–1216.

4. Zignani M, Tabatabay C, Gurny R; Topical semi-solid drug delivery: kinetics and tolerance of ophthalmic hydrogels; *Adv. Drug Deliv. Rev*. (1995) 16, 51–60.

5. Bhattarai N, Gunn J, Zhang M; Chitosan-based hydrogels for controlled, localized drug delivery; *Adv. Drug Deliv. Rev.* (2010) 62, 83–99.

6. Järvien K, Järvien T, Urtti A; Ocular absorption following topical delivery; *Adv. Drug Deliv. Rev.* (1995) 16, 3–19.

7. Almeida H, Amaral MH, Lobão P, Lobo J; In situ gelling systems: a strategy to improve the bioavailability of ophthalmic pharmaceutical formulations; *Drug Discov. Today*.(2014) 19, 400-414

8. De Groote M A, Fang F C; NO Inhibitions: Antimicrobial Properties of Nitric Oxide; *Clin. Infect. Dis.* (1995) 21, 162–165.

9. Bishop A, Andderson J E; NO signaling in the CNS: from the physiological to the pathological; *Toxicology.* (2005) 208, 193-205.

10. Scatena R, Bottoni P, Pontoglio A, Giardina B, Pharmacological modulation of nitric oxide release: new pharmacological perspectives, potential benefits and risks; *Curr. Med. Chem.* (2010) 17, 61-73.

11. Heyne G W, Kiland, J A, Kaufman P L, Gabel, B T; Effect of nitric oxide on anterior segment physiology in monkeys; *Invest. Ophthalmol. Visual Sci.* (2013) 54, 5103−5110.

12.Behar-Cohen F F, Goureau O, D'Hermies F, Courtois Y; Decreased intraocular pressure induced by nitric oxide donors is correlated to nitrite production in the rabbit eyes*; Invest. Ophthalmol. Visual Sci*. (1996) 37, 1711−1715.

13. Al-Sa'doni H H, Ferro A; Current status and future possibilities of nitric oxide-donor drugs: focus on S-nitrosothiols; *Mini Rev. Med. Chem*. (2005) 5, 247–254.

14. Laursen B E, Stankevicius E, Pilegaard H, Mulvany M, Simonsen U; Potential Protective Properties of a Stable, Slow-releasing Nitric Oxide Donor, GEA 3175, in the Lung; *Cardiovasc. Drug Rev*. (2006) 24, 247–260.

15. Yasuda H; Solid tumor physiology and hypoxia-induced chemo/radio-resistance: Novel strategy for cancer therapy: Nitric oxide donor as a therapeutic enhancer; *Nitric Oxide*. (2008) 19, 205–216.

16. Griffiths M J D, Evans T W; Inhaled Nitric Oxide Therapy in Adults*; N. Engl. J. Med.* (2005) 2683-2695.

17. Greenough A; Inhaled nitric oxide in the neonatal period; *Expert. Opin. Investig. Drugs.* (2000) 1601-1609.

18. Thatcher G R J, Weldon H; NO problem for nitroglycerin: organic nitrate chemistry and therapy; *Chem. Soc. Rev*. (1998) 27, 331-337.

19. Torfgard K E, Ahlner J; Mechanisms of action of nitrates; *Cardiovasc. Drugs Ther*. (1994) 8, 701-717.

20. Davies K M, Wink D A, Saavedra J E, Keefer L K; Chemistry of the Diazeniumdiolates. Kinetics and Mechanism of Dissociation to Nitric Oxide in Aqueous Solution; *J. Am. Chem. Soc.* (2001) 123, 5473-5481.

21. Pavlos C M, Xu H, Toscano J P; Controlled photochemical release of nitric oxide from O2-substituted diazeniumdiolates; *Free Rad. Biol. Med*. (2004) 37, 745-752.

22. Williams R J P; Nitric oxide in biology: its role as a ligand; *Chem. Soc. Rev*. (1996) 25, 77-83.

23. Pipes D W, Meyer T J; Comparisons between polypyridyl nitrosyl complexes of osmium(II) and ruthenium(II), *Inorg. Chem*. (1984) 23, 2466-2472.

24. Marks G S, McLaughlin B E, Jimmo S L, Poklewska- Koziell M, Bien J F, Nakatsu K; Time-dependent increase in nitric oxide formation concurrent with vasodilation induced by sodium nitroprusside, 3-morpholinosydnonimine, and S-nitroso-N-acetylpenicillamine but not by glyceryl trinitrate; *Drug Metab. Dispos*. (1995) 23, 1248-1252.

25. Feelisch MJ; The biochemical pathway of nitric oxide formation from nitrovasodilatators appropriate of exogenous NO donors and aspects of preparation and handling of aqueous NO solution; *J. Cardiovasc. Pharmacol. Ther*. (1991) 25-33.

26. Bettache N, Carter T, Corrie J E, Ogden D B, Trentham D R; Photolabile donors of nitric oxide: Ruthenium nitrosyl chlorides as caged nitric oxide, *Methods. Enzymol.* (1996) 268, 266-281.

27. Clarke M J, Gaul J B; Chemistry relevant to the biological effects of nitric oxide and metallonitrosyl*s; Struct. Bonding*. (1993) 81, 147-181.

28. Dodsworth E S, Vleck A A, Lever A B P; Factorization of Ligand-Based Reduction Potentials; *Inorg. Chem*. (1994) 33, 1045-1049.

29. Ford P C; Polychromophoric Metal Complexes for Generating the Bioregulatory Agent Nitric Oxide by Single- and Two-Photon Excitation; *Acc. Chem. Res.* (2008) 41, 190-200.

30. Ford P C; Photochemical delivery of nitric oxide; *Nitric Oxide*. (2013) 35, 56-64.

31. Tasker H S, Jones H O; CCXII—The action of mercaptans on acid chlorides. Part II. The acid chlorides of phosphorus, sulphur, and nitrogen; *J. Chem. Soc*. (1909) 95, 1910-1918.

32. V. R. Zhelyaskov, K. R. Gee and D. W. Godiwin; Control of NO Concentration in Solutions of Nitrosothiol Compounds by Light, *Photochem. Photobiol.* (1998) 67, 282-288.

33. Shishido S M, Barozzi Seabra A, Loh W, de Oliveira M; Thermal and photochemical nitric oxide release from *S*-nitrosothiols incorporated in Pluronic F127 gel: potential uses for local and controlled nitric oxide release; *Biomaterials.* (2003) 24, 3543-3553.

34. Sexton D J, Muruganandam A, Mckenny D J, Mutus B; Visible light photochemical release of nitric oxide from *s*-nitrosoglutathione: potential photochemotherapeutic applications; *Photochem. Photobiol.,* (1994) 59, 463-467.

35. Chegaev K, Fraix A, Gazzano E, Eldein G, Abd-Ellatef F, Blangetti M, Rolando B, Conoci S, Riganti C, Fruttero R, Gasco A, Sortino S; Light-Regulated NO Release as a Novel Strategy to Overcome Doxorubicin Multidrug Resistance; *ACS Med. Chem. Lett*. (2017) 8, 361−365.

36. Sortino S, Marconi G, Condorelli G; New insight on the photoreactivity of the phototoxic anti-cancer flutamide: photochemical pathways selectively locked and unlocked by structural changes upon drug compartmentalization in phospholipid bilayer vesicles; *Chem. Commun.* (2001) 1226-1227.

37. Sortino S, Giuffrida S, De Guidi G, Chillemi R, Petralia S, Marconi G, Condorelli G, Sciuto S; The Photochemistry of Flutamide and its Inclusion Complex with β-Cyclodextrin. Dramatic Effect of the Microenvironment on the Nature and on the Efficiency of the Photodegradation Pathways *Photochem. Photobio.* (2001) 73, 6–13.

38. Kirejev V, Kandoth N, Gref R, Ericson M B, Sortino S; A polymer-based nanodevice for the photoregulated release of NO with two-photon fluorescence reporting in skin carcinoma cells; *J. Mater. Chem. B*. (2014) 2, 1190-1195.

39. Nitric Oxide: Biology and Pathobiology, ed. L. J. Ignarro, Elsevier Inc. (2010).

40. Special Journal Issue on Nitric Oxide Chemistry and Biology, *in Arch. Pharmacal Res*, ed. L. J. Ignarro, (2009).

41. Sortino S; Photoactivated nanomaterials for biomedical release applications; *J. Mater. Chem*. (2012) 22, 301-318.

42. S. Sortino; Nanostructured molecular films and nanoparticleswith photoactivable functionalities; *Photochem. Photobiol. Sci*. (2008) 7, 911-924.

43. Juzeniene A, Peng Q Mohan J; Milestones in the development of photodynamic therapy and fluorescence diagnosis; *Photochem. Photobiol. Sci*. (2007) 6, 1234-1245.

44. Raab O; Ueber die wirkung fluoreszierender stoffe auf infusorien. *Z. Biol.* (1900) 39, 524–546.

45. Fingar V; Vascular effects of photodynamic therapy*; J. Clin. Laser Med. Surg.* (1996) 14, 323–328.

46. Photodynamic therapy of subfoveal choroidal neovascularization in age- related macular degeneration with verteporfin: one-year results of randomized clinical trials—TAP report. Treatment of age-related macular degeneration with photodynamic therapy (TAP Study group); *Arch. Ophthalmol* .(1999) 1329–1345.

47. Dougherty T J, Gomer C J, Henderson B W; Photodynamic therapy; *J. Natl. Cancer. Inst.* (1998) 90, 889–905.

48. Fraix A and Sortino S; Combination of PDT photosensitizers with NO photodonors; *Photochem. Photobiol. Sci*. (2018) 17, 1709–1727.

49. Fraix A, Kandoth N, Manet I, Cardile V, Graziano A C E, Gref, Sortino S; An engineered nanoplatform for bimodal anticancer phototherapy with dual-color fluorescence detection of sensitizers *Chem. Commun.* (2013) 49, 4459–4461.

50. Misko T P, Schilling R J, Salvemini D, Moore W M, Currie M G; A fluorometric assay for the measurement of nitrite in biological samples; *Anal. Biochem*. (1993) 214, 11–16.

51. Fang F G, Nitric Oxide and Infection, *Kluer Academic/Plemum Publiscer* (1999).

52. Seggio M, Tessaro A L, Nostro A, Ginestra G, Graziano A C E, Cardile V, Acierno S, Russo P, Catanzano O, Quaglia F, Sortino S; Contact lenses delivering nitric oxide under daylight for reduction of bacterial contamination; *Int. J. Mol. Sci.* (2019) 20, 3735-3744.

53. Marino N, Perez-Loret M, Blanco A R, Venura A, Quaglia F, Sortino S; Photo-antimicrobial polymeric films releasing nitric oxide with fluorescence reporting under visible light *Mater. Chem. B.* (2016) 4, 5138-5143.

54. Caruso E B, Petralia S, Conoci S, Giuffrida S, Sortino S; *J. Am. Chem. Soc*. (2007) 129, 480-481.

55. Conoci S, Petralia S and Sortino S, EP2051935A1/US20090191284, 2006.

56. Seggio M, Nostro A, Ginestra G, Quaglia F, Sortino S; A thermoresponsive gel photoreleasing nitric oxide for potential ocular applications; *J. Mater. Chem. B* (2020) 8, 9121-9128.

57. Callari F L, Sortino S; Amplified nitric oxide photorelease in DNA proximity; *Chem. Commun.* (2008) 1971–1973.

58. Zalipsky S, Gilon C, Zilkha A; Attachment of drugs to polyethylene glycols; *Eur. Polym. J.* (1983) 19, 1177–1183.

59. Chambon F, Winter H H; Linear viscoelasticity at the gel point of a crosslinking PDMS with imbalanced stoichiometry*; J. Rheol.* (1987) 31, 683.

60. Di Bari I, Picciotto R, Granata G, Blanco A R, Consoli G M L, Sortino S; A bactericidal calix[4]arene-based nanoconstruct with amplified NO photorelease; *Org. Biomol. Chem*. (2016) 14, 8047–8052.

61. Taladriz-Blanco P, de Oliveira M G; Enhanced Photochemical nitric oxide release from a flutamide derivative incorporated in pluronic F127 micelles; *J. Photochem. Photobiol. A*. (2014) 293, 65–71.

62. Malanga M, Seggio M, Kirejev V, Fraix A, Di Bari I, Fenyvesi E, Ericson M B, Sortino S; A phototherapeutic fluorescent β-cyclodextrin branched polymer delivering nitric oxide; *Biomater. Sci* (2019) 7, 2272–2276.

63. Sodano F, Cavanagh R J, Pearce A K, Lazzarato L, Rolando B, Fraix A, Abelha T F, Vasey C E, Alexander C, Taresco V, Sortino S; Enhancing doxorubicin anticancer activity with a novel polymeric platform photoreleasing nitric oxide; *Biomater. Sci.* (2020) 8, 1329–1344.

64. Carré M C, Mahieuxe B, André J C, Viriot L M; Fluorimetric nitrite analysis using 2,3-diaminonaphthalene: an improvement of the method; *Analysis*. (1999) 27, 835-838.

65. McClements D J; Nanoemulsions versus microemulsions: terminology, differences, and similarities; *Soft. Matter.* (2012) 8, 1719-1729.

66. Shlaes D M, Sahm D, Opiela C, Spellberg B, The FDA Reboot of Antibiotic Development; *Antimicrob. Agents Chemother*. (2013) 57, 4605-4607.

67. Taubes G, The bacteria fight back; *Science.* (2008) 321, 356-361.

68. Cohen M L, Changing patterns of infectious disease; *Nature.* (2000) 406, 762-767.

69. Laxminarayan R, Duse A, Wattal C, Zaidi A K, Wertheim H F, et al.; Antibiotic resistance- the need for global solution; *Lancet Infect. Dis*. (2013) 13, 1057-1098.

70. Robertson C A, Hawkins Evans D, Abrahamse H; Photodynamic therapy: a new antimicrobial approach to infectious disease; *Photochem. Photobiol*.B. (2009) 96, 1–8.

71. Sortino S; Light-controlled nitric oxide delivering molecular assemblies; *Chem. Soc. Rev.* (2010) 39**,** 2903-2913.

72. Fraix A, Catanzano O, Di Bari I, Conte C, Seggio M, Parisi C, Nostro A, Ginestra G, Quaglia F, Sortino S; Visible light-activatable multicargo microemulsions with bimodal photobactericidal action and dual colour fluorescence; *J. Mater. Chem. B* (2019) 7, 5257-5264.

73. Montalti M, Credi A, Prodi L, Gandolfi M T; Handbook of Photochemistry, CRC, Boca Raton, 3rd edn, 2006.

74. Parisi C, Seggio M, Fraix A**,** Sortino S; A High-Permorming Metal-Free Photoactivatable NO Donor with a Green Fluorescent Reporter; *ChemPhotoChem*. (*2020)* 4, 742– 748.

75. Buldt A, Karst U; Determination of Nitrite in Waters by Microplate Fluorescence Spectroscopy and HPLC with Fluorescence Detection; Anal. Chem. (1999) 71, 3003–3007.

76. Uchiyama S, Santa T, Fukushima T, Homma H, Imai K; Effects of the substituent groups at the 4- and 7-positions on the fluorescence characteristics of benzofurazan compounds; *J. Chem. Soc. Perkin Trans. 2*, (1999) 2525–2532.

77. Szejtli J; *Cyclodextrin Technology;* Kluwer: Dordrecht, 1998.

78. Szejtli J; Past, present and futute of cyclodextrin research. *Pure Appl. Chem.* (2004) 76, 1825 –1845.

79. Loftsson, T.; Douchene, D.;Cyclodextrins and their pharmaceutical applications; *Int. J. Pharm.* (2007) 329, 1-11.

80. Davis M E, Brewster M E, Cyclodextrin-based pharmaceutics: past, present and future; *Nat. Rev. Drug Discov.* (2004) 3, 1023-1035.

81. Harada A, Furue M, Nozakura S; Inclusion of Aromatic Compounds by a β-Cyclodextrin–Epichlorohydrin Polymer; *Polym. J.* (1981) 13*,* 777-781.

82. Mourtzis N, Paravatou M, Mavridis I M, Roberts M L, Yannakopoulou K; Synthesis, characterization, and remarkable biological properties of cyclodextrins bearing guanidinoalkylamino and aminoalkylamino groups on their primary side; *Chem. Eur. J.* (2008) 14, 4188-4200.

83. Yannakopoulou K, Jicsinszky L, Aggelidou C, Mourtzis N, Robinson T M, Yohannes A, Nestorovich E M, Bezrukov S, Karginov V A; Symmetry Requirements for Effective Blocking of Pore Forming Toxins: Comparative Study with α-, β-, and γ-Cyclodextrin Derivatives; *Antimicrob. Agents Chemother*. (2011) 55, 3594 –3597.

84. Mazzaglia A, Sciortino M T, Kandoth N, Sortino S, Cyclodextrin-based nanoconstructs for photoactivated therapies*; J. Drug Del. Sci. Tec*. (2012) 22, 235-242.

85. Monti S, Sortino S; Photoprocesses of photosensitizing drugs within cyclodextrin cavities; *Chem. Soc. Rev.* (2002) 31, 287–300.

86. Chidlow G, Melena J, Osborne N N; Betaxolol, a β1-adrenoceptor antagonist, reduces Na+ influx into cortical synaptosomes by direct interaction with Na+ channels: comparison with other β-adrenoceptor antagonists; *Br. J. Pharmacol.* (2000) 130, 759–766.

87. Van Buskirk E M, Weinreb R N, Berry D P, Lustgarten J S, Podos S M, Drake M M; Betaxolol in patients with glaucoma and asthma; *Am. J. Ophthalmol*. (1986) 101, 531-534.

88. Schmetterera L, Polak K; Role of Nitric Oxide in the Control of Ocular Blood Flow; *Prog. Retin. Eye Res.* (2001) 20, 823-847.

89. Jeong H, Park S, Park K, Kim M, Hong J; Sustained Nitric Oxide-Providing Small Molecule and Precise Release Behavior Study for Glaucoma Treatment; *Mol. Pharmaceutics*. (2020) 17, 656−665.

90. Aliancy J, Stamer W D, Wirostko B, A Review of Nitric Oxide for the Treatment of Glaucomatous Disease, *Ophthalmol Ther*. (2017) 6, 221–232.

91. M. Seggio, S. Payamifar, M. Malanga, A. Fraix, E. Kalydi, P. Kasal, O. Catanzaro, C. Conte, F. Quaglia, S. Sortino; Visible Light-Activatable Cyclodextrin-Conjugates for the Efficient Delivery of Nitric Oxide with Fluorescent Reporter and their Inclusion Complexes with Betaxolol; *NJC* (2021) DOI: 10.1039/d1nj00039j.

92. Synthesis of 2I-O-propargylcyclomaltoheptaose and its peracetylated and hepta(6-O-silylated) derivatives, (2020) In book: Carbohydrate Chemistry: Proven Synthetic Methods, Volume 5 (forthcoming) Publisher: CRC Press, Taylor & Francis Group.

93. Bonger K M, Van den Berg R J B H N, Heitman L H, IJzerman A P, Oosterom J, Timmers C M, Overkleeft H S, Van der Marel G A; Synthesis and evaluation of homo-bivalent GnRHR ligands; *Bioorg. Med. Chem*.(2007) 15, 4841-4856.

94. Klein E, DeBonis S, Thiede B, Skoufias D A, Kozielski F, Lebeau L; New chemical tools for investigating human mitotic kinesin Eg5; *Bioorg. Med. Chem*. (2007) 15, 6474–6488

95. Buldt A, Karst U; Determination of Nitrite in Waters by Microplate Fluorescence Spectroscopy and HPLC with Fluorescence Detection; *Anal. Chem.* (1999) *71*, 3003-3007.

96. Sveen C, Macia N, Zaremberg V, Heyne B; Unveiling the Triplet State of a 4-Amino-7-Nitrobenzofurazan Derivative in Cyclohexane; *Photochem. Photobiol*. (2015) 91, 272-279.

97. Benesi A, Hildebrand J H; A Spectrophotometric Investigation of the Interaction of Iodine with Aromatic Hydrocarbon; *J. Am. Chem. Soc*. (1949) 2703-2707.

98. Duro-Castano A, Movellan J, Vicent M J, Smart branched polymer drug conjugates as nano-sized drug delivery systems; *Biomater. Sci*. (2015) 3, 1321-1334.